SEMMELWEIS EGYETEM

DOKTORI ISKOLA

Ph.D. értekezések

3451.

SZÁSZ CSENGE

Gyermekkori betegségek klinikuma, élettana és prevenciója

című program

Programvezető: Dr. Szabó Attila, egyetemi tanár

Témavezető: Dr. Veres-Székely Apor, PhD

OPTIMIZATION OF IN VITRO BIOASSAYS TO INVESTIGATE FIBROBLAST FUNCTIONS

PhD thesis

Csenge Szász, MD

Semmelweis University Doctoral School

Károly Rácz Conservative Medicine Division

Supervisor: Apor Veres-Székely, Ph.D

Official reviewers: Orsolya Cseprekál, MD, Ph.D.

Judit Erzsébet Pongrácz, Ph.D., Prof.

Head of the Complex Examination Committee:

Károly Liliom, Ph.D., Dr. Habil.

Members of the Complex Examination Committee:

Marcell Cserhalmi, Ph.D.

Ágnes Varga, Ph.D.

Budapest

2026

Table of Contents

List of Abbreviations

AA	acetic acid
Abs	absorbance
ATCC	American Type Culture Collection
CAFs	cancer associated fibroblasts
CAR T-cell	chimeric antigen receptor T-cell
DAMP	danger associated molecular signals
DiI	1,1'-Dioctadecyl-3,3,3',3'-Tetramethylindocarbocyanine Perchlorate
DMEM-F12	DMEM/Nutrient Mixture F-12
DMEM	Dulbecco's Modified Eagle Medium
DSS	dextran sulfate sodium salt
Dx	dextran 40
ECM	extracellular matrix
EGF	epidermal growth factor
EGFR	EGF receptor
EMT	epithelial-to-mesenchymal transition
Ex/Em	Excitation/Emission
FAP	fibroblast activation protein
FBS	foetal bovine serum
Fc	ficoll 400
FDA	Food and Drug Administration
Fluo	fluorescence
Gef	gefitinib
GFP	green fluorescent protein
HCl	hydrochloric acid
HEPES	N-(2-hydroxyethyl)piperazine-N′-(2-ethanesulfonic acid)
IL	interleukin
IPF	idiopathic pulmonary fibrosis
LDH	lactate dehydrogenase
MTT	3-[4,5-dimethylthiazol-2-yl]-2,5 diphenyl tetrazolium bromide
NaOH	sodium-hydroxide
Nint	nintedanib

OD	optical density
PBS	phosphate buffered saline
PDD	phenotypic drug discovery
PDGF	platelet-derived growth factor
PEG	polyethylene glycol
PI	propidium iodide
PTFE	polytetrafluoroethylene
RFP	red fluorescent protein
RPMI	Roswell Park Memorial Institute
RT	room temperature
SD	standard deviation
Sor	sorafenib
SRB	sulforhodamine B
TAS	Transient Agarose Spot assay
TCA	trichloroacetic acid
TDD	targeted drug discovery
TGF-β	transforming growth factor beta
TME	tumour microenvironment
TNF-α	tumour necrosis factor alpha
TRIS	tris(hydroxymethyl)aminomethane
UV	Ultraviolet
WGA	Wheat germ agglutinin
α-SMA	alpha smooth muscle actin

1. Introduction

Fibrosis is the unregulated accumulation of scar tissue due to the permanent activation of tissue repair mechanisms even after the initiating injury has been resolved successfully. Therefore, it is not defined as a distinct disease, but rather as an outcome of multiple different pathological processes. Mechanical and chemical injuries (1, 2), radiation (3), acute hypoxic-ischaemic injury (4), chronic oxidative stress (5) and chronic inflammatory processes (6) may all lead to constant fibroblast activation and deposition of extracellular matrix (ECM), which replaces the functional parenchyma over time, resulting in loss of function and eventually organ failure (7). Since it is a universal mechanism, a wide variety of organs can be affected. Interstitial lung diseases of autoimmune, environmental or idiopathic origin may all present with fibrotic changes (8). In the heart, several chronic conditions, like heart failure, hypertension, ischaemic cardiomyopathy or genetic cardiomyopathies trigger the accumulation of extracellular matrix in the interstitial and perivascular area that restricts cardiac function over time (9). Besides failed regeneration following acute kidney injury (10), common diseases of increasing prevalence in the western world, like diabetic nephropathy, hypertension and obesity (11, 12) can all lead to chronic inflammation that triggers fibrosis leading to chronic kidney disease (13), predicted to become the fifth most common cause of death worldwide by 2040 (12). Moreover, even atherosclerotic plaques have been confirmed to contain fibrotic lesions (14). Given that the above-mentioned conditions cover only a fraction of fibrotic diseases, it does not come as a surprise that fibrosis was estimated to contribute to 50% of death cases worldwide (15).

The main executors of fibrosis, the fibroblast cells have three prominent functions that define their role, namely collective migration, proliferation and the synthesis of ECM elements, mainly collagens (16-18). Following tissue damage, these functions appear sequentially, though overlap partially during physiological tissue repair, where transient fibroblast activation is necessary to restore tissue integrity (19). In fibrosis, dysregulation of the restorative processes leads to permanent fibroblast activation and ECM deposition (Figure 1). The main molecular pathways and cellular executors of tissue repair and its progression into fibrosis are detailed in the sections bellow.

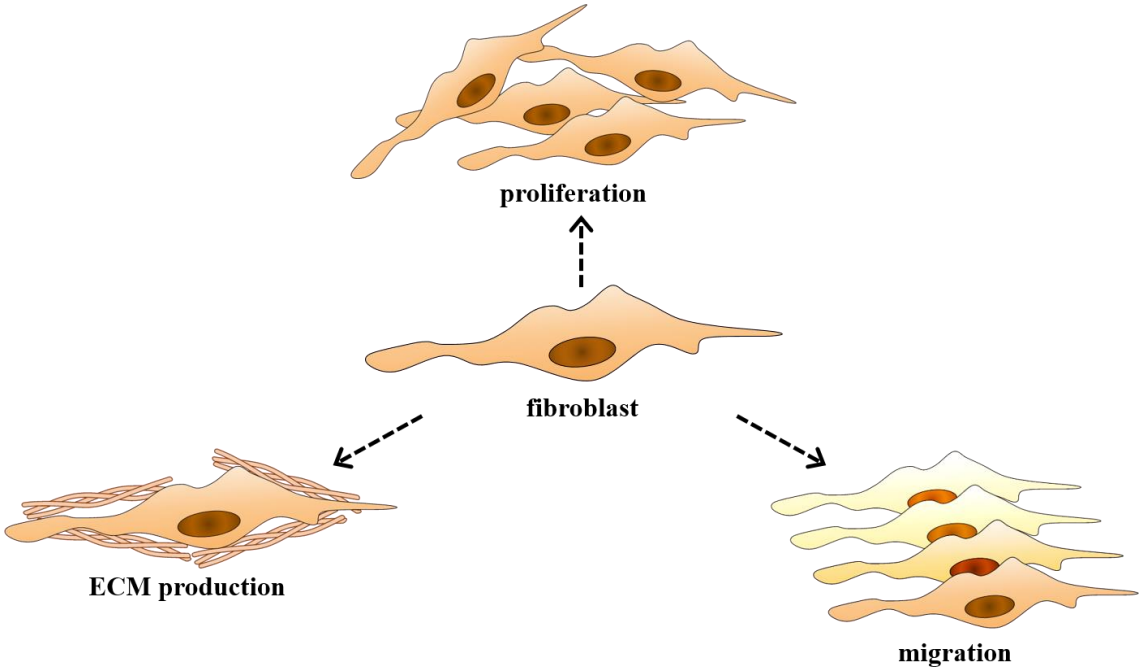

Figure 1: Schematic representation of the main functions of fibroblasts. ECM, extracellular matrix.

Initially, upon injury, danger associated molecular signals (DAMPs) released from the damaged tissue activate macrophages that respond with inflammatory cytokines to recruit neutrophil granulocytes and monocytes (20, 21). Mechanical changes in the ECM due to the soft granulation tissue filling the wound bed and cytokines including platelet-derived growth factor (PDGF) produced by tissue resident cells and macrophages promote the migration of fibroblasts (18, 22), which is facilitated by the epidermal growth factor (EGF) produced by monocytes, platelets and macrophages as well (23). In this stage, fibroblasts forming contractile bundles composed of cytoplasmic actin that exert relatively low contractile forces are referred to as proto-myofibroblasts (24). This form of movement is collective cell migration, the coordinated migration of a physically and functionally linked cell group that retain a higher-than-individual level of organization and are able to modify their tissue surrounding while migrating (25). This process plays an important role in many biological and pathological phenomena in addition to fibrosis throughout our lifespan, including embryonic development, wound healing and reepithelization, fibrosis, tumour invasion and metastasis (26). Then, transforming growth factor beta (TGF-β) released from macrophages and arriving fibroblasts as a para- and autocrine signal, together with EGF and cytokines (e.g. interleukin-1 (IL-1), IL-6, tumour necrosis factor α (TNF-α)) induces fibroblast proliferation, production of ECM

elements, mainly collagens, and myofibroblast activation. These factors can be stored locally linked to various components of the ECM. Besides chemokines, mechanical forces acting along the newly forming granulation tissue also play a role in cell migration and activation of TGF-β, the central cytokine in tissue fibrosis (18, 23).

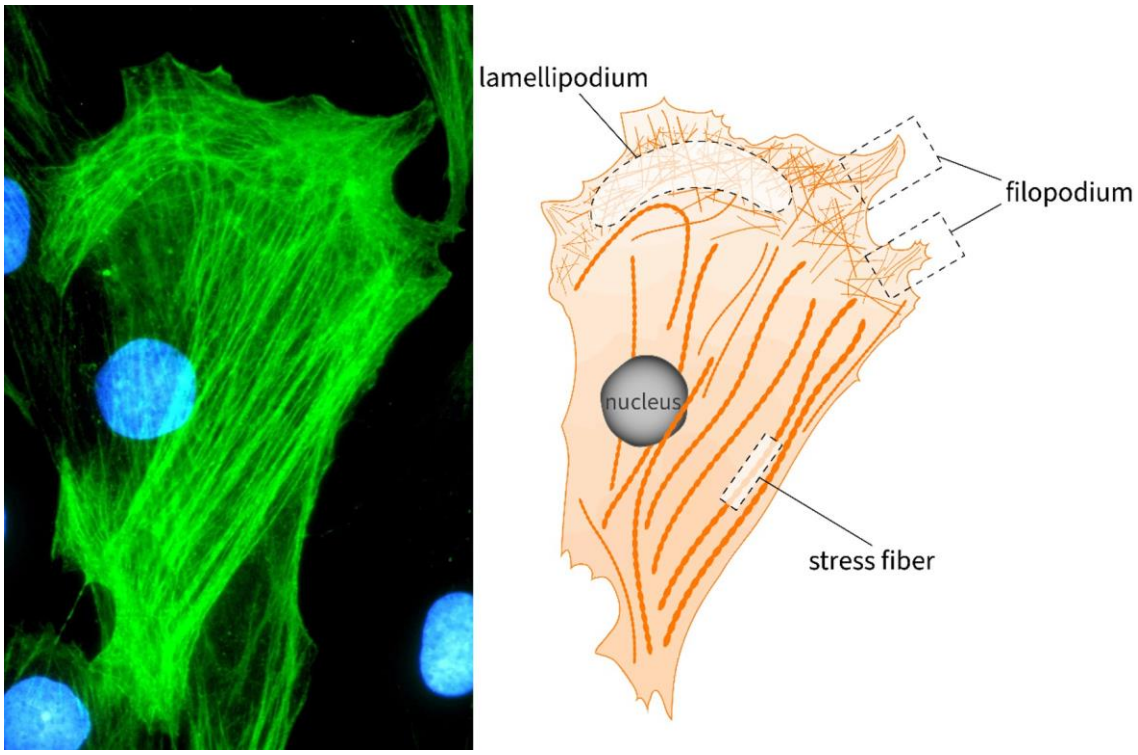

Figure 2: Fluorescent labelling and schematic representation of stress fibres in fibroblasts. The α-smooth muscle actin filaments in a fibroblast cell were labelled fluorescently with phalloidin. The schematic figure illustrates the organization of the filaments into stress fibres responsible for cell contraction and the formation of lamellipodia and filopodia on the leading edge as the initial step of migration (27). (Figure origin: (28))

The heterogeneous population of active, alpha smooth muscle actin (α-SMA) expressing myofibroblast cells mostly develops from resident tissue fibroblasts of mesenchymal origin, however increasing evidence shows that immune cells, local epithelial and endothelial cells are able to transform into myofibroblasts as well through epithelial- or endothelial-mesenchymal transition (19). A main characteristic of myofibroblasts is the formation of α-SMA stress fibres that can exert high contractile forces, thereby stiffening and stabilizing the connective tissue (Figure 2). Compared to proto-myofibroblasts, active myofibroblasts have a relatively lower capacity to produce ECM molecules (18). Whilst during physiological tissue repair, once the tissue integrity is restored, myofibroblasts are deactivated or cleared by apoptosis, their permanent

activation leads to fibrosis. Various factors seem to be responsible for the survival of myofibroblasts, one of which is that the altered balance of the mitochondrial pro- and anti-apoptotic proteins allows the evasion of apoptosis (29). Moreover, the abnormal collagen production and ECM contraction lead to the increased dissociation of TGF-β from its regulator, the latency associated protein, also supported by an elevated autocrine production, and cause long-term epigenetic changes that promote fibrosis (30, 31).

Although the burden of fibrosis is evident and concerning, the therapeutic options are highly limited. The only targeted compounds approved by the Food and Drug Administration (FDA) are the multikinase inhibitor nintedanib and the antifibrotic agent, pirfenidone aiming to inhibit fibroblast functions, however their use is restricted. Nintedanib is indicated for the treatment of idiopathic pulmonary fibrosis (IPF) in adults, other chronic interstitial fibrosing lung diseases and advanced or recurrent non-small cell lung cancer, while pirfenidone is only used in IPF, however, due to the severe, mainly gastrointestinal side effects, a high rate of patients discontinues therapy (32-34). Sadly, even in individuals following therapeutic regimen, the drugs are only capable of somewhat decreasing the progression and extending the average survival from 2 to 5 years (35).

Beyond their well-described importance in tissue repair and fibrosis, currently growing evidence is being gathered about the diverse role of fibroblasts and the tumour microenvironment (TME) in tumour progression and metastasis. It's been shown that fibrotic tissue formation around the tumour is part of the initial immune reaction aimed at isolating and eliminating cancer cells, however, in certain types of cancer, the accumulating stiff scar tissue, so called desmoplastic stroma becomes the main issue, which suggests a shift in fibroblast function towards tumour supporting behaviour (36). The secreted factors of cancer cells, the transforming ECM and the oxidative stress due to the immune reactions and the hypoxic environment often present inside tumours may all contribute to the activation of cancer associated fibroblasts (CAFs) (37). Populations of CAFs with an altered gene expression panel have been identified in several tumour types. Although these groups carry various markers, α-SMA is often present indicating a myofibroblast-like phenotype (38). Similarly to fibroblasts in wound healing and fibrosis, CAFs can develop from multiple different cell types, resulting in a heterogeneous group. While some subtypes exhibit tumour suppressing behaviour by supporting immune

surveillance and producing stroma to inhibit growth, others promote cancer development by immunosuppression, metabolite production and ECM remodelling. Whether these activities and pro- or anti-tumour and functions altogether are exerted by the same cells depending on the environment or by different CAF subpopulations remains to be clarified (36). With the crucial role of CAFs in tumour progression being now revealed, multiple preclinical and clinical trials aim to target this cell type to inhibit tumour progression or overcome therapy resistance. Fibroblast activation protein (FAP), a type-II transmembrane serine protease is an important marker of CAFs, the presence of which has been linked to immunosuppressive phenotype. Therefore, FAP became one of the main investigated targets, along with the application of inhibitory antibodies, prodrugs or protoxins, vaccines and chimeric antigen receptor (CAR) T-cell therapy against it. Nevertheless, in certain cases, the systemic inhibition of FAP led to severe cachexia and bone marrow insufficiency. Other approaches include the inhibition of pathways involved in ECM production or CAF-cancer cell communication (e.g. TGF-β signalling) (36, 39). While CAFs are present in several different cancer types, their importance varies widely. However, beyond the modulation of CAF functions, cancer cells, the central cellular components of tumours themselves share numerous functional characteristics with fibroblasts. Their proliferative and migratory capacity are fundamental for tumour growth, invasion and metastasis formation. Moreover, certain cancer cell types have been shown to secrete collagen isoforms that serve as important signals in cancer progression and modulation of the TME (40, 41). These functions are influenced by the same growth factors that play pivotal role in fibrosis. The increased autocrine PDGF production, the upregulated expression of PDGF receptor and the chronic activation of the receptor signalling pathway have all been shown to facilitate cell proliferation, invasiveness, size and chemotherapeutic resistance of different tumour types (42). While TGF-β acts as a tumour suppressor initially by arresting cell cycle and inducing apoptosis, in the later stages, it promotes the epithelial-to-mesenchymal transition (EMT) of cancer cells, thereby enhancing invasiveness, metastasis formation and expression of ECM proteins (43, 44). The overexpression or mutation of EGF receptor (EGFR) is the central abnormality in several malignancies and often the main cause of therapeutic resistance. The EGFR-regulated pathways potentiate cell proliferation, survival and motility of cancer cells (45). The ligands of the above-mentioned receptors are widely used in in vitro

cancer-related studies as activating agents to investigate the relevance of the pathway and to discover potential therapeutic targets among the elements (46-51).

The diversity of cells and pathways involved as well as the obstacles faced along the rocky way of drug discovery all call for high-throughput, time- and cost-effective standardized methods that allow the rapid selection of biologically relevant, specific compounds.

Lately, targeted drug discovery (TDD) has been the leading approach in industrial drug development, where the clearly defined target interactions and the well-described mechanism of action seemed to be desirable, since it allowed the accurate prediction of time and costs required for the validation, as well as designing of the assay flow. However, retrospectively, the success rate of TDD in the discovery of clinically translatable drugs was lower than expected, leading to rising interest towards the development and application of phenotypic drug discovery (PDD) (52). Instead of focusing on a single target, PDD investigates the complex alterations of a disease-related phenotype in a relevant disease model system even without knowing the exact target or mechanism of action, which can be determined later during the process (53). This means that the validating assays are partially developed in parallel with the PDD campaign, making it less predictable compared to TDD (54). However, a huge advantage of PDD is that the involvement of multiple pathways can not only provide more disease-relevant targets, but also better understanding of the disease pathomechanism itself, while allowing the early elimination of candidates with undesirable mechanisms like protein synthesis or DNA replication inhibitors (55).

Among the complex interactions of heterogeneous cell populations modulating both tissue fibrosis and cancer associated fibrosis, capturing few main routes that significantly modify disease progression without causing major adverse effects due to interference with general pathways posts a real challenge, which is emphasized by the fact that effective therapeutic options are still to be discovered. The PDD approach in this context may be able to reveal new therapeutic targets and offer a better understanding of the phenotypic changes as well.

Since permanently activated fibroblasts are the leading cellular components in both pathologies, establishing a reliable, standardized near-high throughput screening system for the investigation of the main functional/phenotypic characteristics of fibroblasts,

namely migration, proliferation and collagen production could facilitate the effective evaluation of potential therapeutic compounds. Various assays were described in the literature as candidates to assess cell proliferation based on different principles, of which MTT (3-[4,5-dimethylthiazol-2-yl]-2,5 diphenyl tetrazolium bromide), a mitochondrial dehydrogenase enzyme activity based colorimetric assay paired with lactate dehydrogenase (LDH) assay to detect cell death in parallel are used in our laboratory routinely (56). In case of migration, the current gold standard scratch assay's (57) replicability and throughput fail to reach the level desirable to test high number of compounds available in low quantities in early phase drug discovery. Therefore, our group optimized a novel alternative using agarose droplet as a biocompatible, inert physical barrier to create cell-free area, called Transient Agarose Spot (TAS) assay. Combined with persistent staining of viable cells, the final assay became highly automated, with increased throughput, reproducibility, and decreased assay time, cell- and reagent requirement. Given the large number of members in the collagen superfamily and the complexity of collagen biosynthesis that is greatly dependent on the surrounding structures in vivo, to date there has been no gold standard method to investigate total collagen production (14, 58). We optimized a staining method based on Sirius Red, a traditional histological dye, to detect the total collagen production in cell cultures and adjusted the in vitro assay conditions to better approximate the natural circumstances and maximize collagen biosynthesis. The parallel application of these assays could allow a thorough evaluation of fibroblast functions as well as the observation of subtle differences in the effect of compounds targeting fibroblasts. Beyond being available for most research laboratories with its cost-effectiveness and simplicity, our robust system offers a suitable alternative for industrial application.

2. Objectives

In fibrosis, the approved therapeutic options are highly limited, their use is restricted to a handful of diseases, with the purpose being the decrease of disease progression, and serious side effects occur often due to the involvement of universal pathways. Although in cancer, there are multiple therapeutic modalities available, their applicability depends on the exact type of malignancy, moreover, therapeutic resistance can develop over time due to mutations. Therefore, discovering new, specific therapeutic options is emerging in both diseases, calling for standardized near-high-throughput in vitro screening systems.

Fibroblast and cancer cells share the ability of proliferation, migration and collagen production, functional characteristics that are crucial in the progression of numerous diseases. The aim of our work was to create a microplate-based in vitro assay pool for the assessment of new therapeutic candidates in a cost-effective, near-high throughput manner. Besides optimizing well-known methods, we developed new assays to investigate all the above-mentioned phenotypic characteristics in a standardized system. During our project, we focused on the following objectives:

Cell migration

1) To develop a damage-free agarose-based collective cell migration assay, the TAS assay designed for 96-well plate.
2) To compare the performance of the TAS assay to the current gold standard scratch assay.
3) To automate the detection and evaluation steps using a new generation microplate reader.
4) To demonstrate the main considerations in the selection of suitable labelling technique.

Collagen production

5) To optimize Sirius Red staining for the detection of total collagen production in vitro.
6) To assess the major influencing factors and adjust the experimental conditions to achieve maximal collagen production in vitro.

3. Methods

3.1. Cell lines and treatments

Cell lines were cultured in their adequate media under standard cell culture conditions (37°C, humidified, 5% CO_2). Cell lines were obtained from American Type Culture Collection (ATCC), Manassas, VA, USA, József Tóvári, National Institute of Oncology, Budapest, Hungary or the peritoneal dialysate of two paediatric patients undergoing peritoneal dialysis at the Pediatric Center, Semmelweis University (31224-5/2017/EKU) as indicated bellow (Table 1). Dulbecco's Modified Eagle Medium (DMEM), DMEM/Nutrient Mixture F-12 (DMEM-F12), McCoy's 5A Medium and Roswell Park Memorial Institute (RPMI) 1640 medium were purchased from Thermo Fisher Scientific, Waltham, MA, USA. All media were supplemented with 1% penicillin/streptomycin (Merck, Kenilworth, NJ, USA). Heat-inactivated foetal bovine serum (FBS) was purchased from Invitrogen (Waltham, MA, USA). Cells were seeded (n = 5-10 wells/treatment groups) into 96-well tissue culture plates (Sarstedt, Newton, MA, USA) at the densities indicated in Table 1.

During in vitro experiments, recombinant epidermal growth factor (EGF, 10 ng/mL, #236-EG, R&D Systems, Minneapolis, MN, USA), recombinant platelet-derived growth factor BB (PDGF-BB, 10 ng/mL, #520-BB, R&D Systems), recombinant transforming growth factor beta 1 (TGB-β, 1 nM, #PHG9204, Thermo Fisher Scientific), and a dilution series of kinase inhibitors (0 – 10 μM) including nintedanib (Nint, Vichem Chemie Research, Budapest, Hungary), gefitinib (Gef, Vichem) or sorafenib (Sor, Vichem) were used. Control cells were treated only with the corresponding solvents (EGF, PDGF-BB: phosphate buffered saline (PBS), Nint, Gef, Sor: DMSO (Merck), TGF: 4 mM hydrochloric acid (HCl)) in equal volumes. The effect of volume exclusion was investigated by the supplementation of the culture media with dextran 40 (Dx) (40 kDa, 50 mg/mL, Reanal Ltd., Budapest, Hungary), dextran sulfate sodium salt (DSS) (40 kDa, 100 μg/mL, MP Biomedicals, LLC, Irvine, CA, USA), polyethylene glycol (PEG) (20 kDa, 50 mg/mL, Merck) or ficoll 400 (Fc) (400 kDa, 50 mg/mL, Pharmacia Fine Chemicals, Uppsala, Sweden).

Table 1: Summary of the cell cultures, their respective culture media and seeding density used for the in vitro experiments.

Cell line	ATCC code	Cell type	Media	Seeding density/well
MTT/LDH assay				
LCLC-103H	#ACC-384	human lung cancer cell	RPMI 1640	6×10^3
CCD-19Lu	#CCL-210	human lung fibroblast	DMEM	6×10^3
A549	#CRM-CCL-185	human lung carcinoma epithelial cell		6×10^3
TAS assay				
MRC-5	#CCL-171	human lung fibroblast	DMEM	2×10^4
CCD19-Lu	#CCL-210	human lung fibroblast		10^4
NRK-49F	#CRL-1570	rat kidney fibroblast		10^4
A549	#CRM-CCL-185	human lung carcinoma epithelial cell		$1.5/2\times10^4$
Caco-2	#HTB-37	human colon carcinoma cell		6×10^4
HT-29	#HTB-38	human colon carcinoma cell	McCoy's 5A Medium	4×10^4
LCLC-103H	#ACC-384	human lung cancer cell	RPMI 1640	7.5×10^3
HCT-116	#CCL-247	human colon carcinoma cell		2×10^4
RFP expressing HCT-116		human colon carcinoma cell		
GFP expressing HCT-116		human colon carcinoma cell		
Scratch assay				
MRC-5	#CCL-171	human lung fibroblast	DMEM	4×10^5
Sirius Red assay				

CCD-19Lu	#CCL-210	human lung fibroblast	DMEM	10^4
A549	#CRM-CCL-185	human lung carcinoma epithelial cell		10^4
Immunofluorescence staining				
CCD-19Lu	#CCL-210	human lung fibroblast	DMEM	6×10^4

ATCC, American Type Culture Collection; DMEM, Dulbecco's Modified Eagle Medium; RPMI, Roswell Park Memorial Institute; DMEM-F12, DMEM/Nutrient Mixture F-12; GFP, green fluorescent protein; RFP, red fluorescent protein

3.2. Transient Agarose Spot (TAS) assay

To perform TAS assay, 0.1% agarose (Merck) was prepared in sterile water by stirring and heating. A 2 µL droplet of 90°C agarose was placed in the middle of each well on a 96-well plate and left to polymerize for 15 minutes at room temperature (RT) before cell seeding. After 24 hours of incubation in cell culture medium containing 10% FBS, the droplets were removed by pipette tip and cells were washed with 200 µL of sterile PBS to eliminate debris and unattached cells. 100 µL of culture medium supplemented with the corresponding treatment was added for 72 hours. In a set of experiments, MRC-5 cells were incubated with 0.1 mg/mL1,1'-Dioctadecyl-3,3,3',3'-Tetrame-thylindocarbocyanine Perchlorate (DiI) solution (#D282, Thermo Fisher Scientific) for 2 hours before the agarose droplet removal.

3.3. Scratch assay

To perform scratch assay, MRC-5 cells were seeded into 12-well plates. Followed by 24 hours of incubation, media was removed, and the confluent cell layer was scraped with one movement using a 200 µL pipette tip. Wells were washed with 2 mL of sterile PBS to eliminate debris and unattached cells, and treatment of recombinant EGF diluted in 1 mL of culture medium containing 0.1% FBS was applied.

3.4. Data acquisition by microscopy for TAS assay

Brightfield or fluorescent images of each well were taken at specific time points during treatment using an Olympus IX81 microscope system (Olympus Corporation, Tokyo, Japan) with 4× objective. Cell-free gap areas were annotated manually by computer mouse, digitizer board without display and tablet or automatically using ImageJ

1.48v software (National Institutes of Health, Bethesda, Rockville, MD, USA) applying the macros described in Table 2. ***Highlighted parameters*** were determined and verified for each experiment.

Table 2: Macros used in ImageJ for the automatic annotation of cell-free gap areas.

Brightfield images	Fluorescent images

run("Find Edges");
setAutoThreshold("Default");
//run("Threshold...");
setThreshold(*0, 20*);
run("Analyze Particles...",
"size=*2,000,000*-Infinity show=Outlines
summarize");
close();
	run("RGB Stack");
	run("Next Slice [>]");
	run("Delete Slice");
	run("Next Slice [>]");
	run("Delete Slice");
	run("Find Edges", "slice");
	setAutoThreshold("Default");
	//run("Threshold...");
	setThreshold(***0, 20***);
	run("Analyze Particles...",
	"size=***2,000,000***-Infinity show=Outlines
	display clear
	summarize slice");
	close();

Gap areas were determined as ratio (%) of the initial gap area at 0 h:

$$\text{gap area [\%]} = \text{actual gap area} / \text{initial gap area} \times 100$$

In certain cases, gap closure was described by the absolute value decrease in cell-free area:

$$\Delta \text{ gap area [pixel}^2\text{]} = \text{initial gap area - actual gap area}$$

3.5. Cell confluency

Fluorescent images of DiI labelled MRC-5 cells were taken using an Olympus IX81 microscope system with 4× objective and analysed with ImageJ 1.48v software. The quantity of black pixels was determined by setting colour threshold and measuring the labelled area. The gel spot was defined by annotation and the confluency was calculated based on the following equation:

$$\text{confluency [\%]} = [1 - ((\text{black pixel area} - \text{gel spot area}) / (\text{total area} - \text{gel spot area}))] \times 100$$

3.6. Cell staining and data acquisition by microplate reader

To investigate microplate reader-based evaluation, various staining methods were tested with detailed protocols provided in Table 3. Kahle's solution was prepared using

26% ethanol (Molar Chemicals Kft., Halásztelek, Hungary), 3.7% formaldehyde (Molar Chemicals Kft.), and 2% glacial acetic acid (Merck).

Table 3: Summary of the dyes, cell fixation and staining protocols and detection parameters used for microplate reader-based detection of TAS assay.

	Fixation	Dye	Staining	Detection	Ex/Em (nm)
SRB	10% TCA at 4 °C for 1 hour	Sulforhodamine B sodium salt (#S1402, Merck)	0.4% SRB in 1% AA for 30 minutes	abs	565/ -
				fluo	550/605
FastGreen	Kahle's solution at RT for 15 minutes	FastGreen FCF (#F7252, Merck)	0.1% FastGreen in 1% AA for 5 minutes	abs	624/ -
methylene blue		Methylene blue solution acc. To Loeffler (#42335, Molar Chemicals)	1% methylene blue in H_2O for 5 minutes	abs	668/ -
Cresyl Violet		Cresyl Fast Violet – Certistain (#K2247947, Merck)	0.14 mg/mL in 6.8 mM sodium ace-tate + 83 mM AA mix for 20 minutes	abs	590/ -
				fluo	583/627
PI		Propidium Iodide Staining Solution (#51-66211E, BD Pharmingen)	0.5 µM in PBS for 5 minutes	fluo	550/605
DiI	-	1,1'-Dioctadecyl-3,3,3',3'-Tetrame-thylindocarbocyanine Perchlorate (#D282, Thermo Fisher Scientific)	0.1 mg/mL in cell culture medium for 24 hours	fluo	538/582
WGA		Wheat Germ Agglutinin Alexa Fluor 488 conjugate (#W11261, Thermo Fisher Scientific)	0.01 mg/mL in cell culture medium for 4 hours	fluo	470/515

Calcein AM	Calcein AM (#C3099, Thermo Fisher Scientific)	10 µM in cell culture medium for 1 hour	fluo	490/533
Cell Tracker	Cell Tracker Green CMFDA (#C7025, Thermo Fisher Scientific)	5 µM in cell culture medium for 1 hour	fluo	470/515
Hoechst	Hoechst 33342 trihydrochloride (#B2261, Merck)	0.5 µg/mL (1:10 000) in cell culture medium for 4 hours	fluo	355/455
Autofluorescence	-	-	abs	285/ -

TCA, trichloroacetic acid; RT, room temperature; AA, acetic acid; abs, absorbance; fluo, fluorescence; Ex/Em, Excitation/Emission

Stained or green and red fluorescent protein expressing cells were used to detect signal with the microplate reader. Absorbance or fluorescence signal of each well was measured using a CLARIOstar Plus microplate reader equipped with MARS 285 v4.01 software (BMG Labtech, Ortenberg, Germany) at the wavelengths provided in Table 3. Readings were performed using the well scanning function at 30×30 points/well focusing on a 4 mm diameter circle in the middle of the well with the focal height set to 3.2 mm and bottom optic for fluorescence detection. To clearly discriminate cell-covered and cell-free areas, the gain parameters were manually adjusted for the fluorescence values to be positioned in the upper third of the measurement range. Cell-free gap areas were defined as the number of scan points that fell below a manually set threshold and presented as the percentage ratio (%) of the initial gap area.

3.7. MTT cell proliferation assay

MTT assay was performed to determine the mitochondrial dehydrogenase activity of attached viable cells. MRC-5 cells were seeded in 96-well plates, incubated for 24 hours in culture medium containing 0.1% FBS and treated with recombinant PDGF-BB in the presence or absence of nintedanib. Thereafter 10 µL of MTT reagent, containing 5 mg/mL thiazolyl blue tetrazolium bromide (diluted in sterile H_2O) was added to each well containing the cells and the 100 µL supernatant and incubated at 37°C for 4 hours. Subsequently, supernatant was removed and intracellular MTT crystals were solubilized

in 1:1 mixture of ethanol and DMSO. Absorbance was measured at 570 nm and at 690 nm as background in a CLARIOstar Plus microplate reader equipped with MARS 285 v4.01 software.

3.8. LDH cytotoxicity assay

The extent of cell death was investigated using a colorimetric method based on the release of lactate-dehydrogenase (LDH) in the supernatant upon cell damage. 40 µL of supernatant was mixed with equal volume of LDH reagent containing 109 mM lactate, 3.3 mM β-nicotinamide-adenine-dinucleotide-hydrate (#N7004), 2.2 U/mL diaphorase (#D2197), 3 mM tris(hydroxymethyl)aminomethane (TRIS), 30 mM N-(2-hydroxyethyl)piperazine-N′-(2-ethanesulfonic acid) (HEPES), 10 mM NaCl, 350 µM thiazolyl blue tetrazolium bromide (all reagents were purchased from Merck) in a sterile 96-well plate and incubated at 37°C for 1 hour. Absorbance was measured at 570 nm and at 690 nm as background in a CLARIOstar Plus microplate reader equipped with MARS 285 v4.01 software.

3.9. Sirius Red histological staining (Picrosirius)

To visualize the collagen accumulation, slides with histological samples from fibrotic mouse lungs were deparaffinised by submerging in xylene for 10 minutes at RT, followed by rehydration in descending ethanol concentrations (96-90-80-70%), 1 minute for each. After that, slides were stained with dye solution containing 0.1% Direct Red 80 and 1.2% picric acid for 1 hour at RT, which was removed quickly using distilled water. To remove excess dye, slides were rinsed with 0.1M HCl solution for 2 minutes at RT. Ascending concentrations of ethanol (70-80-90-96% absolute ethanol) were applied, 1 minute each for dehydration, after which slides were cleared in xylene for 10 minutes at RT and covered using DPX Mountant for Histology (Merck).

3.10. Sirius Red collagen detection assay for cells

CCD-19Lu and A549 cells were cultured in 10% FBS for 24 hours followed by another 24 hours in 1% FBS to reach full confluence. Subsequently, cells were incubated for 48 hours with 1 nM TGF-β dissolved in FBS-free DMEM containing 200 µM ascorbate (Merck) unless otherwise indicated. After treatment, the supernatant was separated, and cells were washed with 200 µL of PBS. 50 µL of Kahle's fixing solution was applied at RT for 15 minutes followed by another washing step. Next, cells were

incubated in 50 µL of Sirius Red solution containing 0.1% Direct Red 80 and 1% acetic acid in distilled water at RT for 1 hour, then washed with 400 µL of 0.1 M HCl. 100 µL 0.1 M sodium-hydroxide (NaOH) was added to elute the bound dye. All reagents were purchased from Merck. The absorbance was determined as optical density (OD) at 540 nm with CLARIOstar microplate reader with MARS Data Analysis Software v4.01 using NaOH as blank.

3.11. Sirius Red collagen detection assay for cell culture medium

To conduct the optimization steps for collagen detection in the supernatant, a dilution series of rat tail-derived Collagen type I (#A10483-01; Thermo Fisher Scientific) was prepared in distilled water or DMEM and various 96-well microplates were compared for the washing and centrifugation including flat-bottom (Sarstedt), V-bottom (Thermo Fisher Scientific), or 0.45 µm low-binding hydrophilic polytetrafluoroethylene (PTFE) filter plate (Merck).

In the final assay, the culture supernatant measuring 100 µL was transferred into a V-bottom 96-well plate, stained with 50 µL of Sirius Red solution containing 0.1% Direct Red 80 and 3% acetic acid in distilled water and mixed thoroughly. After incubating at RT for 30 minutes, the plate was centrifuged at 3000×g for 6 minutes to pellet collagen-dye precipitates. Unbound dye solution was removed by multichannel pipette, thereafter wells were washed with 150 µL 0.1 M HCl and centrifuged again. After eluting the collagen-bound dye with 100 µL of NaOH and transferring the solution into a clear flat-bottom 96-well plate, absorbance was measured at 540 nm with CLARIOstar microplate reader with MARS Data Analysis Software v4.01 using NaOH as blank.

3.12. Immunofluorescence staining

CCD19-Lu cells were seeded into 4-well chambers (Sarstedt) medium containing 10% FBS for 7 days. Subsequently, after rinsed with 500 µL PBS, cells were fixed in 300 µL BD Cytofix/Cytoperm™ (BD Biosciences, Franklin Lakes, NJ, USA) at RT for 15 minutes then rinsed again with 500 µL BD Perm/Wash™ (BD Biosciences). Primary antibodies against procollagen 1α2 (sc-166572; mouse, 1:100, Santa Cruz Biotechnology, Dallas, TX, USA) or collagen type I alpha 1 (sc-293182; mouse, 1:100, Santa Cruz Biotechnology) were diluted in BD Perm/Wash™ and applied at RT for 1 hour. Cells were washed with 500 µL BD Perm/Wash™ for 2 minutes, incubated with goat anti-

mouse Alexa Fluor® 568-conjugated IgG secondary antibody (A11004; 1:500, Thermo Fischer Scientific) at RT for 1 hour and washed again with 500 µL BD Perm/Wash™ for 2 minutes. Controls were prepared omitting the primary antibody to ensure specificity and avoid autofluorescent signal. Nuclei were labelled with Hoechst 33342 DNA staining (1:5000) for 15 minutes, cells were washed with 500 µL BD Perm/Wash™, finally slides were cover slipped using ProLong™ Gold Antifade Mountant (Thermo Fischer Scientific).

3.13. Data acquisition by microscopy for Sirius Red assay

Brightfield, fluorescent or polarized light illumination images were taken using Olympus IX81 microscope system (Olympus Corporation, Tokyo, Japan) with 20× or 100× objectives. Right before the elution step, samples from the stained collagen solution or supernatant were resuspended in HCl, dripped onto a slide and cover slipped. Images taken from the same field were merged in ImageJ 1.48v software after conversion from coloured to 8-bit format.

3.14. Statistical analysis

Statistical evaluation was performed using GraphPad Prism 8.01 or 9.1.2 software (GraphPad Software Inc., San Diego, CA, USA). Unpaired t test with Welch's correction was used for the comparison of two independent groups. Two-way ANOVA, Brown-Forsythe and Welch ANOVAs or ordinary two-way ANOVA with Dunnett's tests were applied for multiple comparisons and Pearson's correlation for correlation analyses. $p \leq 0.05$ was considered as statistically significant. Curves from the dilution series were compared by linear regression analysis. Unless otherwise indicated, results are illustrated as mean ± standard deviation (SD) of the corresponding treatment groups. The applied tests, significances, and number of elements (n) are indicated in each figure legend.

Descriptive statistics were performed to evaluate the performance of *Sirius Red collagen detection assay for cell culture medium*. Linearity was determined based on the range of the collagen concentration for which a linear curve could be fitted, while meeting the criteria of regression (R^2) < 0.95. The limit of detection was determined based on the minimal collagen concentration at which the absorbance was significantly different from the baseline. Accuracy was defined as the mean difference between nominal and measured collagen concentrations in the linear range. Intra-assay variability was defined

based on the average coefficient of variations from the samples of linear range measured in a single experiment. Inter-assay variability was determined as the coefficient of variation derived from the mean values of samples of linear range measured in six independent experiments. Non-linear asymmetric sigmoidal 5 parameter logistic curve was fitted on the collagen concentration-absorbance correlation graph.

4. Results

4.1. Optimization of TAS assay

4.1.1. Agarose spot stability and optimal cell density

The stability of the agarose spot was investigated over several days using MRC-5 cells. Upon removal after 24 hours, rapid cell migration and reduction in gap size was observable, however the permanent spot inhibited migration even in a 7-day interval allowing change of medium and flexible initiation of the migration experiment.

To examine the effect of cell density on the confluence, MRC-5 cells were seeded with different cell counts around the agarose spot and plated for 24 hours. The confluence elevated in parallel with the increase in cell density, reaching a plateau phase at 20×10^3 cells/well. After agarose spot removal, gap closure was similarly accelerated at higher cell densities, arriving at the maximum at 20×10^3 cells/well. Taken together, the confluence and the rate of gap closure seemed to correlate (Figure 3).

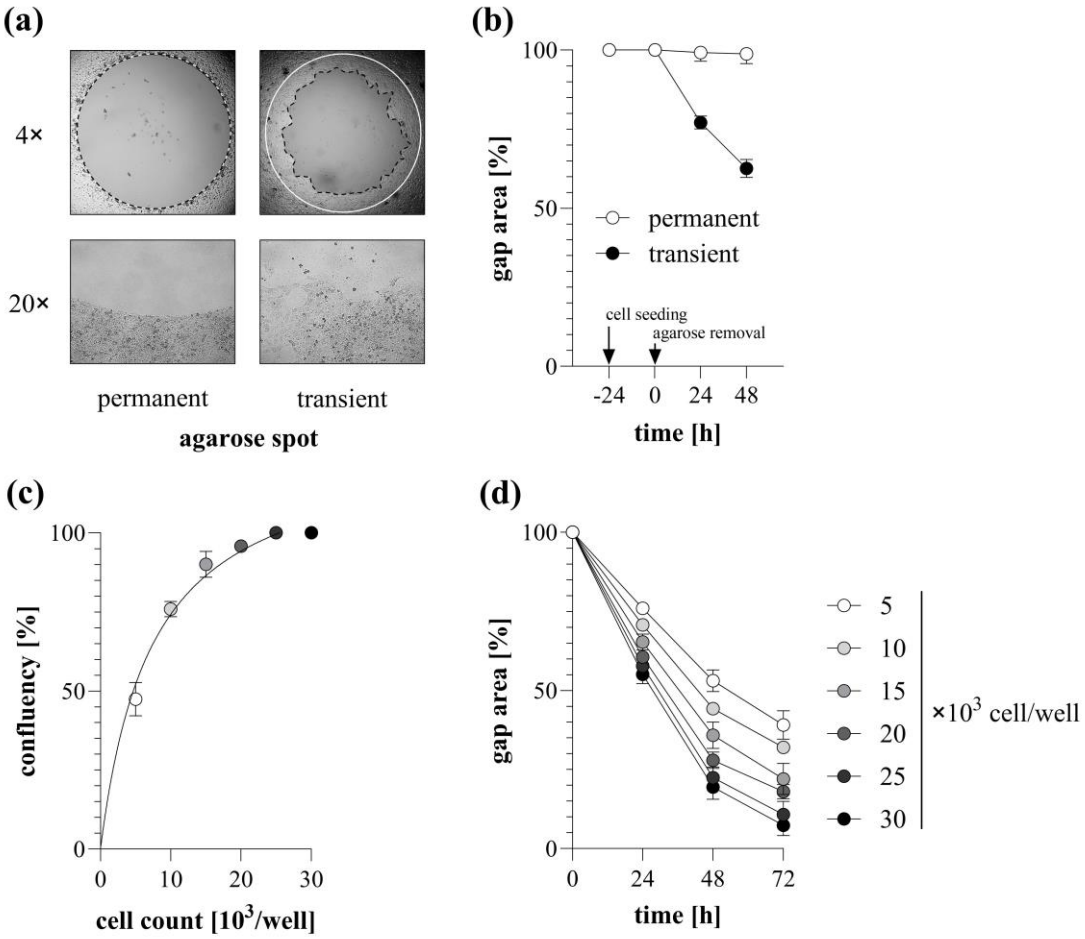

Figure 3: The effect of agarose spot and cell density on the migratory capacity of MRC-5 cells. **(a)** Brightfield microscopic images of cell-free gap areas were annotated manually. Lines indicate the gap edges at 0 (white) and 48 (black) hours. Images taken with 20× objective show the edge of the cell-free area at 48 hours. **(b)** The gap closure was monitored for 72 hours after cell seeding. Results are presented as mean ± SD (n = 6). **(c)** The effect of cell density on the confluence and **(d)** on the rate of gap closure was determined. Results are presented as mean ± SD (n = 5).

4.1.2. Applicability of TAS assay to investigate fibroblast migration

The migration of MRC-5 and NRK-49F cells was investigated following various treatments. The addition of FBS to the culture medium increased the rate of gap closure in a dose dependent manner (Figure 4a, c, e). Treatment with EGF accelerated cell migration as well (Figure 4b, d, f).

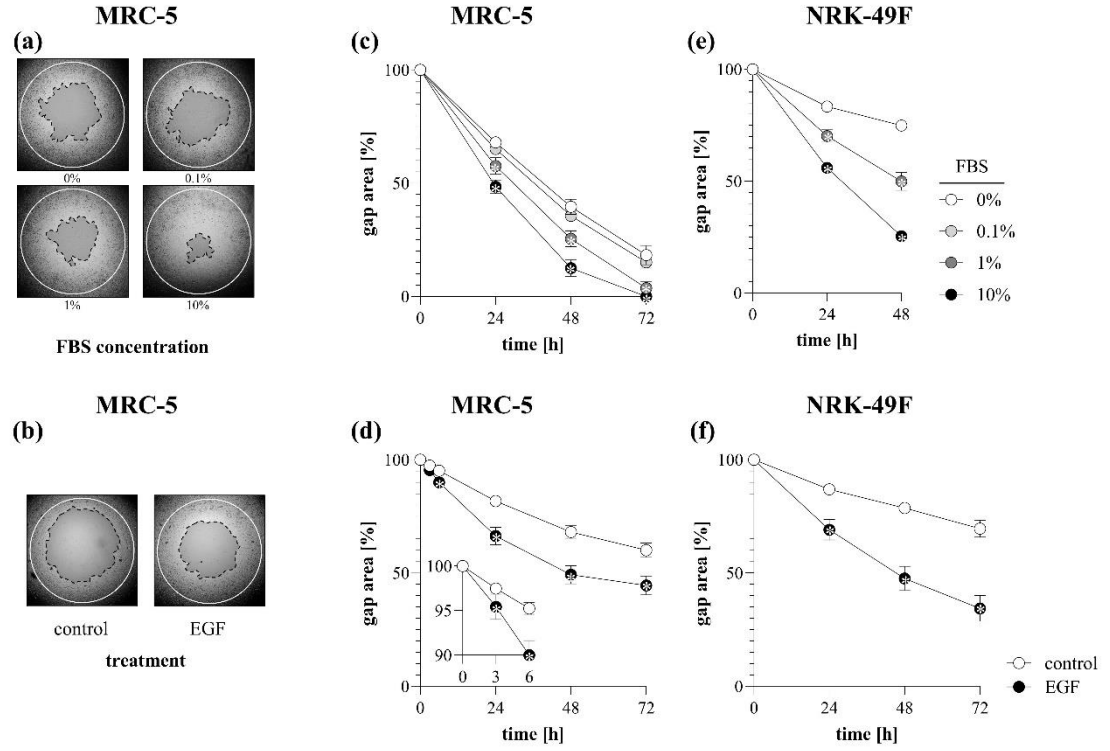

Figure 4: The effect of nutrient supplementation (FBS) and growth factor addition (EGF) on the migration of MRC-5 lung fibroblasts and NRK-49F rat kidney fibroblasts. Migration was investigated with TAS assay. **(a, b)** Brightfield microscopic images of the gap size were taken. Lines indicate the gap edges at 0 (white) and 48 (black) hours. **(c-f)** Gap closure was followed for 72 hours after gel removal. Results are presented as mean ± SD (n = 8). * $p < 0.05$ vs. 0% FBS **(c, e)** or control **(d, f)** at the concerning time (two-way ANOVA). FBS, foetal bovine serum; EGF, epidermal growth factor.

4.1.3. Applicability of TAS assay to investigate cancer cell migration

The migration of A549, Caco-2 and HT-29 cell lines was investigated after supplementation of FBS dilution series (Figure 5a-c) or treatment with EGF (Figure 5d-f). While FBS accelerated the rate of gap closure in A549, EGF did not have an effect contrary to the colon cancer cells, where EGF could increase migration.

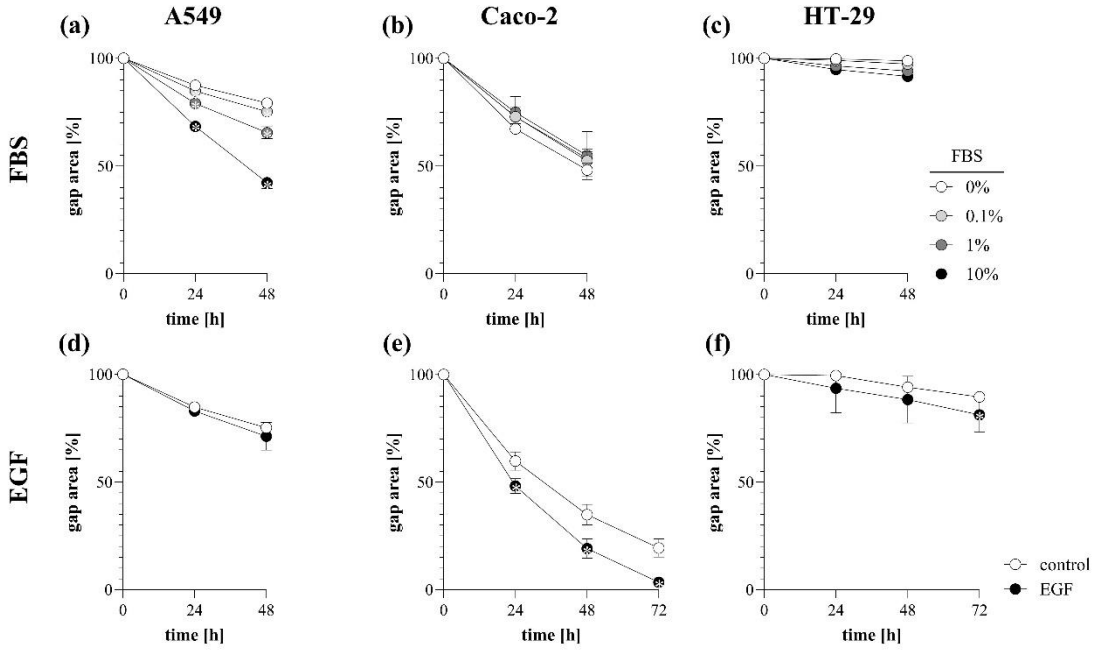

Figure 5: The effect of nutrient supplementation (FBS) **(a-c)** and growth factor addition (EGF) **(d-f)** on the migration of A549 lung adenocarcinoma epithelial cells, Caco-2 and HT-29 colon cancer cells. Migration was investigated with TAS assay. Gap closure was monitored for 48-72 hours after gel removal. Results are presented as mean ± SD (n = 8). *p < 0.05 vs. 0% FBS **(a-c)** or 0% control **(d-f)** at the concerning time (two-way ANOVA).

4.1.4. Comparison of different gap annotation methods

To examine the accuracy and reproducibility of different methods, brightfield and fluorescent images of the same field of DiI labelled cells were annotated using different manual techniques and automatic annotation (Figure 6a). Both brightfield and fluorescent images of MRC-5 were suitable for the automatic method and gap sizes showed a strong positive correlation with the manual annotation (Figure 6b). However, from the NRK-49F cells only the fluorescent images could be processed automatically because the software was unable to recognize the edges of the cell-free area.

Regarding the time requirement, while the digitizer board and tablet could accelerate the manual evaluation, automatic annotation largely shortened and simplified the process (Figure 6c).

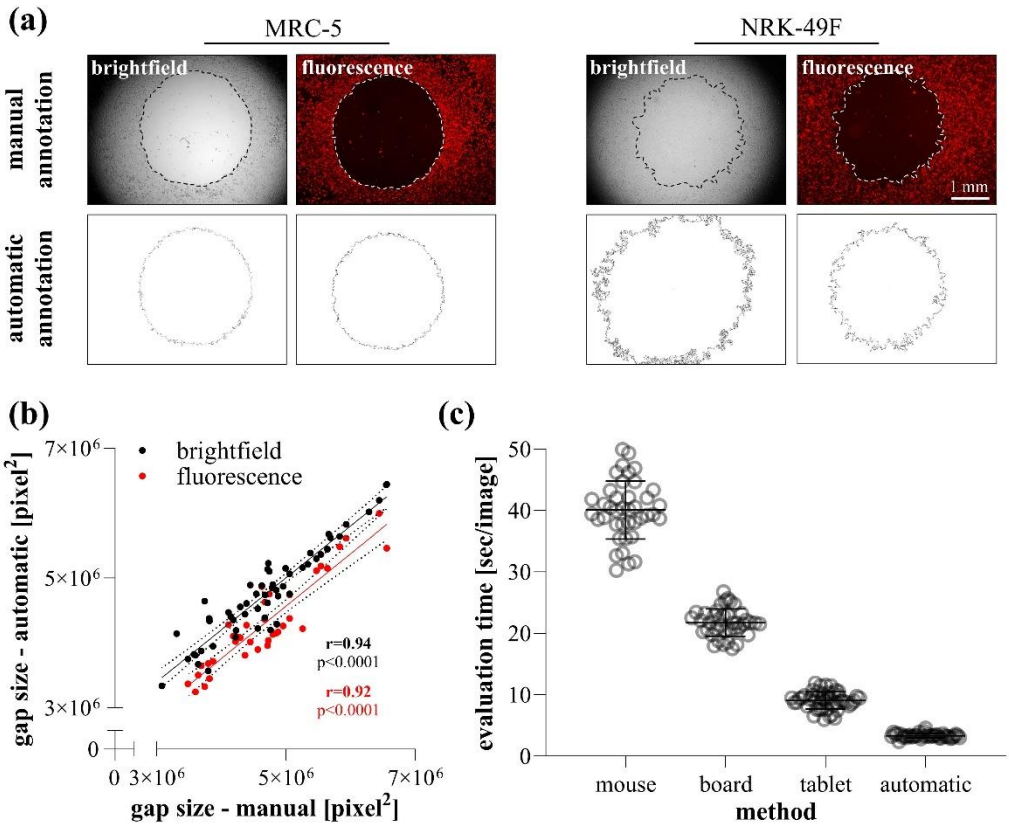

Figure 6: Comparison of data evaluation methods in TAS assay. **(a)** Brightfield and fluorescent images of DiI-stained MRC-5 and NRK-49F cells were taken. **(b)** The same images of MRC-5 cells (n = 40) were analysed after manual or automatic annotation to compare the gap areas. Pearson's correlation coefficients (r) and p values are indicated. **(c)** The required evaluation times were compared.

4.1.5. Comparison of scratch and TAS migration assay

Scratch assay on 12-well plate and TAS assay on 96-well plates were performed in parallel on MRC-5 cells to compare the sensitivity and reproducibility. When examining the initial gap sizes from numerous independent experiments, in the case of scratch assay confidence interval fell between 23% and 30% while for TAS assay it was significantly lower, falling at only 9%, similar to measuring the agarose spot without cells (Figure 7a, b, c). Beside the inconsistent initial gap size, in scratch assay the gap closure is uneven and can only be documented by a series of images, while for TAS assay the whole cell-free area fits in one field of view (Figure 7d).

The migration kinetics were similar with both methods, however when examining the relative and absolute gap size values, the intra-group variance determined by the coefficient of variation of group means was on average 3 times higher in scratch assay (Figure 7e).

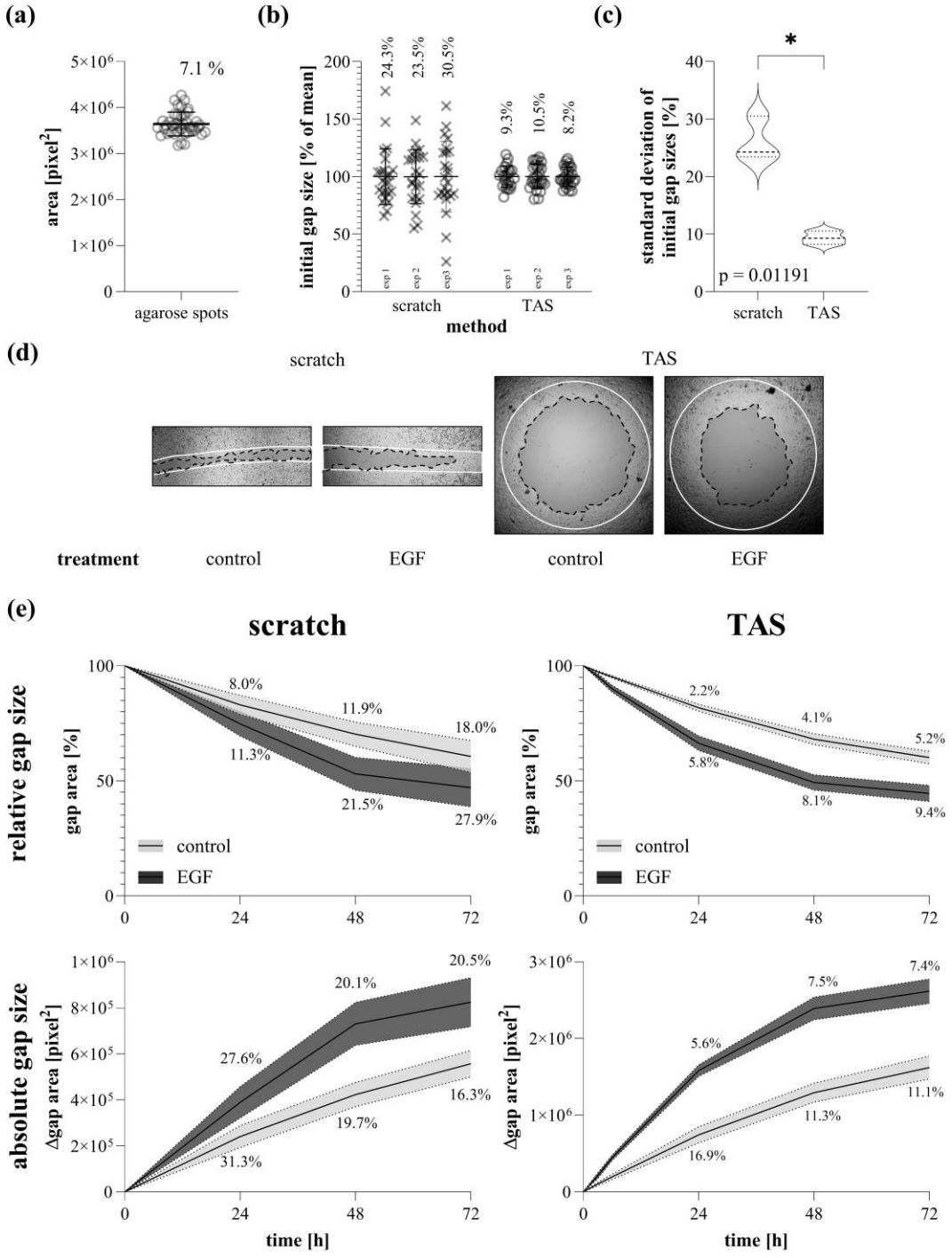

Figure 7: Evaluation of the reproducibility of scratch assay and TAS assay. Reproducibility was compared by measuring the initial gap size and following the gap closure kinetics of control and EGF-treated MRC-5 cells. **(a)** Consistency of agarose spot sizes (n = 40) was determined by graphical analysis. **(b)** Consistency of initial gap sizes was determined in independent experiments (n = 24–30 in each 3-3 experiments). **(c)** The standard deviation of the initial gap sizes of scratch and TAS assays was compared from 3 independent experiments. *p < 0.05 (unpaired t test with Welch's correction) **(d)** Evenness of gap closure was investigated on control and EGF-treated cells, as

demonstrated in representative microscopic images, where lines indicate the gap edges at 0 (white) and 48 (black) hours after gel removal. **(e)** Relative (percentage of initial gap size) and absolute ($\Delta pixel^2$) alterations in gap sizes were followed for 72 hours. Results are presented as mean ± deviation (n = 6). Line widths and percentage values indicate the coefficient of variation of the concerning groups.

4.1.6. Principle and validation of micro plate reader-based data acquisition

Green fluorescent protein (GFP)-expressing HCT-116 cells of TAS assay plates were examined using the well scanning mode of the microplate reader, resulting in an intensity heatmap containing 708 scan points where fluorescence or absorbance values transition sharply from the cell-free to the full-confluent area. Cell-free area was determined as the number of scan point falling below a manually set threshold value (Figure 8a). Optimal threshold was between 10-25% of the maximal intensity values, within which the resulting cell-free areas correlated perfectly with each other (Figure 8b).

To validate the microplate reader-based evaluation, TAS assay plates of GFP- and red fluorescent protein (RFP)-expressing HCT-116 cells were detected with microscopy and microplate reader as well. The acquired gap sizes showed a perfect correlation between the two methods (Figure 8c, d), moreover upon FBS stimulation, a linear dose-response relationship was observable with very high correlation coefficients (Figure 8e).

Absorbance of unstained non-fluorescent cells was scanned in the ultraviolet (UV) range, however cell free area was detectable only after the replacement of medium with PBS. To improve visualization, various colorimetric and fluorescent staining methods were tested for detection with the microplate reader. All stains allowed clear differentiation between cells and cell-free gap area (Figure 8f).

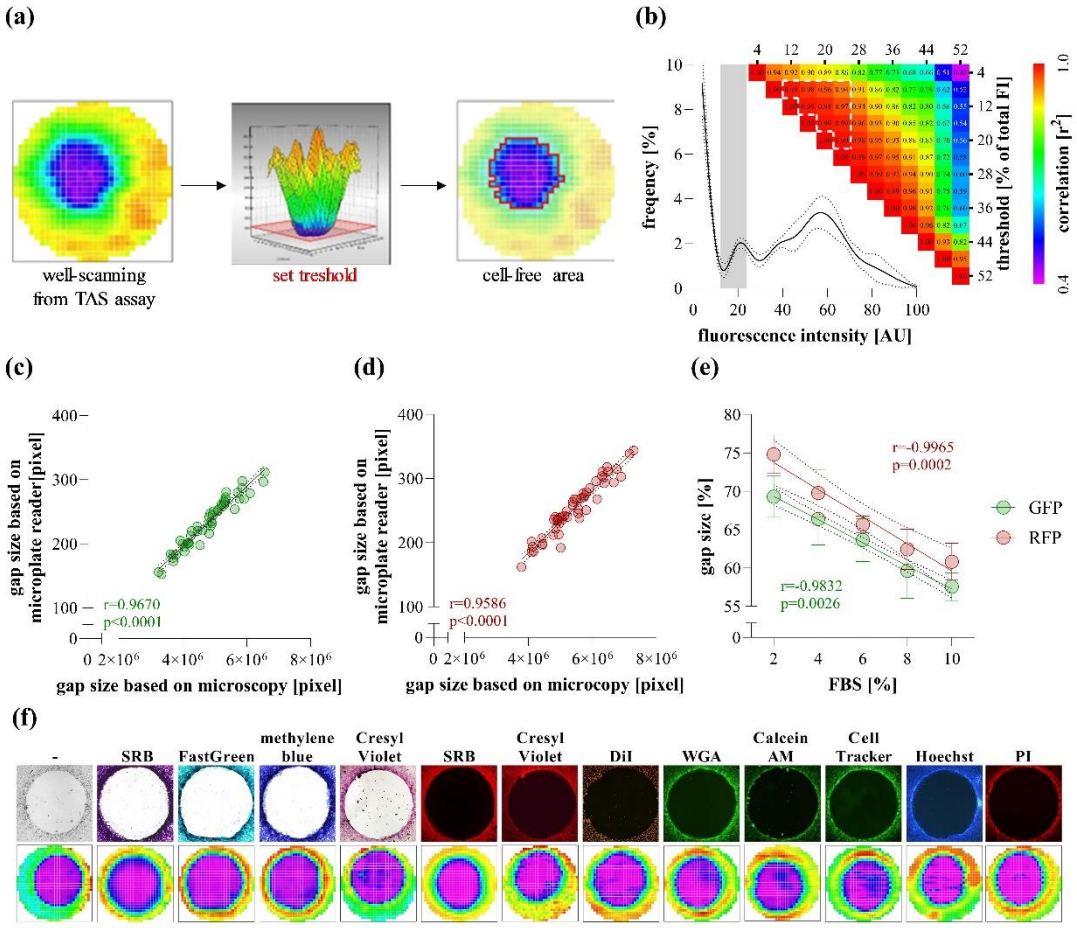

Figure 8: Microplate-reader based evaluation of TAS assay. **(a)** TAS assay wells containing GFP-expressing HCT-116 cells (n = 50) were detected using the well scanning mode of the microplate reader. A threshold value was set manually based on the generated intensity heatmap to determine the cell-free area. **(b)** Cell-free area was selected setting different threshold values based on the intensity distribution of the heatmap pixels and a correlation matrix was generated to establish the optimal threshold (highlighted with white outline). Cell-free areas of TAS assay plates with GFP **(c)** or RFP **(d)** expressing HCT-116 cells (n = 50) were evaluated using microscope and microplate reader as well, the acquired gap sizes were correlated. **(e)** To demonstrate the applicability of microplate reader-based evaluation, cells were stimulated with a dilution series of FBS, and gap closure was investigated after 72 hours (n = 10/group). **(f)** UV absorbance of unstained cells and signal of various colorimetric and fluorescent dyes was detected with microscopy and microplate reader as well. Results are presented as mean ± SD. Significance values (p) and Pearson's correlation coefficients (r) are indicated.

4.1.7. Optimization of Hoechst staining

The applicability of Hoechst DNA staining was verified on RFP- or GFP expressing and non-fluorescent HCT-116 cells. Gap sizes of Hoechst-stained cells determined by microplate-reader showed very high correlation with GFP and RFP signal as well as with the gap size determined by microscopy (Figure 9a).

The compatibility of Hoechst with living cells was tested on A549 and LCLC-103H cell lines. We found that even very low dye concentration resulted in a stable fluorescent signal, meanwhile, although higher concentrations yielded a higher initial intensity, they decreased to a similar value over time (Figure 9b). Fluorescent signal was stably detectable even after 72 hours after a 4-hour staining period with 1:10.000 dilution (Figure 9c). Cytotoxic effects emerged only at high concentrations (1:1000 dilution), especially when the medium was not changed after the staining period (continuous staining) (Figure 9d). After stimulation with FBS dilution series, a dose-dependent acceleration in gap closure was observable with very high correlation coefficient using the microplate reader for detection (Figure 9e).

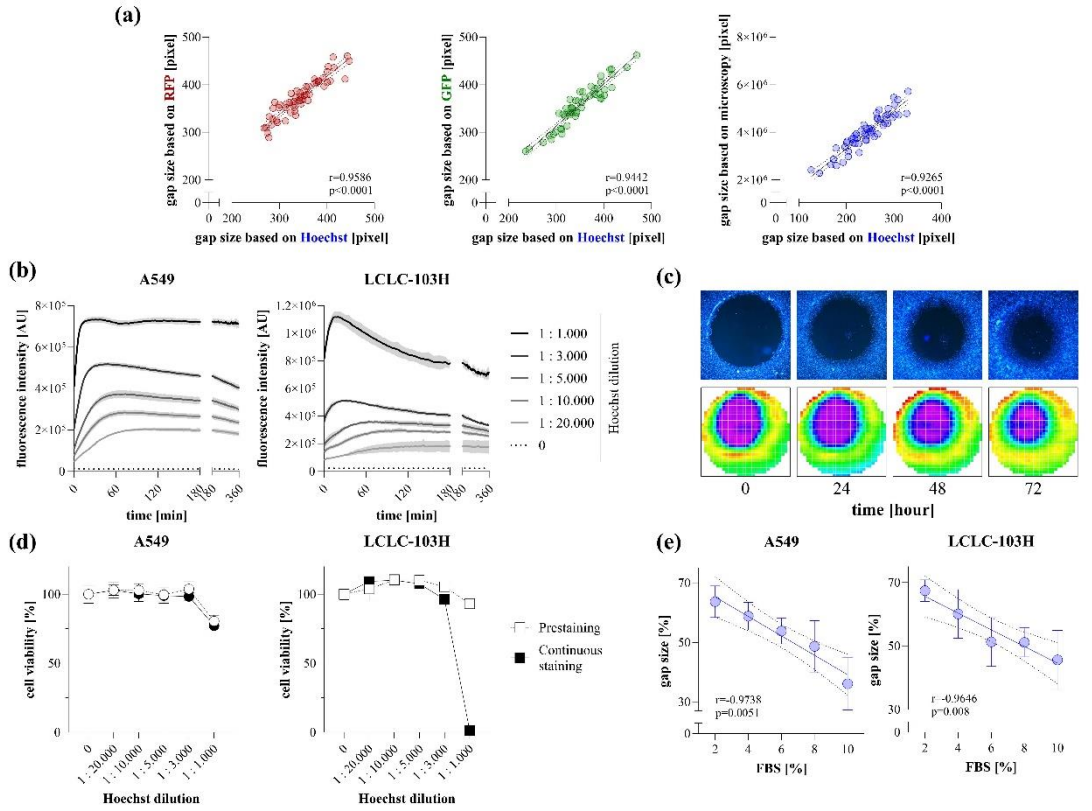

Figure 9: The validation of Hoechst staining. Validation was carried out on GFP- or RFP-expressing and non-fluorescent HCT-116 cells. **(a)** Gap sizes detected based on Hoechst fluorescence intensity were correlated with GFP/RFP signal and microscopy-based evaluation (n=50). Staining kinetics, stability, cytotoxicity, and applicability were investigated on A549 and LCLC-103H cells. **(b)** Staining kinetics with various Hoechst concentrations (n=5/group) were monitored every 2 minutes. **(c)** Stability of the staining was followed for 72 hours both with microscopy (top line) and microplate reader (bottom line). **(d)** Cytotoxicity was assessed with MTT assay at 72 hours following a 4-hour prestaining period or continuous staining. **(e)** To demonstrate the applicability of microplate reader-based evaluation, cells (n=10/group) were stimulated with dilution series of foetal bovine serum (FBS) for 72 hours. Results are presented as mean ± SD. Significance values (p) and Pearson's correlation coefficients (r) are indicated.

4.2. Optimization of Sirius Red assay

4.2.1. Detection of cell-associated collagens by Sirius Red staining

Sections of lung tissue from mice and lung fibroblast cell cultures were stained with Sirius Red according to the standard histological procedure and microscopic images were taken with brightfield and polarized light illumination techniques. On the brightfield images of tissue samples, large collagen positive areas were visible in red colour, which were mostly organised into a complex system of fibres, as the polarized light images revealed. Meanwhile in the adherent cells, collagen positivity was observable mainly in the cytoplasm and thin fibrils produced minimal light scattering only at the cell edges (Figure 10a). In line with these findings, immunostaining of pro-collagen I and collagen I showed predominantly intracellular and perinuclear positivity (Figure 10b).

To investigate the collagen production of cell cultures, unstimulated and TGF-β induced CCD-19Lu lung fibroblasts were grown in 96-well plates, brightfield images were taken (Figure 10c), and collagen amount was measured by Sirius Red assay for cells. The volume exclusion effect of macromolecular crowding on the collagen production was tested by supplementing the culture media with various polymers (dextran, dextran sulphate sodium, polyethylene glycol or Ficoll). While TGF-β increased the production of cell-associated collagens, macromolecules had no effect on the process (Figure 10d).

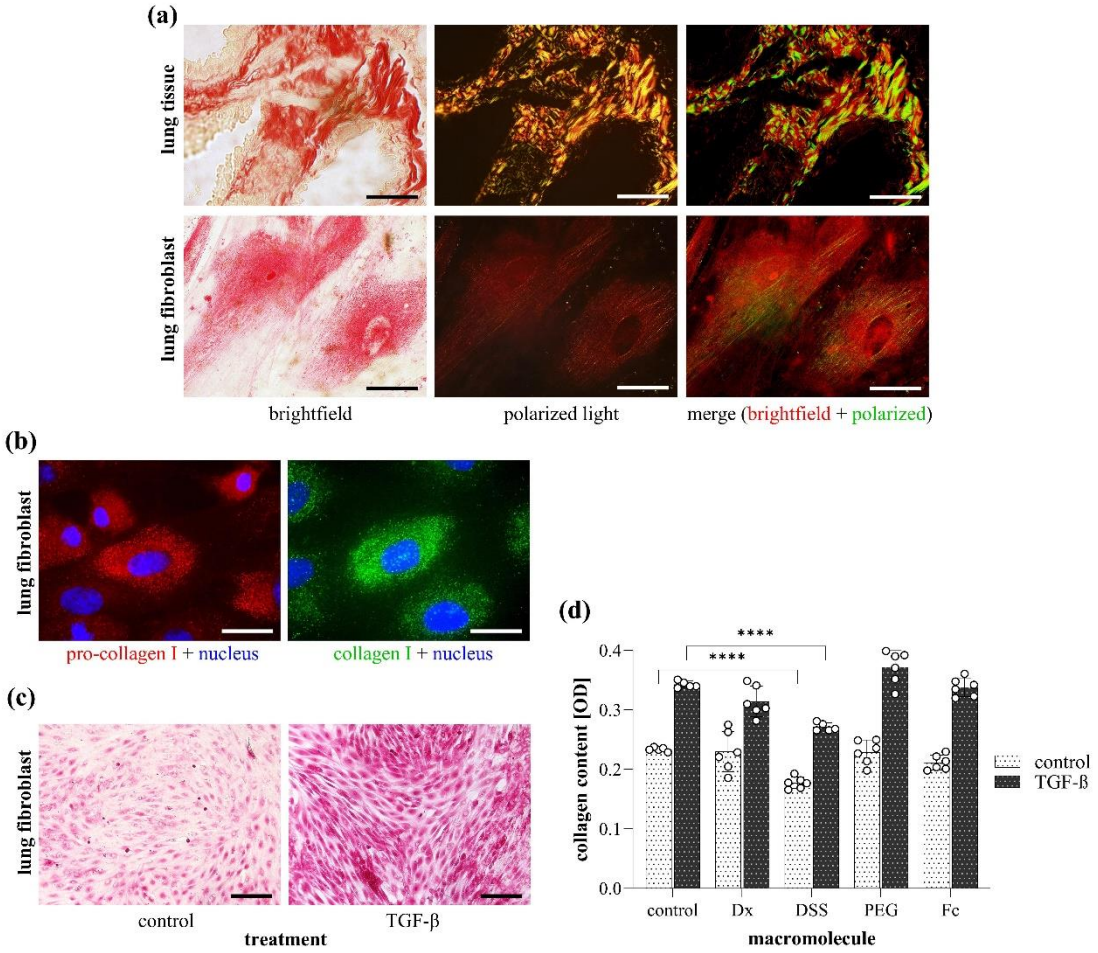

Figure 10: Investigation of cell-associated collagen production on TGF-β treated CCD-19Lu lung fibroblasts. **(a)** Brightfield, polarized light illumination and merged images were taken of fibrotic mouse lung sections and cell cultures stained with Picrosirius. Scale bar: 50 µm. **(b)** Cells were labelled with antibodies against pro-collagen I and collagen I, and fluorescent images were taken. Scale bar: 50 µm. **(c)** Brightfield images of control and TGF-β stimulated cells stained with Sirius Red were taken. Scale bar: 200 µm. **(d)** The volume exclusion effect of macromolecular crowding on the collagen production of TGF-β stimulated cells was investigated by Sirius Red assay for cells adding dextran (Dx), dextran sulphate sodium (DSS), polyethylene glycol (PEG) or Ficoll (Fc) to the culture medium. The amount of cell-associated collagens was determined by the optical density (OD) of their eluates. Results are presented as mean ± SD, dots represent individual values (n = 6). ****p < 0.0001 (two-way ANOVA with Dunnett's test).

4.2.2. Detection of collagens in cell culture medium with Sirius Red staining

To establish the protocol for collagen staining in the supernatant, collagen solutions in different solvents were stained with Sirius Red and dye-collagen precipitates were separated by centrifugation. Microscopic images revealed strong, specific labelling of fibrillary collagens (Figure 11a).

When testing staining solutions with different dye concentrations, whereas a higher dye content resulted in a higher signal intensity, the intra-assay variability multiplied. The background of this phenomenon may be the auto-precipitation and the instability of dye crystals in the supersaturated solution (Figure 11b). Collagen solutions dissolved in DMEM or H_2O were stained with dye solutions containing different acetic acid concentrations to determine the importance of pH. In DMEM, low acid concentrations resulted in a decreased binding capacity of Sirius Red, probably due to the alkaline pH shift caused by buffers present in the medium (Figure 11c).

Performing the staining and washing steps at RT led to reliable and accurate data, however we found that cooling the reagents and incubating the assay at 4°C could further increase the sensitivity if necessary (Figure 11d). Measurements after 15 minutes of incubation revealed strong formation of dye-collagen complexes, which could not be increased with the elongation of the incubation time (Figure 11e). Different plate types were investigated to select the most applicable option for the centrifugation and washing steps, with V-bottom plates giving the best results. Flat-bottom and filter plates did not allow firm attachment of the pellet due to their large surface or bound the precipitates causing a loss of signal intensity (Figure 11f).

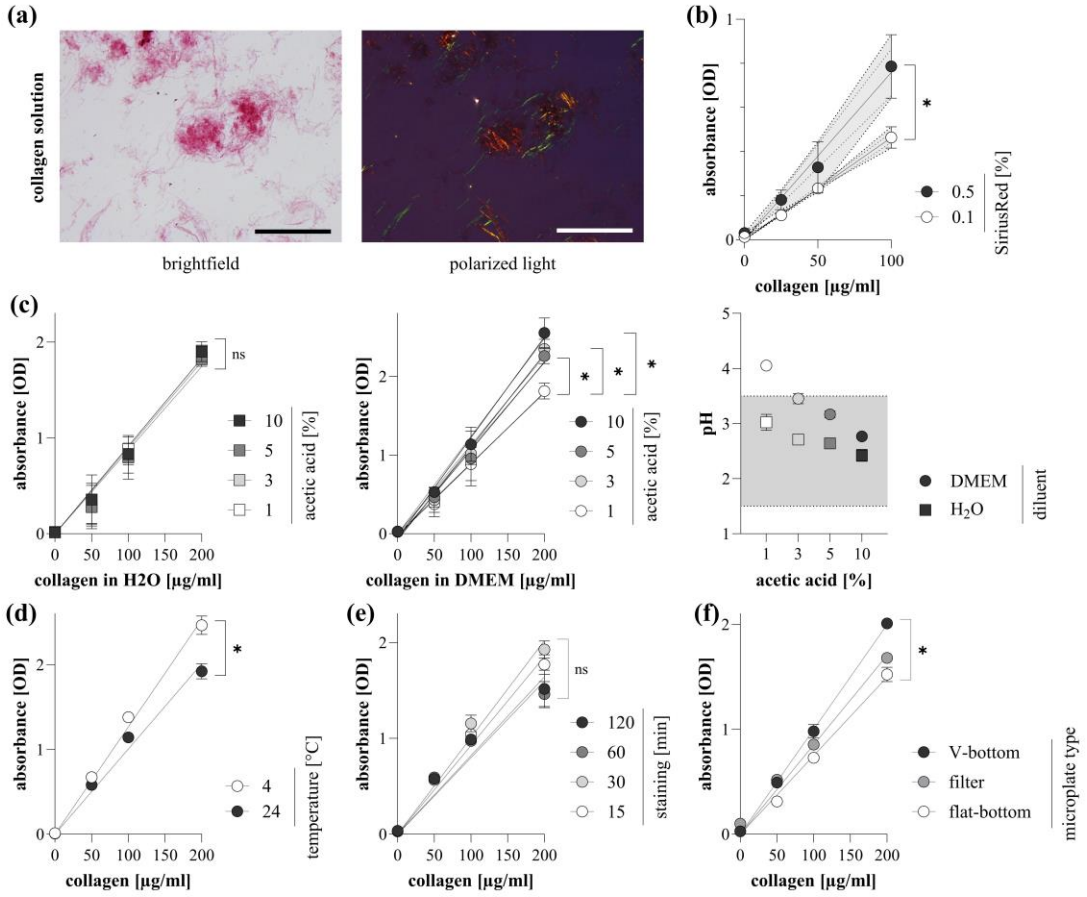

Figure 11: Optimization of the staining conditions for collagen detection in the cell culture medium. **(a)** To visualize collagen-dye precipitates, images of Sirius Red-stained collagen I solution (200 µg/mL in DMEM) were taken with brightfield and polarized light illumination techniques. Scale bar: 200 µm. **(b, c)** The effect of dye- and acetic acid concentrations on the staining efficiency of Sirius Red was investigated on collagen solutions diluted in distilled water (H_2O) or culture medium (DMEM). The pH of the resulting mixtures was determined as well. The grey bar shows the optimal pH range for labelling with Sirius Red based on literary data. **(d, e, f)** Different staining temperatures, incubation times and plate types used for the washing steps were also compared. The labelling efficiency of Sirius Red-stained collagens was determined by the optical density (OD) of their eluates. Results are presented as mean ± SD (n = 6). ns: non-significant, * $p < 0.05$ (linear regression).

To validate the Sirius Red staining procedure of the cell culture medium based on the results detailed above, a wide range of collagen dilution series were stained according to the established setup: samples were incubated in 0.1% Sirius Red solution containing 3% acetic acid for 30 minutes at RT and washed in V-bottom plates. The obtained data confirmed the good quality of our assay characterized by a wide range detection, high sensitivity, and very low intra-and inter-assay variability (< 10%) (Figure 12).

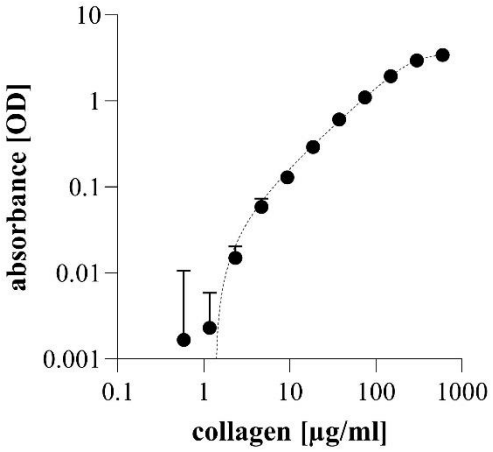

Linearity:	0–300 µg/ml
Limit of detection:	2 µg/ml
Accuracy:	±3.5 µg/ml
Intra-assay variability:	7.7 %
Inter-assay variability:	9.5 %

Figure 12: Validation of the Sirius Red assay for cell culture supernatant. To describe the performance of the established assay, a wide range of collagen I series (0 - 600 µg/mL) was diluted in culture medium (DMEM), incubated with 0.1% Sirius Red in 3% acetic acid for 30 minutes at room temperature and washed in V-bottom plate. The amount of Sirius Red-stained collagens was determined by the optical density (OD) of their eluates. The efficiency of the method was described by determining linearity, sensitivity, and precision. Results are presented as mean ± SD (n = 6). Dashed line indicates the asymmetric sigmoidal 5 parameter logistic curve fitting.

4.2.3. Optimization of in vitro experimental conditions to detect collagen production of fibroblasts

To investigate the effect of FBS concentration on the collagen biosynthesis of CCD19-Lu fibroblasts, cells treated with different FBS concentrations, and their supernatants were stained in parallel with Sirius Red. We experienced that while the FBS supplementation slightly elevated the cell-associated collagen production, an exponential increase in signal intensity occurred in the cell medium samples (Figure 13c). Microscopic images revealed flake-like aggregates of FBS and Sirius Red causing high non-specific signal (Figure 13a, b).

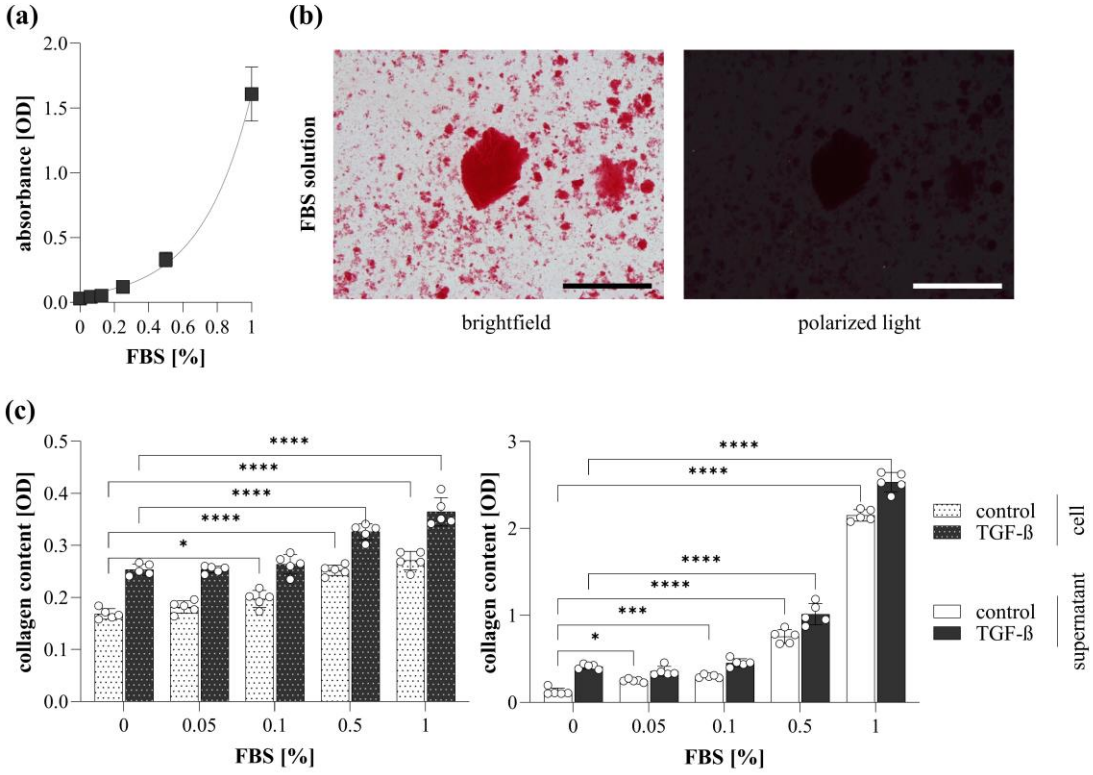

Figure 13: Effect of foetal bovine serum (FBS) on the collagen detection in the culture medium. **(a)** FBS dilution series was prepared in culture medium (DMEM) and stained with Sirius Red to investigate non-specific binding. **(b)** To visualize dye aggregates in 1% FBS solution, brightfield and polarized light illumination images were taken. Scale bar: 200 µm. **(c)** To investigate the effect of different FBS concentrations on the collagen production, TGF-β treated CCD-19Lu cells and their supernatants were stained with Sirius Red. The amount of Sirius Red-stained collagens was determined based on the optical density (OD) of their eluates. Results are presented as mean ± SD, dots represent individual values (n = 5). * $p < 0.05$; *** $p < 0.001$; **** $p < 0.0001$ (two-way ANOVA with Dunnett's test).

The effect of ascorbate, an essential cofactor of collagen biosynthesis was investigated as well. Ascorbate did not form aggregates with Sirius Red, the precipitates separated from the culture medium showed light scattering parts under polarized light illumination (Figure 14a, b). Addition of ascorbate to the culture medium elevated the level of both cell-associated and soluble collagens in a dose-dependent manner (Figure 14c).

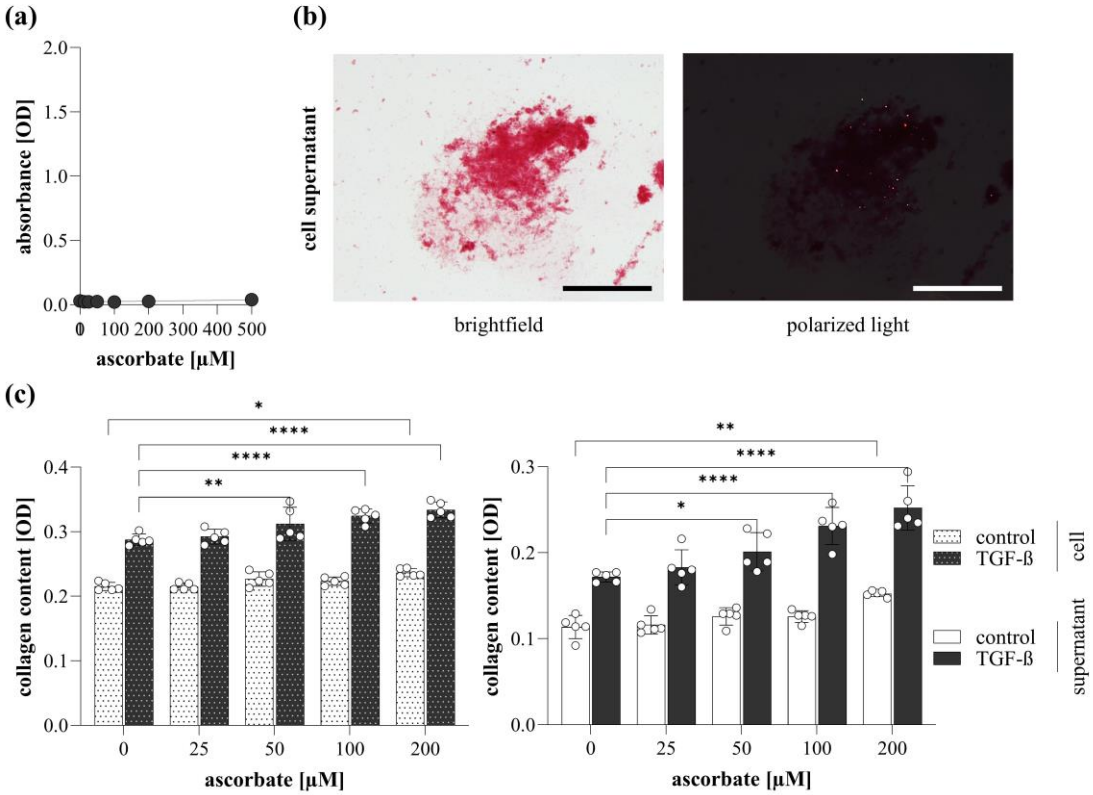

Figure 14: Effect of ascorbate on the collagen detection in the culture medium. **(a)** Ascorbate dilution series was prepared in culture medium (DMEM) and stained with Sirius Red to investigate non-specific binding. **(b)** To visualize dye aggregates in a culture medium (200 µm ascorbate, TGF-β treatment), brightfield and polarized light illumination images were taken. Scale bar: 200 µm. **(c)** To investigate the effect of different ascorbate concentrations on the collagen production, TGF-β treated CCD-19Lu cells and their supernatants were stained with Sirius Red. The amount of Sirius Red-stained collagens was determined based on the optical density (OD) of their eluates. Results are presented as mean ± SD, dots represent individual values (n = 5). * $p < 0.05$; ** $p < 0.01$; **** $p < 0.0001$ (two-way ANOVA with Dunnett's test).

4.3. Representative in vitro measurements to investigate the effect of kinase inhibitors on cell proliferation, migration and collagen production

The effect of the antifibrotic agent nintedanib was investigated on CCD-19Lu lung fibroblast cells, while the anticancer compounds sorafenib and gefitinib were tested using A549 lung carcinoma epithelial cells. MTT and LDH assays were performed to investigate cell proliferation and the cytotoxic effect of the compounds. The cells and their supernatants were stained with Sirius Red to determine collagen production. TAS assay was carried out to assess changes in migratory capacity, represented as the rate of gap closure 72 hours after treatment using the following equation: gap closure [%] = 100 – [(initial gap size – actual gap size) / initial gap size×100].

Nintedanib decreased proliferation, cell-attached and soluble collagen production, and fibroblast migration in a dose-dependent manner without inducing cell death (Figure 15a-c). Sorafenib decreased proliferation, collagen levels and cell migration as well, however, the highest applied concentration appeared to be cytotoxic. This may be the reason behind the increased collagen content in the supernatant of the group treated with 10 μM, since the collagen content of the detached cells has been labelled too (Figure 15d-f). Gefitinib ameliorated proliferation only at the highest concentration and its inhibitory effect on collagen production reached the level of significance only in case of cell-associated collagens, however, it also inhibited cell migration in a dose-dependent manner (Figure 15g-i).

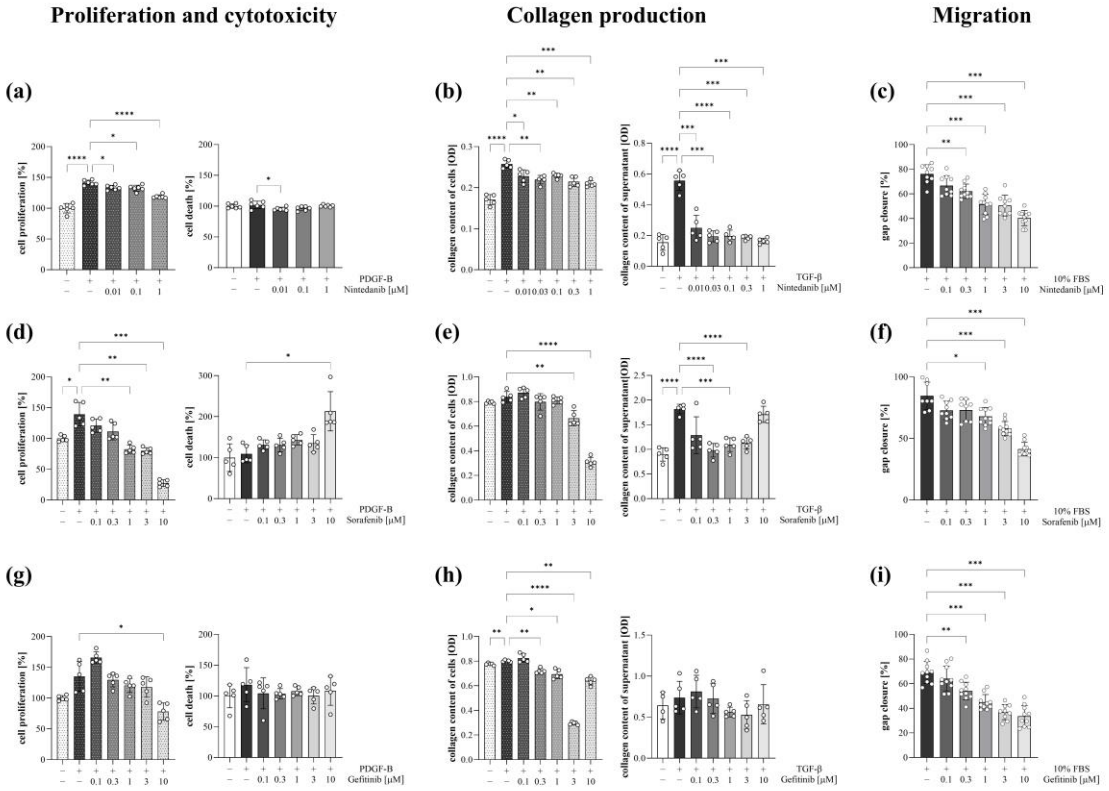

Figure 15: Effect of kinase inhibitors on the proliferation, cell death, collagen production and migration of fibroblasts and cancer cells. The effect of nintedanib **(a-c)** was tested using CCD19-Lu lung fibroblasts. The effect of sorafenib **(d-f)** and gefitinib **(g-i)** was investigated on A549 lung cancer epithelial cells. **(a, d, g)** Cell proliferation and cytotoxicity were measured via MTT and LDH assay (n=5). **(b, e, h)** Cell-associated and soluble collagen amounts were determined with Sirius Red assay for cells or supernatant based on the optical density (OD) of their eluates (n=5). Dots represent individual values. **(c, f, i)** Cell migration was investigated on Hoechst-stained cells for 72 hours via microplate reader-based quantification (n=10). Results are presented as mean ± SD. * $p < 0.05$; ** $p < 0.01$; *** $p < 0.001$; **** $p < 0.0001$ (Brown–Forsythe and Welch ANOVA with Dunnett's T3 test).

5. Discussion

Collective migration, proliferation and collagen production are the three main functions of fibroblast cells that can be examined separately, all of them being important phenotypic characteristics of cancer cells as well (Figure 16). Having a reliable system to investigate fibroblast and cancer cell functions and their pathological changes – using methods with low compound- and cell requirements, preferably compatible with 96-well plates – is a crucial step towards the development and efficient sorting of potential therapeutics against fibrotic and malignant diseases.

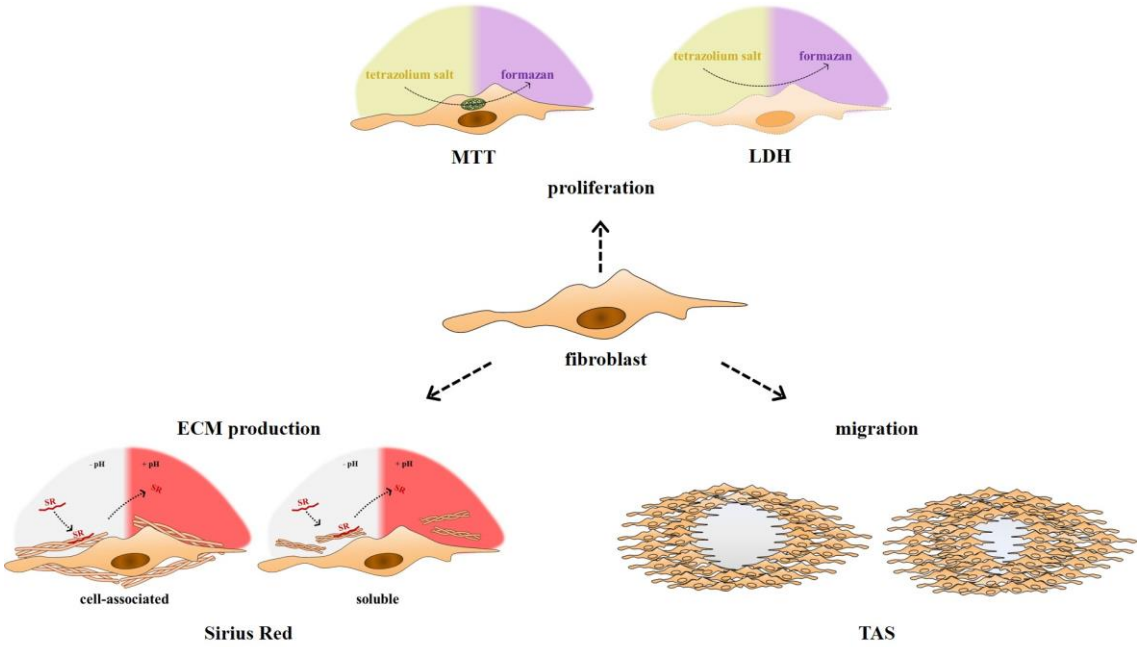

Figure 16: In vitro assays used to test the main functional characteristics of fibroblasts and cancer cells.

Assays using various principles are available to measure the rate of cell proliferation, including ATP production, enzyme activity, DNA synthesis or membrane permeability (59). In our experiments, MTT and LDH assays were applied to determine changes in cell proliferation, reduced apoptosis and possible cytotoxicity. MTT assay is a colorimetric assay based on the mitochondrial dehydrogenase activity of viable cells, which converts the substrate thiazolil tetrazolium into purple coloured formazan end-product trapped inside the cells. After being eluted at the end of the assay, the measured absorbance of formazan is proportionate with the number of viable cells (60). LDH assay is performed from the supernatant of the same sample (61). The parallel determination of cell proliferation and cell death is crucial to ensure that the decreased proliferation rate is

not due to cytotoxicity caused by the inhibition of main metabolic pathways. Moreover, it can detect decreased apoptotic activity, an important trait of activated fibroblasts and cancer cells (29, 62). We optimized the assay conditions to create a standardized 96-well plate based system where cells can be induced by various growth factors relevant in the examined disease model. In the representative measurements, recombinant human PDGF, a common growth factor in fibrosis and certain types of cancer was used as an inductor of proliferation. Since cell proliferation is the outcome of the interactions between a chain of signalling molecules, the effectiveness of specific receptor inhibitors and general kinase inhibitors, as well as the modulators of the downstream elements can be tested with a single, straightforward assay (42).

The most common method to assess collective migration is scratch assay that investigates migration on a confluent layer of adherent cells plated in 6- or 12-well plates, where a cell-free gap area is generated by scratching the surface with a pipette tip and gap closure is followed subsequently by graphical analysis (63). Although the assay's low cost and simplicity justify its widespread use, it comes with considerable disadvantages, starting at the high material and reagent requirement that limit throughput. Besides the influence of physical damage to the cells and surface caused by the scratching itself, the resulting gap area is uneven, leading to a high intra- and inter-assay variability (64, 65). Moreover, due to the large well size, the gap area cannot be photographed in a single field of view. To overcome these limits, our group developed an alternative, named Transient Agarose Spot (TAS) assay. As a first step, droplets of heated agarose solution were placed in the middle each well on a 96-well plate and left to polymerize. Agarose is a widely used non-toxic, biocompatible material without immunogenic properties (66). Subsequently, cells were seeded around the droplet and incubated until adhering and reaching near-full confluence. The agarose drops remained stable for several days, inhibited under-agarose cell migration and allowed cell treatment and medium exchange (Figure 3a, b).Thereafter, the agarose droplet could easily be removed by pipette tip without harming the cells or the surface, leaving a cell-free area where cells were able to migrate. The migration kinetics was followed by graphical analysis of microscopic images taken at certain time points after treatment (Figure 17).

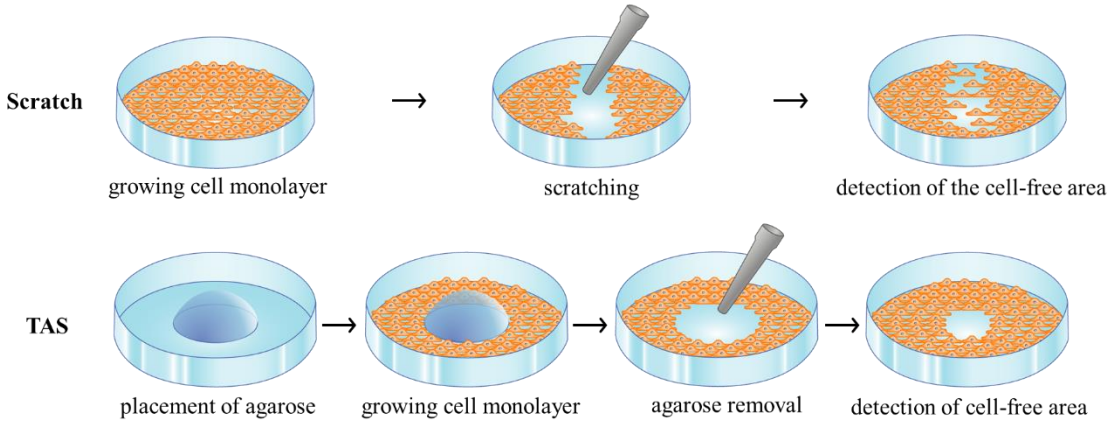

Figure 17: Comparison of the execution of Scratch and Transient Agarose Spot (TAS) collective cell migration assays.

Initially, we investigated the influence of cell density on the rate of gap closure. The effect of this factor was clear and growing cells to a near-full confluence proved to be optimal for migration without formation of overlapping cell layers that could interfere with the evaluation (Figure 3c, d). Our finding is further supported by studies showing that collective migration requires the maintenance of cell-cell cohesions (67, 68). Increasing the concentration of FBS in the culture medium elevated the gap closure rate in a dose-dependent manner (Figure 4a, c, e; Figure 5a-c) due to the presence of growth factors, and chemoattractants known to facilitate cell migration (69, 70). Moreover, the nutrient content increases metabolic activity, which elevates the proliferation rate through autocrine signalling leading to the prolonged activation of receptor tyrosine kinases that further promotes migration (71). By the addition of growth factors like EGF (Figure 4b, d, f; Figure 5d-f), the effect of inductor signals may be examined more specifically. We performed the TAS assay on various fibroblast, epithelial and cancer cell lines, which taken together with the independence from inductor signals highlights its diverse applicability in processes where cell migration is of importance (Figure 4; Figure 5), like wound healing or cancer progression.

In the first version of TAS assay, the cell-free area was detected by microscopy and brightfield images were annotated manually using ImageJ software to measure the gap size, which is easy to use even without previous experience. Nevertheless, the evaluation process is monotonous and labour-intensive, therefore different approaches were tested to replace manual annotation with computer mouse. While digitizer board (without screen) and tablet (with screen) accelerated the evaluation only slightly,

automatic annotation with the help of macros described in the method section shortened evaluation time per image by magnitudes (Figure 6c). It should be noted that macro parameters need to be adjusted previously for the accurate detection of gap edges. Certain cell types, like MRC-5 lung fibroblasts were recognized perfectly by the software, however in case of some more flattened cell types, for example NRK-49F kidney fibroblasts, the program could not identify the cell edges accurately (Figure 6a). Therefore, out of various non-toxic dyes tested to enhance the contrast between the cells and the cell-free area, the lipophilic membrane staining DiI was applied in our experimental setup for a stable fluorescent signal. With slight adjustments in the macros, this allowed the accurate recognition of gap edges (Figure 6b). Similar software were developed to shorten the evaluation time of scratch assay as well that were able to approximate the precision of manual annotation. One example is the TScracth program that operates as a MATLAB graphical user interface, however it has not been updated recently (72). Another approach, the free Automatic Invasiveness Measure (AIM) software determines the cell-free area based on the local entropy of the images (73). Although these tools provide clear advantages in terms of assay evaluation, they could not overcome a number of drawbacks originating from the technique.

Next, we compared the performance of TAS assay with the current gold standard scratch assay using EGF-stimulated MRC-5 cells. An immediate advantage of TAS assay appeared while photographing the gaps. Compared to scratch assay that required multiple images to cover the elongated wound and the identification of the same area needed extra precautions (74), the circular gap of TAS assay could fit in a single field of view, which would allow automated documentation (Figure 7c). The standard deviation of the initial gap sizes in TAS assay was one third of scratch assay in accordance with the literature (Figure 7b, c) (75). Considering that this might lead to an even higher deviation further along the assay, it limits the applicability of scratch assay. The gap closure rate was similar in the two assays, however TAS assay provided a higher resolution due to the lower standard deviation. To avoid bias originating from normalization to the inconsistent initial gap sizes, the absolute areas were also determined as $pixel^2$ and compared, which resulted in the same intra-assay variability, in favour of TAS assay (Figure 7d). As a result of the low intra-assay variability, TAS assay is able to detect differences in the migration kinetics as early as 3 hours after treatment.

It is important to note that TAS assay is different from under-agarose migration assay, an experimental setup designed to investigate single cell migration of spermatocytes and leukocytes driven by chemoattractant gradient (76, 77). While in TAS assay the agarose drop's function is to block migration, during the under-agarose method, the permanent agarose layer serves as a reservoir for the applied treatments, and the outcome is determined by the number of cells migrated under the agarose.

In summary, TAS assay stands as an improved alternative to scratch assay that maintained the favourable properties, meanwhile eliminating most of the disadvantages (Table 4).

Table 4: Comparison of the advantages of scratch assay and TAS assay

Assay characteristics	Scratch Assay	TAS Assay
Cost-effective	+	+
Minimal equipment	+	+
Easy to perform	+	+
Consistent gap size	-	+
Well reproducible	-	+
Easy gap relocation during repetitive imaging	-	+
Intact cells and plate surface	-	+
Small surface and volumes (96-well based)	-	+
Low intra- and inter-assay variation	-	+
Automatable	-	+

However, the microscopy-based detection and the evaluation steps still require human resources and special adjustments, thereby limiting the assay throughput and efficiency that significantly confines the possibility of industrial utilization (65).

Therefore, we aimed to automate data acquisition and analysis by transferring them into a microplate-reader to decrease assay time and elevate throughput. New-generation microplate readers like the devices produced by BMG LABTECH (Ortenberg, Germany), Tecan (Männedorf, Switzerland), and Molecular Devices (San Jose, CA, USA) feature well-scanning mode, a function designed to perform multiple measurements in a single well for the detection of cell-based assays with non-

homogenous cell distribution, where a single central measurement would not be representative of the whole area.

We have been using the CLARIOstar Plus microplate reader (BMG LABTECH, Ortenberg, Germany) combined with MARS software to detect 30×30 scan points in a circular area with 4 mm diameter in the middle of each well of a 96-well plate. Subsequently, the software generated a heatmap based on the absorbance or fluorescence intensity values. In the region of interest, we could clearly distinguish a high and a low (near-blank) intensity group of scan points that corresponded well to the cell-rich and cell-free areas allowing accurate threshold selection (Figure 8a, b).

Red (RFP) and green (GFP) fluorescent protein expressing colon cancer cells were utilised to validate the microplate reader-based detection. The gap sizes of the same samples determined by graphical analysis based on microscopic images or by the microplate reader showed a very high correlation. The dose-dependent migration enhancing effect of FBS was detectable as well (Figure 8c-e). While fluorophore expressing cell lines are practical when one type of pathology is investigated, their availability is limited. The intrinsic UV absorbance of cells at a specific wavelength could serve as an alternative, since it was detectable, nevertheless, it required the replacement of culture media with PBS to avoid false positive signal derived from certain components (e.g. phenol red, FBS) (78). Therefore, various absorbance based and fluorescent dyes with different staining principles were tested, all of them being suitable for microplate reader-based detection (Figure 8f).

Considering several aspects, the DNA stain Hoechst proved to be highly compatible with the experimental setup of TAS assay. Hoechst is a cost-effective, non-toxic cell-permeable dye that is suitable for the long-term labelling of viable cells even at low concentrations due to its slow elimination (Figure 9b, d) (79). Furthermore, the dye gains increased fluorescence intensity upon binding to the minor groove of double stranded DNA, which further ensures an optimal signal-to-noise ratio throughout the whole experiment (Figure 9c) (80) compared to esterase-dependent dyes for example, where leaking dye molecules increase background signal over time (81). Another advantage of Hoechst is that unlike colorimetric methods or the fluorescent DNA stain propidium iodide, its application does not require cell fixation, which would convert the assay into an end-point measurement as opposed to kinetic assay with multiple measuring

points (79). Membrane dyes may be used instead of Hoechst, as demonstrated at the automated graphical analysis (Figure 6a), however, besides higher costs, hydrophobic lipid dyes are more difficult to handle in water-based cell culture media (82). Taken together, Hoechst proved to be suitable for the microplate reader-based detection and evaluation of cancer cell migration, providing similar results to fluorophore expressing cells (Figure 9a, e). At the same time, we would like to draw attention to the fact that Hoechst interacts with drug transporters, e.g. several ATP binding cassette (ABC) transporters, which are known to be responsible for multidrug resistance in cancer cells (83, 84). Therefore, in experimental setups, where this might be a concern, it is advisable to review platforms, like DrugBank for common pathways, perform transporter-binding assays or conduct experiments with the examined compound in the presence and absence of Hoechst to exclude possible interference. As the results of the original TAS assay confirm (Figure 6), in case of disturbance, membrane dyes like DiI can be an efficient alternative. The investigated stains can be applied on different cell types, however, the dye uptake kinetics and the intensity might show individual variations hence we advise to perform optimization steps similar to the workflow described in section *4.1.7 Optimization of Hoechst staining* before the experiments.

To complete the assay pool for the investigation of fibroblast functions in vitro, a reliable near high-throughput collagen detection method was needed. The collagen superfamily consists of at least 28 genetically distinct members (85), the specific detection of which is possible for example via polymerase chain reaction, Western blot, immunocytochemistry, or enzyme-linked immunosorbent assay, nevertheless these methods are usually time consuming, expensive and/or low-throughput. Moreover, the quantification of total collagens may provide more information about the phenotypic outcome of a disease. Currently, few commercial assay kits are available for total collagen detection, two of which, the Sircol Collagen Assay (Biocolor, Carrickfergus, UK) and the Sirius Red Total Collagen Detection Assay Kit (Chondrex, Woodinville, WA, USA) are Sirius Red-based. Besides the high costs, the relatively low number of samples that can be processed with one kit and the unsolved issue of serum components interfering with the assay due to unspecific binding, other disadvantages include narrow detection range and extra acidic or enzymatic lysing steps, which elongate assay time (86, 87).

For the optimization of total collagen quantification in vitro, we chose to investigate Sirius Red staining. The Picrosirius staining method that traditionally combines Sirius Red and picric acid has a long history in histology, starting as a potential staining for amyloid plaques, but being mostly utilised later for collagen labelling (88, 89). The elongated dye molecule has four anionic azo groups under acidic conditions that form ionic bonds with the cationic amino acid residues of collagen, allowing the dye to associate along the triple helix. This enables Sirius Red to bind to water-soluble and insoluble collagen forms as well, verified in various mature and pro-collagen types (fibrillary I, II, III, V or network forming IV) (89-91). Upon microscopic observation, thick fibres of collagens I and III show increased birefringence under polarized light when stained with Sirius Red due to the highly organized crystalline-like structure (92). In addition to tissue samples, collagen can be visualized in adherent cell cultures as well, as seen in Figure 10.

Sirius Red-stained slides are usually evaluated by experienced pathologist based on a scoring system, however, the staining method is not only suitable for visualization (93, 94). Taking advantage of the dye's chemical properties, after removing the unbound dye from the system, the bound molecules can be eluted with alkaline solution to quantify collagen amount based on optical density (95). This approach of labelling fixed cells and releasing the dye offers a simpler and less time-consuming solution compared to the above-mentioned kits that require sample digestion.

Upon treatment with the profibrotic TGF-β, fibroblasts have shown more intense labelling (Figure 10c), however, even after 7 days of culturing, there was no significant fibre alignment, as it is visible on the microscopic images (Figure 10a). Supporting these findings, immunostaining showed mainly intracellular and perinuclear localization of pro-collagen I and collagen I (Figure 10b). Collagen biosynthesis is a complex process including several intra- and extracellular steps, in the course of which the singular collagen strands go through various post-translational modifications and form triple helical procollagen molecules that are transported to the extracellular space in a soluble form. The maturation involves the cleavage of terminal peptides, after which the resulting insoluble tropocollagens align in a quarter-staggered structure and crosslinks are formed (58, 96). The presence of ECM elements, like fibronectins and integrins is crucial in the maturation and organization of the final reticular or fibrillary structure (97). Therefore,

the development of in vitro models to investigate collagen biosynthesis and maturation is challenging, because due to lack of tissue environment, cell-attached collagen fibres fail to form, leaving high amount of soluble precursors in the supernatant that are usually discarded at the beginning of the assays (14, 98). To simulate the in vivo tissue environment, the culture medium was supplemented in previous studies with macromolecules for their volume exclusion effect (99, 100). The reduction of the available aqueous environment facilitates the optimal alignment of collagen precursors and enzymes to perform the modifications required for collagen maturation (101, 102). However, these studies lasted for several weeks to reach a significant elevation in the level of cell-attached collagens (101). In line with these findings, in our experiments, after the addition of dextran, polyethylene glycol or Ficoll and culturing for 7 days, we could not detect increased collagen deposition (Figure 10d).

Since assay time is an important feature in high-throughput drug development, instead of extending the duration of the assay, we optimized the detection of soluble precursors in the cell supernatant. After mixing with the staining solution, the precipitates of soluble collagens and Sirius Red dye (Figure 11a) can be pelleted down by centrifugation, allowing the removal of the excess dye with acidic wash solution. Subsequently, the bound dye can be eluted to measure the optical density.

First, we examined the effect of staining environment on Sirius Red binding using collagen solution. The dye showed strong, stable signal at the concentration described in the original protocol used in the literature for histological staining (Figure 11b) (89). The elevation of acetic acid concentration in the staining solution from 1% to 3% improved the signal intensity. This may be due to the pH shift caused by the buffer capacity of the cell culture medium (Figure 11c) (89). As mentioned above, acidity is important in the formation of ionic groups necessary for dye binding (95). It has been shown previously that lowering the temperature of the reagents and transferring the incubation to 4°C could increase binding capacity (103). Similarly, we experienced higher sensitivity compared to performing the assay at room temperature, which may be useful at samples with low collagen concentration (Figure 11d). Meanwhile, the lower temperature did not cause any technical difficulties. We investigated the effect of incubation time as well, where stable signal was reached at 15 minutes and did not improve with further incubation (Figure 11e). Studies suggest that longer incubation time in fixed tissue samples is required due

to the slow dye diffusion between the tightly packed collagen fibres (89, 104). As the in vitro assays were performed in 96-well plate, we tested different types of plates to perform multiple staining and washing steps on the cell supernatant. The transparent V-bottom plate proved to be the most suitable due to its small bottom surface that allowed firm attachment of the collagen-dye precipitates (Figure 11f). When testing the performance of the optimized staining process, we found that the efficacy and sensitivity were similar to the commercially available assay kits (Figure 12).

As a next step, we aimed to adjust the conditions of the in vitro experiments to determine the total collagen production of fibroblast cells. Collagen production is mostly investigated on prolonged or hyper-confluent fibroblast cultures stimulated by TGF-β treatment (100). Therefore, in our experiments, fibroblasts were cultured in medium containing high amount FBS to facilitate proliferation due to its nutrient and growth factor content (71). Nevertheless, FBS is rich in albumin that is known to have multiple basic amino acid residues with high non-specific binding ability towards various macromolecules including Sirius Red, which was well supported by our findings on FBS containing medium stained with Sirius Red (Figure 13a-b) (86, 95). Based on our findings, FBS supplementation only had a moderate effect on the amount of cell-attached collagen production of TGF-β stimulated fibroblasts, meanwhile masking the specific signal of soluble collagens completely in the supernatant (Figure 13c). Moreover, previous studies achieved to increase collagen production in highly confluent fibroblast cultures under serum deprivation (105, 106). Taken together, we recommend the application of FBS-free media during cell treatment for the accurate determination of collagen content in both cells and their supernatant.

Lastly, the effect of ascorbic acid (ascorbate, vitamin C) supplementation was investigated. Ascorbate is a well-known cofactor of prolyl and lysyl hydroxylase enzymes that perform post-translational modifications crucial for triple helix formation (107). It was shown to stabilize the collagen mRNA, thereby increasing collagen production on the transcriptional level as well (108, 109). The significance of ascorbate is further highlighted by the symptoms of scurvy, the nutritional deficiency of ascorbate, where a systemic weakening and abnormality of connective tissue is observable (110). The addition of ascorbate to the culture media increased collagen production in a dose-dependent manner without the formation of non-specific aggregates (Figure 14).

Therefore, we recommend supplementation with 200 μM ascorbate in the culture media for the in vitro experiments.

To demonstrate the applicability of the screening system for the investigation of cell proliferation, cytotoxicity, collagen production and migration, we performed representative measurements on fibroblast and cancer cells. The effect of three kinase inhibitor compounds with different targets was tested. Nintedanib exhibited dose-dependent inhibitory effect on all the examined functions of lung fibroblasts due to its diverse targets (Figure 15a-c). The general inhibition of fibroblast activity by nintedanib has been reported in numerous fibrosis- (111, 112) and cancer-related (113, 114) studies. Sorafenib acts as a multikinase inhibitor as well, which is reflected in our results. In accordance with the literary data obtained using various cancer cell types including A549 (115-117), the compound decreased proliferation and migration (Figure 15d, f). The A549 lung adenocarcinoma epithelial cell line was shown to expresses different collagen isoforms (118, 119), therefore, we investigated the effect of sorafenib on collagen levels and experienced decreased secretion (Figure 15e). In contrast with the preceding compounds, gefitinib acts predominantly as an EGFR inhibitor. While it's being used to inhibit the migration and proliferation of cancer cells in vitro (120, 121), its single molecular target might explain the limited effect observed in our experiments.

6. Conclusions

Despite the increasing number of patients affected by fibrosis or cancer, numerous difficulties arise regarding their effective long-term treatment, therefore, there is a constant demand for new therapeutic options. Fibroblasts and cancer cells have similar functional characteristics, namely proliferation, migration and the production of extracellular matrix proteins, like collagen. Monitoring these cellular functions simultaneously enables us to assess the effect of novel potential antifibrotic and anticancer compounds in a manner that meets the advantages of phenotypic drug discovery.

The near-high throughput in vitro screening system built by our research group is optimized for 96-well plates, thereby allowing the examination of multiple compounds utilizing low amounts of cells and compounds. The assays were designed to require relatively short time and minimal manual work, as well as low material requirements, maintaining high reproducibility, linearity and low intra- and inter-assay variability. Their simplicity, cost-effectiveness and reliability make them available not only for a wide range of research laboratories, but they might also meet the requirements of industrial circumstances.

In conclusion, we obtained the following findings regarding the main objectives:

1) The execution of the agarose placement and removal during TAS assay on a 96-well plate did not damage the surface or the cells, therefore it did not interfere with the subsequent cell migration, ensuring thereby that the evaluation of factors influencing the migration rate remained unbiased.

2) The thorough and systematic comparison of the TAS assay to the current gold standard scratch assay prove that TAS assay was a considerable alternative in many aspects including a low variability in gap size leading to recognition of changes in migration at earlier time points.

3) Transferring the detection and evaluation in a new generation microplate reader for automation resulted in a significant decrease of assay time and manual work, maintaining the performance meanwhile.

4) The selection of the most suitable labelling technique and the optimization of Hoechst staining showed not only the applicability of Hoechst in a wide range of cell

types and experimental setups, but it also presented a systematic method that may help the development of other staining protocols.

5) The optimization of Sirius Red staining for the detection of total collagen production in vitro resulted in a time-efficient protocol that could assess the cell-attached and soluble forms of collagen in parallel, overcoming the difficulties of modelling collagen biosynthesis in vitro and providing more information about the changes in collagen production.

6) Along the assessment of the major influencing factors, the elimination of fetal bovine serum from the cell culture before the experiments could prevent the high false positive signal due to nonspecific binding, while during the adjustment of the experimental conditions, the addition of ascorbic acid increased collagen production.

7. Summary

Fibrotic processes become activated in several acute tissue injuries and chronic diseases, resulting in organ failure over time and contributing significantly to death cases worldwide. Similarly, cancer is another leading cause of mortality in most developed regions. Moreover, fibroblast and cancer cells share similar functional characteristics of proliferation, collective migration and production of extracellular matrix elements. In order to alleviate the medical burden imposed by these diseases, we aimed to develop an efficient screening system for the investigation of new therapeutic options.

Following induction with different growth factors playing central role in fibrosis and cancer progression, the effect of kinase inhibitors on proliferation, a crucial phenomenon in the course of these diseases was examined with the well-known enzyme activity-based MTT assay with optimized conditions for our experimental setup. To distinguish between proliferation inhibition and cytotoxicity, it was paired with LDH test.

To overcome the disadvantages of the current gold standard assay for collective cell migration, the scratch assay, we developed a novel migration test called TAS assay. Instead of creating gap in an already formed monolayer of cells, TAS assay applies agarose spot as a removable physical barrier prior to cell seeding to avoid the modifying effect of physical damage on cell migration and ensure a uniform, small, easily traceable initial gap, resulting in a cost-effective, precise migration assay. The implementation of cell staining even allowed the transfer of the detection and evaluation into a microplate reader, resulting in a highly automated test and a significant shortening of assay time.

Finally, to address the challenges of modelling and measuring collagen production in vitro, we established a Sirius Red collagen stain-based assay. Since the non-polymerized soluble collagens in the supernatant represent an important fraction of total collagens and are usually discarded, the aim was to optimize the staining procedure for their labelling as well. Furthermore, the cell culture conditions were also adjusted to minimize the effect of interfering factors and achieve maximal collagen production.

The resulting near-high throughput in vitro screening system consists of cost-effective, simple, relatively fast assays that enable the simultaneous measurement of the main fibroblast and cancer cell functions to obtain comprehensive understanding about the effect of the tested compounds.

8. References

1. Marinova M, Solopov P, Dimitropoulou C, Colunga Biancatelli RM, Catravas JD. Acute exposure of mice to hydrochloric acid leads to the development of chronic lung injury and pulmonary fibrosis. Inhalation toxicology. 2019;31(4):147–60.
2. Cabrera-Benítez NE, Parotto M, Post M, Han B, Spieth PM, Cheng W-E, et al. Mechanical stress induces lung fibrosis by epithelial–mesenchymal transition. Critical care medicine. 2012;40(2):510–7.
3. Fijardo M, Kwan JYY, Bissey P-A, Citrin DE, Yip KW, Liu F-F. The clinical manifestations and molecular pathogenesis of radiation fibrosis. EBioMedicine. 2024;103.
4. Chen Y, Lin L, Tao X, Song Y, Cui J, Wan J. The role of podocyte damage in the etiology of ischemia-reperfusion acute kidney injury and post-injury fibrosis. BMC nephrology. 2019;20:1–11.
5. Brosius FC. New insights into the mechanisms of fibrosis and sclerosis in diabetic nephropathy. Reviews in Endocrine Metabolic Disorders. 2008;9:245–54.
6. Nichols D, Chmiel J, Berger M. Chronic inflammation in the cystic fibrosis lung: alterations in inter-and intracellular signaling. Clinical reviews in allergy immunology. 2008;34:146–62.
7. Henderson NC, Rieder F, Wynn TA. Fibrosis: from mechanisms to medicines. Nature. 2020;587(7835):555–66.
8. Liu M, Zeng X, Wang J, Fu Z, Wang J, Liu M, et al. Immunomodulation by mesenchymal stem cells in treating human autoimmune disease-associated lung fibrosis. Stem cell research & therapy. 2016;7(1):63.
9. Frangogiannis NG. Cardiac fibrosis. Cardiovascular research. 2021;117(6):1450–88.
10. Zuk A, Bonventre JV. Acute kidney injury. Annual review of medicine. 2016;67:293–307.
11. Sharma K. Obesity, oxidative stress, and fibrosis in chronic kidney disease. Kidney international supplements. 2014;4(1):113–7.
12. Reiss AB, Jacob B, Zubair A, Srivastava A, Johnson M, De Leon J. Fibrosis in chronic kidney disease: pathophysiology and therapeutic targets. Journal of Clinical Medicine. 2024;13(7):1881.

13. Panizo S, Martínez-Arias L, Alonso-Montes C, Cannata P, Martín-Carro B, Fernández-Martín JL, et al. Fibrosis in chronic kidney disease: pathogenesis and consequences. International journal of molecular sciences. 2021;22(1):408.

14. Chen CZ, Raghunath M. Focus on collagen: in vitro systems to study fibrogenesis and antifibrosis _ state of the art. Fibrogenesis tissue repair. 2009;2:1–10.

15. Plikus MV, Wang X, Sinha S, Forte E, Thompson SM, Herzog EL, et al. Fibroblasts: Origins, definitions, and functions in health and disease. Cell. 2021;184(15):3852–72.

16. Jeon H, Hidai H, Hwang DJ, Healy KE, Grigoropoulos CP. The effect of micronscale anisotropic cross patterns on fibroblast migration. Biomaterials. 2010;31(15):4286–95.

17. Rokonay R, Veres-Székely A, Szebeni B, Pap D, Lippai R, Béres NJ, et al. Role of IL-24 in the mucosal remodeling of children with coeliac disease. Journal of translational medicine. 2020;18(1):36.

18. Younesi FS, Miller AE, Barker TH, Rossi FM, Hinz B. Fibroblast and myofibroblast activation in normal tissue repair and fibrosis. Nature Reviews Molecular Cell Biology. 2024;25(8):617–38.

19. Schuster R, Younesi F, Ezzo M, Hinz B. The role of myofibroblasts in physiological and pathological tissue repair. Cold Spring Harbor perspectives in biology. 2023;15(1):a041231.

20. Franklin RA. Fibroblasts and macrophages: Collaborators in tissue homeostasis. Immunological reviews. 2021;302(1):86–103.

21. Adler M, Mayo A, Zhou X, Franklin RA, Meizlish ML, Medzhitov R, et al. Principles of cell circuits for tissue repair and fibrosis. IScience. 2020;23(2).

22. Werner S, Grose R. Regulation of wound healing by growth factors and cytokines. Physiological reviews. 2003;83(3):835–70.

23. Kim D, Kim SY, Mun SK, Rhee S, Kim BJ. Epidermal growth factor improves the migration and contractility of aged fibroblasts cultured on 3D collagen matrices. International Journal of Molecular Medicine. 2015;35(4):1017–25.

24. Hinz B, Phan SH, Thannickal VJ, Galli A, Bochaton-Piallat M-L, Gabbiani G. The myofibroblast: one function, multiple origins. The American journal of pathology. 2007;170(6):1807–16.

25. Haeger A, Wolf K, Zegers MM, Friedl P. Collective cell migration: guidance principles and hierarchies. Trends in cell biology. 2015;25(9):556–66.

26. Friedl P, Gilmour D. Collective cell migration in morphogenesis, regeneration and cancer. Nature reviews Molecular cell biology. 2009;10(7):445–57.

27. SenGupta S, Parent CA, Bear JE. The principles of directed cell migration. Nature Reviews Molecular Cell Biology. 2021;22(8):529–47.

28. Sepsi Z, Bokrossy P, Szász C, Pap D, Szebeni B, Szabó JA, et al. A fibroblastok funkcionális vizsgálata–II. rész: Sejtmigrációs mérések. Gyermekgyógyászat. 2022;73(4):252–4.

29. Hinz B, Lagares D. Evasion of apoptosis by myofibroblasts: a hallmark of fibrotic diseases. Nature Reviews Rheumatology. 2020;16(1):11–31.

30. Balestrini JL, Chaudhry S, Sarrazy V, Koehler A, Hinz B. The mechanical memory of lung myofibroblasts. Integrative Biology. 2012;4(4):410–21.

31. Peng D, Fu M, Wang M, Wei Y, Wei X. Targeting TGF-β signal transduction for fibrosis and cancer therapy. Molecular cancer. 2022;21(1):104.

32. Hughes G, Toellner H, Morris H, Leonard C, Chaudhuri N. Real world experiences: pirfenidone and nintedanib are effective and well tolerated treatments for idiopathic pulmonary fibrosis. Journal of clinical medicine. 2016;5(9):78.

33. Pirfenidone: DrugBank; 2007 [updated 29.01.2025.; cited 2025 17.07.]. Available from: https://go.drugbank.com/drugs/DB04951.

34. Nintedanib DrugBank2015 [updated 11.07.2025.; cited 2025 07.17.]. Available from: https://go.drugbank.com/drugs/DB09079.

35. Santos G, Fabiano A, Mota PC, Rodrigues I, Carvalho D, Melo N, et al. The impact of nintedanib and pirfenidone on lung function and survival in patients with idiopathic pulmonary fibrosis in real-life setting. Pulmonary Pharmacology Therapeutics. 2023:102261.

36. Chen Y, McAndrews KM, Kalluri RJNrCo. Clinical and therapeutic relevance of cancer-associated fibroblasts. 2021;18(12):792–804.

37. Wu F, Yang J, Liu J, Wang Y, Mu J, Zeng Q, et al. Signaling pathways in cancer-associated fibroblasts and targeted therapy for cancer. Signal transduction and targeted therapy. 2021;6(1):218.

38. Lee YE, Go G-Y, Koh E-Y, Yoon H-N, Seo M, Hong S-M, et al. Synergistic therapeutic combination with a CAF inhibitor enhances CAR-NK-mediated cytotoxicity via reduction of CAF-released IL-6. Journal for Immunotherapy of Cancer. 2023;11(2):e006130.

39. Glabman RA, Choyke PL, Sato N. Cancer-associated fibroblasts: tumorigenicity and targeting for cancer therapy. Cancers. 2022;14(16):3906.

40. Cescon M, Rampazzo E, Bresolin S, Da Ros F, Manfreda L, Cani A, et al. Collagen VI sustains cell stemness and chemotherapy resistance in glioblastoma. Cellular Molecular Life Sciences. 2023;80(8):233.

41. Chen Y, Yang S, Tavormina J, Tampe D, Zeisberg M, Wang H, et al. Oncogenic collagen I homotrimers from cancer cells bind to α3β1 integrin and impact tumor microbiome and immunity to promote pancreatic cancer. Cancer cell. 2022;40(8):818–34. e9.

42. Pandey P, Khan F, Upadhyay TK, Seungjoon M, Park MN, Kim B. New insights about the PDGF/PDGFR signaling pathway as a promising target to develop cancer therapeutic strategies. Biomedicine & Pharmacotherapy. 2023;161:114491.

43. Hao Y, Baker D, Ten Dijke P. TGF-β-mediated epithelial-mesenchymal transition and cancer metastasis. International journal of molecular sciences. 2019;20(11):2767.

44. Abe T, Kanno S-i, Niihori T, Terao M, Takada S, Aoki Y. LZTR1 deficiency exerts high metastatic potential by enhancing sensitivity to EMT induction and controlling KLHL12-mediated collagen secretion. Cell Death Disease. 2023;14(8):556.

45. Takeuchi K, Ito F. EGF receptor in relation to tumor development: molecular basis of responsiveness of cancer cells to EGFR-targeting tyrosine kinase inhibitors. The FEBS journal. 2010;277(2):316–26.

46. Grassi ML, de Souza Palma C, Thome CH, Lanfredi GP, Poersch A, Faca VM. Proteomic analysis of ovarian cancer cells during epithelial-mesenchymal transition (EMT) induced by epidermal growth factor (EGF) reveals mechanisms of cell cycle control. Journal of proteomics. 2017;151:2–11.

47. Sheng W, Shi X, Lin Y, Tang J, Jia C, Cao R, et al. Musashi2 promotes EGF-induced EMT in pancreatic cancer via ZEB1-ERK/MAPK signaling. Journal of Experimental & Clinical Cancer Research. 2020;39(1):16.

48. Sheng W, Tang J, Cao R, Shi X, Ma Y, Dong M. Numb-PRRL promotes TGF-β1-and EGF-induced epithelial-to-mesenchymal transition in pancreatic cancer. Cell Death Disease. 2022;13(2):173.

49. Fingas CD, Bronk SF, Werneburg NW, Mott JL, Guicciardi ME, Cazanave SC, et al. Myofibroblast-derived PDGF-BB promotes Hedgehog survival signaling in cholangiocarcinoma cells. Hepatology. 2011;54(6):2076–88.

50. Weigel MT, Dahmke L, Schem C, Bauerschlag DO, Weber K, Niehoff P, et al. In vitro effects of imatinib mesylate on radiosensitivity and chemosensitivity of breast cancer cells. BMC cancer. 2010;10(1):412.

51. Engebraaten O, Bjerkvig R, Pedersen PH, Laerum OD. Effects of EGF, BFGF, NGF and PDGF (bb) on cell proliferative, migratory and invasive capacities of human brain-tumour biopsies In Vitro. International journal of cancer. 1993;53(2):209–14.

52. Moffat JG, Vincent F, Lee JA, Eder J, Prunotto M. Opportunities and challenges in phenotypic drug discovery: an industry perspective. Nature reviews Drug discovery. 2017;16(8):531–43.

53. Quancard J, Bach A, Cox B, Craft R, Finsinger D, Guéret SM, et al. The european federation for medicinal chemistry and chemical biology (EFMC) best practice initiative: phenotypic drug discovery. ChemMedChem. 2021;16(11):1737–40.

54. Berg EL. The future of phenotypic drug discovery. Cell chemical biology. 2021;28(3):424–30.

55. Vincent F, Loria PM, Weston AD, Steppan CM, Doyonnas R, Wang Y-M, et al. Hit triage and validation in phenotypic screening: considerations and strategies. Cell Chemical Biology. 2020;27(11):1332–46.

56. Korzeniewski C, Callewaert DM. An enzyme-release assay for natural cytotoxicity. Journal of immunological methods. 1983;64(3):313–20.

57. Radstake WE, Gautam K, Van Rompay C, Vermeesen R, Tabury K, Verslegers M, et al. Comparison of in vitro scratch wound assay experimental procedures. Biochemistry and Biophysics Reports. 2023;33:101423.

58. Onursal C, Dick E, Angelidis I, Schiller HB, Staab-Weijnitz CA. Collagen biosynthesis, processing, and maturation in lung ageing. Frontiers in Medicine. 2021;8:593874.

59. Kamiloglu S, Sari G, Ozdal T, Capanoglu E. Guidelines for cell viability assays. Food Frontiers. 2020;1(3):332–49.
60. Mosmann T. Rapid colorimetric assay for cellular growth and survival: application to proliferation and cytotoxicity assays. Journal of immunological methods. 1983;65(1-2):55–63.
61. Abe K, Matsuki N. Measurement of cellular 3-(4, 5-dimethylthiazol-2-yl)-2, 5-diphenyltetrazolium bromide (MTT) reduction activity and lactate dehydrogenase release using MTT. Neuroscience research. 2000;38(4):325–9.
62. Jan R. Understanding apoptosis and apoptotic pathways targeted cancer therapeutics. Advanced pharmaceutical bulletin. 2019;9(2):205.
63. Liang C-C, Park AY, Guan J-L. In vitro scratch assay: a convenient and inexpensive method for analysis of cell migration in vitro. Nature protocols. 2007;2(2):329–33.
64. Kam Y, Guess C, Estrada L, Weidow B, Quaranta V. A novel circular invasion assay mimics in vivo invasive behavior of cancer cell lines and distinguishes single-cell motility in vitro. BMC cancer. 2008;8(1):198.
65. Mouritzen MV, Jenssen H. Optimized scratch assay for in vitro testing of cell migration with an automated optical camera. Journal of visualized experiments: JoVE. 2018(138):57691.
66. Salati MA, Khazai J, Tahmuri AM, Samadi A, Taghizadeh A, Taghizadeh M, et al. Agarose-based biomaterials: opportunities and challenges in cartilage tissue engineering. Polymers. 2020;12(5):1150.
67. Matsuzawa K, Himoto T, Mochizuki Y, Ikenouchi J. α-Catenin controls the anisotropy of force distribution at cell-cell junctions during collective cell migration. Cell Reports. 2018;23(12):3447–56.
68. Omelchenko T, Hall A. Myosin-IXA regulates collective epithelial cell migration by targeting RhoGAP activity to cell-cell junctions. Current Biology. 2012;22(4):278–88.
69. Omar Zaki SS, Kanesan L, Leong MYD, Vidyadaran S. The influence of serum-supplemented culture media in a transwell migration assay. Cell biology international. 2019;43(10):1201–4.

70. Lee SY, Yun SH, Jeong JW, Kim JH, Kim HW, Choi JS, et al. Review of the current research on fetal bovine serum and the development of cultured meat. Food science of animal resources. 2022;42(5):775.
71. Liu S, Yang W, Li Y, Sun C. Fetal bovine serum, an important factor affecting the reproducibility of cell experiments. Scientific Reports. 2023;13(1):1942.
72. Gebäck T, Schulz MMP, Koumoutsakos P, Detmar M. TScratch: A novel and simple software tool for automated analysis of monolayer wound healing assays: Short Technical Reports. Biotechniques. 2009;46(4):265–74.
73. Cortesi M, Pasini A, Tesei A, Giordano E. AIM: a computational tool for the automatic quantification of scratch wound healing assays. Applied Sciences. 2017;7(12):1237.
74. De Ieso ML, Pei JV. An accurate and cost-effective alternative method for measuring cell migration with the circular wound closure assay. Bioscience reports. 2018;38(5):BSR20180698.
75. Pijuan J, Barceló C, Moreno DF, Maiques O, Sisó P, Marti RM, et al. In vitro cell migration, invasion, and adhesion assays: from cell imaging to data analysis. Frontiers in cell and developmental biology. 2019;7:107.
76. Heit B, Kubes P. Measuring chemotaxis and chemokinesis: the under-agarose cell migration assay. Science's STKE. 2003;2003(170):pl5–pl.
77. Ahmed M, Basheer HA, Ayuso JM, Ahmet D, Mazzini M, Patel R, et al. Agarose spot as a comparative method for in situ analysis of simultaneous chemotactic responses to multiple chemokines. Scientific reports. 2017;7(1):1075.
78. Ghasemi M, Turnbull T, Sebastian S, Kempson I. The MTT assay: utility, limitations, pitfalls, and interpretation in bulk and single-cell analysis. International journal of molecular sciences. 2021;22(23):12827.
79. Fuchs H, Jahn K, Hu X, Meister R, Binter M, Framme C. Breaking a Dogma: High-Throughput Live-Cell Imaging in Real-Time with Hoechst 33342. Advanced Healthcare Materials. 2023;12(20):2300230.
80. Petersen TW, Ibrahim SF, Diercks AH, van den Engh G. Chromatic shifts in the fluorescence emitted by murine thymocytes stained with Hoechst 33342. Cytometry Part A: the journal of the International Society for Analytical Cytology. 2004;60(2):173–81.

81. Bratosin D, Mitrofan L, Palii C, Estaquier J, Montreuil J. Novel fluorescence assay using calcein-AM for the determination of human erythrocyte viability and aging. Cytometry Part A: the journal of the International Society or Analytical Cytology. 2005;66(1):78–84.

82. Cirulis JT, Strasser BC, Scott JA, Ross GM. Optimization of staining conditions for microalgae with three lipophilic dyes to reduce precipitation and fluorescence variability. Cytometry Part A. 2012;81(7):618–26.

83. Kim M, Turnquist H, Jackson J, Sgagias M, Yan Y, Gong M, et al. The multidrug resistance transporter ABCG2 (breast cancer resistance protein 1) effluxes Hoechst 33342 and is overexpressed in hematopoietic stem cells. Clinical Cancer Research. 2002;8(1):22–8.

84. Swain BM, Guo D, Singh H, Rawlins PB, McAlister M, van Veen HW. Complexities of a protonatable substrate in measurements of Hoechst 33342 transport by multidrug transporter LmrP. Scientific Reports. 2020;10(1):20026.

85. Salamito M, Nauroy P, Ruggiero F. The collagen superfamily: everything you always wanted to know. The collagen superfamily and collagenopathies: Springer; 2021. p. 1–22.

86. Lareu RR, Zeugolis DI, Abu-Rub M, Pandit A, Raghunath M. Essential modification of the Sircol Collagen Assay for the accurate quantification of collagen content in complex protein solutions. Acta biomaterialia. 2010;6(8):3146–51.

87. Coentro JQ, Capella-Monsonís H, Graceffa V, Wu Z, Mullen AM, Raghunath M, et al. Collagen quantification in tissue specimens. Fibrosis: Methods and Protocols: Springer; 2017. p. 341–50.

88. Brigger D, Muckle R. Comparison of Sirius red and Congo red as stains for amyloid in animal tissues. Journal of Histochemistry Cytochemistry. 1975;23(1):84–8.

89. Junqueira LCU, Bignolas G, Brentani RR. Picrosirius staining plus polarization microscopy, a specific method for collagen detection in tissue sections. The Histochemical journal. 1979;11:447–55.

90. Nielsen LF, Moe D, Kirkeby S, Garbarsch C. Sirius red and acid fuchsin staining mechanisms. Biotechnic histochemistry. 1998;73(2):71–7.

91. Walsh BJ, Thornton SC, Penny R, Breit SN. Microplate reader-based quantitation of collagens. Analytical biochemistry. 1992;203(2):187–90.

92. Dayan D, Hiss Y, Hirshberg A, Bubis J, Wolman M. Are the polarization colors of picrosirius red-stained collagen determined only by the diameter of the fibers? Histochemistry. 1989;93:27–9.

93. Courtoy GE, Leclercq I, Froidure A, Schiano G, Morelle J, Devuyst O, et al. Digital image analysis of picrosirius red staining: A robust method for multi-organ fibrosis quantification and characterization. Biomolecules. 2020;10(11):1585.

94. Segnani C, Ippolito C, Antonioli L, Pellegrini C, Blandizzi C, Dolfi A, et al. Histochemical detection of collagen fibers by sirius red/fast green is more sensitive than van gieson or sirius red alone in normal and inflamed rat colon. PloS one. 2015;10(12):e0144630.

95. Marotta M, Martino G. Sensitive spectrophotometric method for the quantitative estimation of collagen. Analytical biochemistry. 1985;150(1):86–90.

96. Canty EG, Kadler KE. Procollagen trafficking, processing and fibrillogenesis. Journal of cell science. 2005;118(7):1341–53.

97. Sorushanova A, Delgado LM, Wu Z, Shologu N, Kshirsagar A, Raghunath R, et al. The collagen suprafamily: from biosynthesis to advanced biomaterial development. Advanced materials. 2019;31(1):1801651.

98. Lareu RR, Arsianti I, Subramhanya HK, Yanxian P, Raghunath M. In vitro enhancement of collagen matrix formation and crosslinking for applications in tissue engineering: a preliminary study. Tissue engineering. 2007;13(2):385–91.

99. Lareu RR, Subramhanya KH, Peng Y, Benny P, Chen C, Wang Z, et al. Collagen matrix deposition is dramatically enhanced in vitro when crowded with charged macromolecules: the biological relevance of the excluded volume effect. FEBS letters. 2007;581(14):2709–14.

100. Chen C, Peng Y, Wang Z, Fish P, Kaar J, Koepsel R, et al. The Scar-in-a-Jar: studying potential antifibrotic compounds from the epigenetic to extracellular level in a single well. British journal of pharmacology. 2009;158(5):1196–209.

101. Zeiger AS, Loe FC, Li R, Raghunath M, Van Vliet KJ. Macromolecular crowding directs extracellular matrix organization and mesenchymal stem cell behavior. PloS one. 2012;7(5):e37904.

102. Gnutt D, Ebbinghaus S. The macromolecular crowding effect–from in vitro into the cell. Biological chemistry. 2016;397(1):37–44.

103. Rodríguez-Rodríguez P, Arribas SM, de Pablo ALL, González MC, Abderrahim F, Condezo-Hoyos L. A simple dot-blot–Sirius red-based assay for collagen quantification. Analytical bioanalytical chemistry. 2013;405:6863–71.

104. Rowshani AT, Scholten EM, Bemelman F, Eikmans M, Idu M, van Groningen MC, et al. No difference in degree of interstitial Sirius red–stained area in serial biopsies from area under concentration-over-time curves–guided cyclosporine versus tacrolimus-treated renal transplant recipients at one year. Journal of the American Society of Nephrology. 2006;17(1):305–12.

105. Coppock DL, Kopman C, Scandalis S, Gilleran S. Preferential gene expression in quiescent human lung fibroblasts. Cell growth differentiation. 1993;4:483–.

106. Coller HA, Sang L, Roberts JM. A new description of cellular quiescence. PLoS biology. 2006;4(3):e83.

107. Szarka A, Lőrincz T. The role of ascorbate in protein folding. Protoplasma. 2014;251(3):489–97.

108. Phillips CL, Tajima S, Pinnell SR. Ascorbic acid and transforming growth factor-β1 increase collagen biosynthesis via different mechanisms: coordinate regulation of proα1 (I) and proα1 (III) collagens. Archives of biochemistry. 1992;295(2):397–403.

109. Kishimoto Y, Saito N, Kurita K, Shimokado K, Maruyama N, Ishigami A. Ascorbic acid enhances the expression of type 1 and type 4 collagen and SVCT2 in cultured human skin fibroblasts. Biochemical biophysical research communications. 2013;430(2):579–84.

110. Bánhegyi G, Benedetti A, Margittai É, Marcolongo P, Fulceri R, Németh CE, et al. Subcellular compartmentation of ascorbate and its variation in disease states. Biochimica et Biophysica Acta -Molecular Cell Research. 2014;1843(9):1909–16.

111. Zhou B-y, Wang W-b, Wu X-l, Zhang W-j, Zhou G-d, Gao Z, et al. Nintedanib inhibits keloid fibroblast functions by blocking the phosphorylation of multiple kinases and enhancing receptor internalization. Acta Pharmacologica Sinica. 2020;41(9):1234–45.

112. Sato S, Shinohara S, Hayashi S, Morizumi S, Abe S, Okazaki H, et al. Anti-fibrotic efficacy of nintedanib in pulmonary fibrosis via the inhibition of fibrocyte activity. Respiratory research. 2017;18(1):172.

113. Andreucci E, Bugatti K, Peppicelli S, Ruzzolini J, Lulli M, Calorini L, et al. Nintedanib-αVβ6 Integrin Ligand Conjugates Reduce TGF β-Induced EMT in Human Non-Small Cell Lung Cancer. International Journal of Molecular Sciences. 2023;24(2):1475.

114. da Silva RF, Dhar D, Raina K, Kumar D, Kant R, Cagnon VHA, et al. Nintedanib inhibits growth of human prostate carcinoma cells by modulating both cell cycle and angiogenesis regulators. Scientific reports. 2018;8(1):9540.

115. Ha T-Y, Hwang S, Moon K-M, Won Y-J, Song G-W, Kim N, et al. Sorafenib inhibits migration and invasion of hepatocellular carcinoma cells through suppression of matrix metalloproteinase expression. Anticancer research. 2015;35(4):1967–76.

116. Zhou Q, Guo X, Choksi R. Activation of focal adhesion kinase and Src mediates acquired sorafenib resistance in A549 human lung adenocarcinoma xenografts. The Journal of pharmacology and experimental therapeutics. 2017;363(3):428–43.

117. Dattachoudhury S, Sharma R, Kumar A, Jaganathan BG. Sorafenib inhibits proliferation, migration and invasion of breast cancer cells. Oncology. 2020;98(7):478–86.

118. Mishra DK, Creighton CJ, Zhang Y, Gibbons DL, Kurie JM, Kim MP. Gene expression profile of A549 cells from tissue of 4D model predicts poor prognosis in lung cancer patients. International journal of cancer. 2014;134(4):789–98.

119. Takai E, Tsukimoto M, Kojima S. TGF-β1 downregulates COX-2 expression leading to decrease of PGE2 production in human lung cancer A549 cells, which is involved in fibrotic response to TGF-β1. PLoS One. 2013;8(10):e76346.

120. Thwe AM, Mossey P, Ellis IR. Effect of tyrosine kinase inhibitors on cell migration and epithelial-to-mesenchymal transition in Asian head and neck cancer cell lines. Journal of Oral Pathology Medicine. 2021;50(10):1031–9.

121. Li X, Li W, Wang J, Wang Q, Liang M, Chen S, et al. Establishment of a novel microfluidic co-culture system for simultaneous analysis of multiple indicators of gefitinib sensitivity in colorectal cancer cells. Microchimica Acta. 2024;191(5):279.

9. Bibliography of the candidate's publications

9.1. Publications related to the thesis

1. Veres-Székely Apor, **Szász Csenge**, Pap Domonkos, Bokrossy Péter, Lenzinger Dorina, Visnovitz Tamás, Mihály Judith, Pálmai Marcell, Varga Zoltán, Őrfi László, Szabó Attila J, Vannay Ádám, Szebeni Beáta

Improvement in Transient Agarose Spot (TAS) Cell Migration Assay: Microplate-Based Detection and Evaluation

INTERNATIONAL JOURNAL OF MOLECULAR SCIENCES 26: 12 Paper: 5584, 13 p. (2025)

Közlemény: 36188672 | Szakcikk (Folyóiratcikk) | Tudományos

IF: 4,9

2. **Szász Csenge**, Pap Domonkos, Szebeni Beáta, Bokrossy Péter, Őrfi László, Szabó Attila J, Vannay Ádám, Veres-Székely Apor

Optimization of Sirius Red-Based Microplate Assay to Investigate Collagen Production In Vitro

INTERNATIONAL JOURNAL OF MOLECULAR SCIENCES 24: 24 Paper: 17435, 17 p. (2023)

Közlemény: 34434633 | Szakcikk (Folyóiratcikk) | Tudományos

IF: 4,9

3. Veres-Székely Apor, Pap Domonkos, Szebeni Beáta, Őrfi László, **Szász Csenge**, Pajtók Csenge, Lévai Eszter, Szabó Attila J, Vannay Ádám

Transient Agarose Spot (TAS) Assay: A New Method **to Investigate Cell Migration**

INTERNATIONAL JOURNAL OF MOLECULAR SCIENCES 23: 4 Paper: 2119, 17 p. (2022)

Közlemény: 32670502 | Szakcikk (Folyóiratcikk) | Tudományos

IF: 5,6

4. **Szász Csenge**, Sepsi Zita, Bokrossy Péter, Pap Domonkos, Szebeni Beáta, Szabó J Attila, Vannay Ádám, Veres-Székely Apor

A fibroblastok funkcionális vizsgálata – I. rész: Bevezetés

GYERMEKGYÓGYÁSZAT 73: 3 pp. 169-170. (2022)

Közlemény: 32828458 | Összefoglaló cikk (Folyóiratcikk) | Tudományos

5. Sepsi Zita, Bokrossy Péter, **Szász Csenge**, Pap Domonkos, Szebeni Beáta, Szabó J Attila, Vannay Ádám, Veres-Székely Apor

A fibroblastok funkcionális vizsgálata – II. rész: Sejtmigrációs mérések

GYERMEKGYÓGYÁSZAT 73: 4 pp. 252-254. (2022)

Közlemény: 33002115 | Összefoglaló cikk (Folyóiratcikk) | Tudományos

6. Bokrossy Péter, Sepsi Zita, **Szász Csenge**, Pap Domonkos, Szebeni Beáta, Szabó J Attila, Vannay Ádám, Veres-Székely Apor

A fibroblastok funkcionális vizsgálata – III. rész: Sejtproliferációs mérések

GYERMEKGYÓGYÁSZAT 73: 5 pp. 327-329. (2022)

Közlemény: 33094468 | Összefoglaló cikk (Folyóiratcikk) | Tudományos

7. Veres-Székely Apor, Szebeni Beáta, Pap Domonkos, Bokrossy Péter, Lévai Eszter, **Szász Csenge**, Szabó J Attila, Vannay Ádám

A fibroblastok funkcionális vizsgálata – IV. rész: Az ECM-termelés mérése

GYERMEKGYÓGYÁSZAT 73: 6 pp. 402-405. (2022)

Közlemény: 33272244 | Összefoglaló cikk (Folyóiratcikk) | Tudományos

9.2. Publications not related to the thesis

8. Zrufkó Réka, Pajtók Csenge, Szebeni Beáta, Veres-Székely Apor, Bernáth Mária, **Szász Csenge**, Bokrossy Péter, Szabó Attila J, Vannay Ádám, Pap Domonkos
The DJ-1-Binding Compound Exerts a Protective Effect in Both In Vitro and In Vivo Models of Sepsis-Induced Acute Kidney Injury
ANTIOXIDANTS 14: 6 Paper: 719, 15 p. (2025)
Közlemény: 36193750 | Szakcikk (Folyóiratcikk) | Tudományos
IF: 6,6

9. Pap Domonkos, Veres-Székely Apor, Szebeni Beáta, Zrufkó Réka, Bokrossy Péter, **Szász Csenge**, Vannay Ádám
Role of PARK7/DJ-1 in Gastrointestinal Diseases
INTERNATIONAL JOURNAL OF CELIAC DISEASE 12: 1 pp. 28-32. (2024)
Közlemény: 35663921 | Összefoglaló cikk (Folyóiratcikk) | Tudományos

10. Veres-Székely Apor, **Szász Csenge**, Pap Domonkos, Szebeni Beáta, Bokrossy Péter, Vannay Ádám
Zonulin as a Potential Therapeutic Target in Microbiota-Gut-Brain Axis Disorders: Encouraging Results and Emerging Questions
INTERNATIONAL JOURNAL OF MOLECULAR SCIENCES 24: 8 Paper: 7548, 28 p. (2023)
Közlemény: 33764732 | Összefoglaló cikk (Folyóiratcikk) | Tudományos
IF: 4,9

11. Pap Domonkos, Pajtók Csenge, Veres-Székely Apor, Szebeni Beáta, **Szász Csenge**, Bokrossy Péter, Zrufkó Réka, Vannay Ádám, Tulassay Tivadar, Szabó Attila J
High Salt Promotes Inflammatory and Fibrotic Response in Peritoneal Cells
INTERNATIONAL JOURNAL OF MOLECULAR SCIENCES 24: 18 Paper: 13765, 19 p. (2023)
Közlemény: 34135659 | Szakcikk (Folyóiratcikk) | Tudományos
IF: 4,9

10. Acknowledgements

I consider myself really lucky for having the support of so many wonderful people during my PhD journey. First, I would like to express my gratitude to my supervisor, Apor Veres-Székely, who was constantly available to answer my questions and concerns. He always provided professional and personal guidance with great accuracy and honesty, meanwhile pushing me to be independent. I learned plenty from him about the importance of organization and critical thinking during scientific projects, a pool of knowledge pointing much further than the frames of this thesis. Furthermore, I am grateful for his unique, humorous personality which brightened the atmosphere as well as his friendship.

I would like to thank to my dear colleagues, Mária Bernáth, Beáta Szebeni and Domonkos Pap, who all provided valuable advice, a wide range of knowledge and a working environment that felt like family. I deeply appreciate being involved in so many different projects and them sharing their expertise with me. I am thankful for Csenge Pajtók and Eszter Lévai, the senior PhD students who welcomed me with kindness and friendship and taught me patiently. I would like to highlight Péter Bokrossy, my great friend and fellow PhD student, who offered constant professional and emotional support during this period. We collected many precious memories that I highly appreciate.

I am grateful for the leader of our research group, Ádám Vannay for his constant supervision and advice, as well as for providing important academic opportunities to expand my knowledge and connections. He enabled me to spend 8 wonderful months on internship abroad, gaining valuable experience in a new field and building friendships.

I would like to thank Prof. Attila Szabó, the director of the Pediatric Center and doctoral program leader for the opportunity to join the scientific community of the Pediatric Center, and conduct my PhD in this highly professional research group gaining experience in a range of scientific fields and methods.

I am grateful for having strong, special connection with my family, who supported my decisions with all their heart. Knowing that I could always count on them to have a conversation, to get advice and reassurance or just a nice home-cooked meal made me feel secure. They are there to lift me up when I encounter difficulties, help me stay focused on the important steps, and are ready to celebrate the successes. Lastly, I really appreciate all my friends for standing by me and being company in relaxation and recharge.

International Journal of
Molecular Sciences

MDPI

Article

Transient Agarose Spot (TAS) Assay: A New Method to Investigate Cell Migration

Apor Veres-Székely [1,2,*], Domonkos Pap [1,2], Beáta Szebeni [1,2], László Őrfi [3,4], Csenge Szász [1], Csenge Pajtók [1], Eszter Lévai [1], Attila J. Szabó [1,2] and Ádám Vannay [1,2]

1 1st Department of Pediatrics, Semmelweis University, 1083 Budapest, Hungary; pap.domonkos@med.semmelweis-univ.hu (D.P.); szebeni.beata@med.semmelweis-univ.hu (B.S.); szaszcsenge3@gmail.com (C.S.); pajtok.csenge@gmail.com (C.P.); levai.eszter@semmelweis-univ.hu (E.L.); szabo.attila@med.semmelweis-univ.hu (A.J.S.); vannay.adam@med.semmelweis-univ.hu (Á.V.)
2 ELKH-SE Pediatrics and Nephrology Research Group, 1052 Budapest, Hungary
3 Department of Pharmaceutical Chemistry, Semmelweis University, 1092 Budapest, Hungary; lorfi@vichem.hu
4 Vichem Chemie Research Ltd., 1022 Budapest, Hungary
* Correspondence: veres-szekely.apor@med.semmelweis-univ.hu

Abstract: Fibroblasts play a central role in diseases associated with excessive deposition of extracellular matrix (ECM), including idiopathic pulmonary fibrosis. Investigation of different properties of fibroblasts, such as migration, proliferation, and collagen-rich ECM production is unavoidable both in basic research and in the development of antifibrotic drugs. In the present study we developed a cost-effective, 96-well plate-based method to examine the migration of fibroblasts, as an alternative approach to the gold standard scratch assay, which has numerous limitations. This article presents a detailed description of our transient agarose spot (TAS) assay, with instructions for its routine application. Advantages of combined use of different functional assays for fibroblast activation in drug development are also discussed by examining the effect of nintedanib—an FDA approved drug against IPF—on lung fibroblasts.

Keywords: fibroblast; migration; agarose; proliferation; collagen deposition; high throughput; assay

Citation: Veres-Székely, A.; Pap, D.; Szebeni, B.; Őrfi, L.; Szász, C.; Pajtók, C.; Lévai, E.; Szabó, A.J.; Vannay, Á. Transient Agarose Spot (TAS) Assay: A New Method to Investigate Cell Migration. *Int. J. Mol. Sci.* **2022**, *23*, 2119. https://doi.org/10.3390/ijms23042119

Academic Editor: Lukas J. A. C. Hawinkels

Received: 21 December 2021
Accepted: 12 February 2022
Published: 14 February 2022

1. Introduction

Idiopathic pulmonary fibrosis (IPF) is an aggressive form of interstitial pneumonias characterized by excessive accumulation of fibroblasts and scar tissue formation, resulting in severe respiratory failure and high mortality rate [1,2]. Fibrosis independently from the etiology of the primary disease can virtually affect any organ, making this a key determinant of health [3]. Indeed, according to certain estimates tissue fibrosis is responsible for 45% of all death in the developed world [4].

Fibroblasts comprise the main cellular components of scar tissue. These cells can be described by their typical molecular biological and functional properties (Figure 1) [5,6] including enhanced migration due to their contractile stress fiber system, increased proliferation, and decreased apoptosis rate, resulting significant cell accumulation [7–10]. Activated fibroblasts are also responsible for the production of extracellular matrix (ECM), the structural element of the scar tissue, mainly composed of collagens and fibronectins [11,12]. These processes lead to excessive deposition of ECM which displaces native cells, leading finally to decreased organ function [13,14].

Nintedanib is one of the two approved drugs against IPF. Several preclinical and clinical studies have confirmed that multikinase inhibitors significantly slow progression of fibrosis by suppressing fibroblasts activation [15]. However, there is no approved pharmaceutical treatment available for other fibroproliferative diseases. Therefore, there is still a clear medical demand to develop antifibrotic drugs and targeting fibroblasts is a promising opportunity.

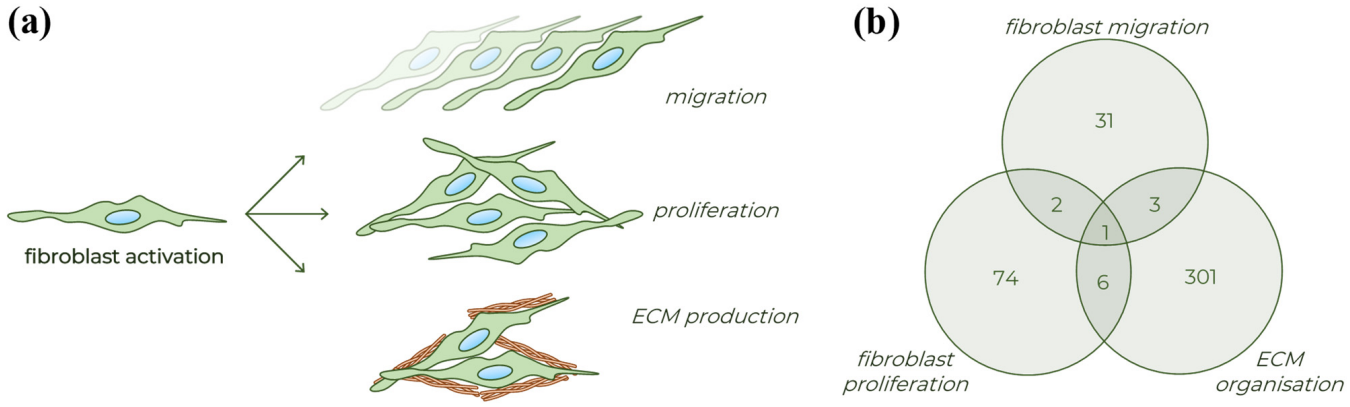

Figure 1. Different processes of fibroblast activation. (**a**) Schematic figure about the typical properties of activated fibroblasts. (**b**) Venn diagram presenting the number of human genes involved in the various fibroblast related biological processes based on the Gene Ontology database (detailed in Table S1).

Several microplate-based assays have been described to investigate the different aspects of fibroblast activation. There are various well-constructed assays to investigate the proliferation (e.g., thiazolyl blue tetrazolium bromide—MTT; bromodeoxyuridine—BrdU) [16] or ECM production (e.g., SiriusRed staining) [17] of fibroblasts, however, the situation is different regarding their migration. The gold standard method is the scratch assay, which is based on graphical analysis of cell-free area created mechanically on a cell monolayer [18]. Despite its simplicity and cost-effectiveness, the scratch assay has significant limitations, including low reproducibility or high intra-assay variability [19–22].

In this article we describe our newly developed in vitro TAS assay, developed primarily for investigating fibroblast migration in a near high-throughput manner. Moreover, we also show how the set of microplate-based assays can be used to determine the main properties of fibroblasts, including migration, proliferation, and collagen deposition.

Beside the huge importance of fibroblast-related experiments, studying cell migration emerges also in other fields of research. Indeed, the adequate re-epithelization requires a proper balance in the migration and proliferation of epithelial cells during the repair process of injured lung, skin, or intestine [23–25]. In addition, the migration and proliferation of cancer cells determine the tumor progression and metastasis [26,27]. Therefore, in the present study we also examined the possible application of TAS assay for investigating the cellular mechanism of re-epithelization or tumor cell migration.

2. Results

2.1. Basic Settings of TAS Assay: Agarose Spot Stability and Optimal Cell Density

The stability of agarose gel spots was investigated over several consecutive days using MRC-5 lung fibroblasts. In 'transient' group, gel spots were removed 24 h after cell seeding, thereafter the rapid reduction in cell-free gap area was observed.

However, when the agarose gel spots were not removed ('permanent' group), the covered area remained cell-free for days, without any signs of under-agarose cell migration, allowing to change the medium and initiate the examination of migration at any time after optional pre-treatment steps (Figure 2).

The effect of cell confluence on the gap closure was also investigated using MRC-5 cells. The higher the cell count we used, the higher the confluence reached before gel removal, reaching the plateau phase at about 20,000 cell/well count (Figure 3a). Similarly, the increasing cell number resulted in accelerated gap closure, which was maximized at about 20,000 cell/well (Figure 3b). Based on the above-mentioned results, the confluency and the kinetics of gap closure showed a strongly positive correlation (Figure S1).

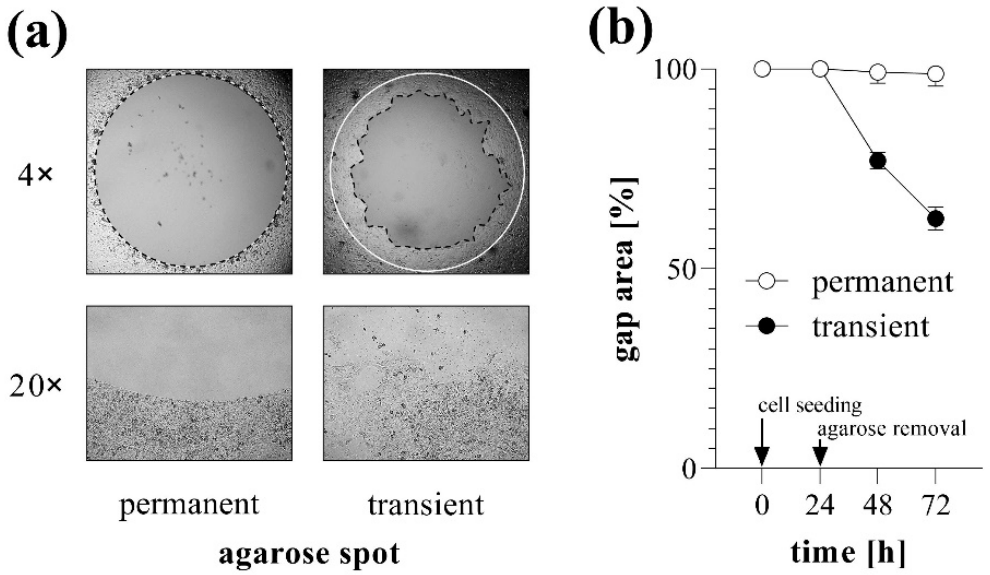

Figure 2. Gap closure in case of permanent and transient agarose spots. To investigate the stability of agarose gel spots, TAS migration assay was performed on MRC-5 cells. (**a**) Cell-free zone areas were analyzed graphically after brightfield microscopy. Lines in representative images indicate the gap edges at 0 (white) and 48 (black) hours after gel removal. Pictures taken with 20× objectives show the edges of cell-free zones. (**b**) The gap closure was monitored for 72 h after cell seeding. Results are presented as mean ± SD (n = 6).

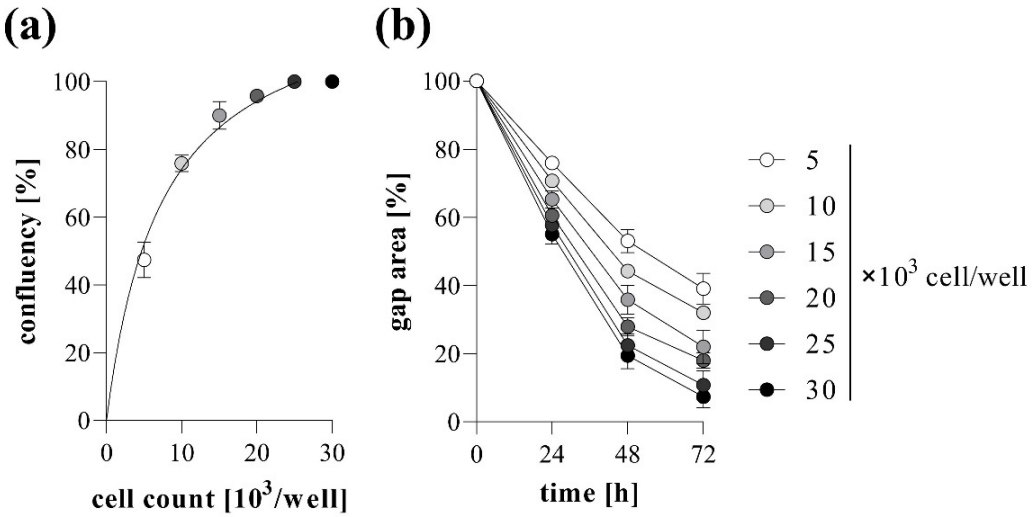

Figure 3. Effect of cell density on gap closure. To determine optimal cell count, TAS migration assay was performed on MRC-5 cells. (**a**) The resulting confluencies and the (**b**) kinetics of gap closure in the case of various cell counts were determined graphically. Results are presented as mean ± SD (n = 5).

2.2. TAS Assay as Fibroblast Migration Assay

Cell migration of MRC-5 lung fibroblasts was investigated by TAS assay following various treatments. We found that addition of FBS into the culture media increased the rate of gap closure in a dose-dependent manner (Figure 4). Moreover, treatment with EGF also increased the extent of gap closure of MRC-5 cells (Figure 5).

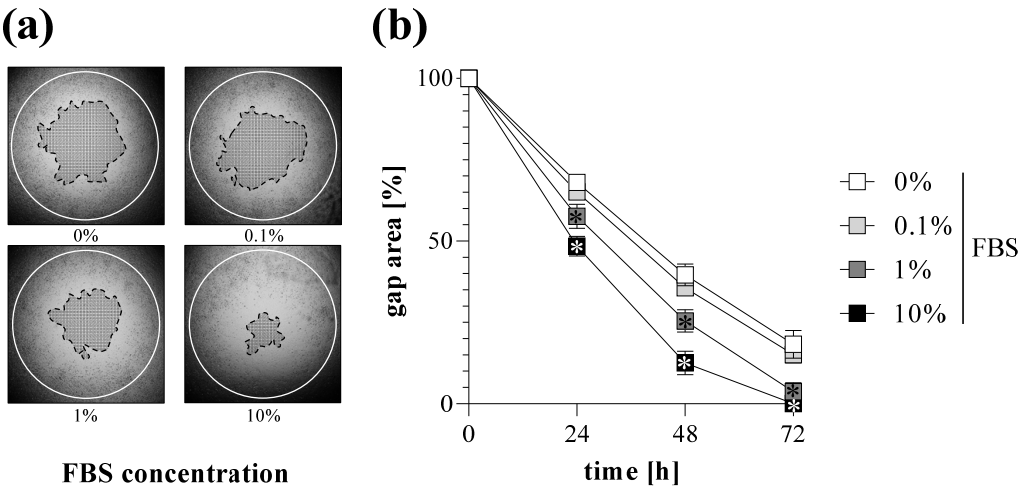

Figure 4. Effect of FBS treatment on gap closure. To determine the effect of serum addition, TAS migration assay was performed on MRC-5 cells. (**a**) Cell-free zone areas were analyzed graphically after brightfield microscopy. Lines in representative images indicate the gap edges at 0 (white) and 48 (black) hours after gel removal. (**b**) The gap closure was monitored for 72 h after gel removal. Results are presented as mean ± SD (n = 8). * $p < 0.05$ vs. 0% FBS at the concerning time (two-way ANOVA).

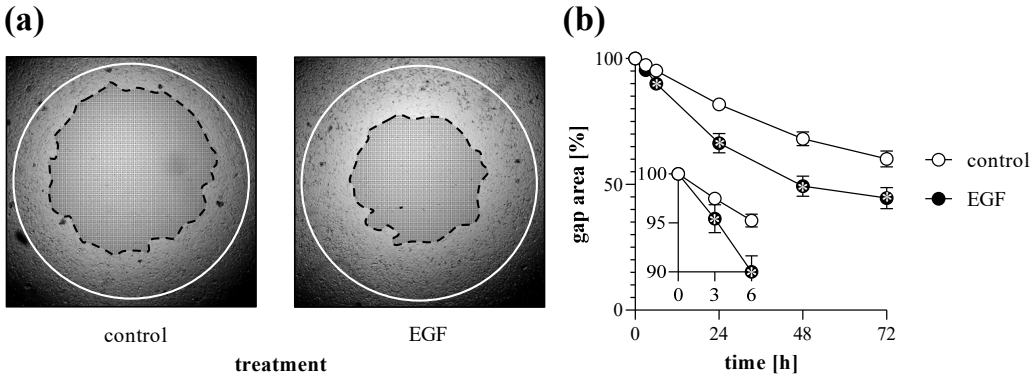

Figure 5. Effect of growth factor treatment on gap closure. To determine the effect of EGF treatment, TAS migration assay was performed on MRC-5 cells. (**a**) Cell-free zone areas were analyzed graphically after brightfield microscopy. Lines in representative images indicate the gap edges at 0 (white) and 48 (black) hours after gel removal. (**b**) The gap closure was monitored for 72 h after gel removal. Results are presented as mean ± SD (n = 8). * $p < 0.05$ vs. 0% control at the concerning time (two-way ANOVA).

2.3. Comparison of Different Gap Annotation Methods

To investigate the accuracy and reproducibility of the different methods, the size of the same gaps was determined by manual (Figure 6a) and automatic annotations (Figure 6b). In the case of brightfield or fluorescence images of MRC-5 cells, the manual or automatic annotation of the gap area showed a very high positive correlation (Figure 6c). While the brightfield images of NRK-49F cells were not suitable for the automatic annotation, because the software could not define the edge of the cell-free area, fluorescent images were appropriate for evaluation (Figure 6b).

Comparing the speed of the annotation methods, we found that although the manual annotation can be significantly accelerated by the use of a digitizer board or tablet, the automatic annotation of the images takes considerably fewer orders of magnitude of evaluation time (Figure 6d).

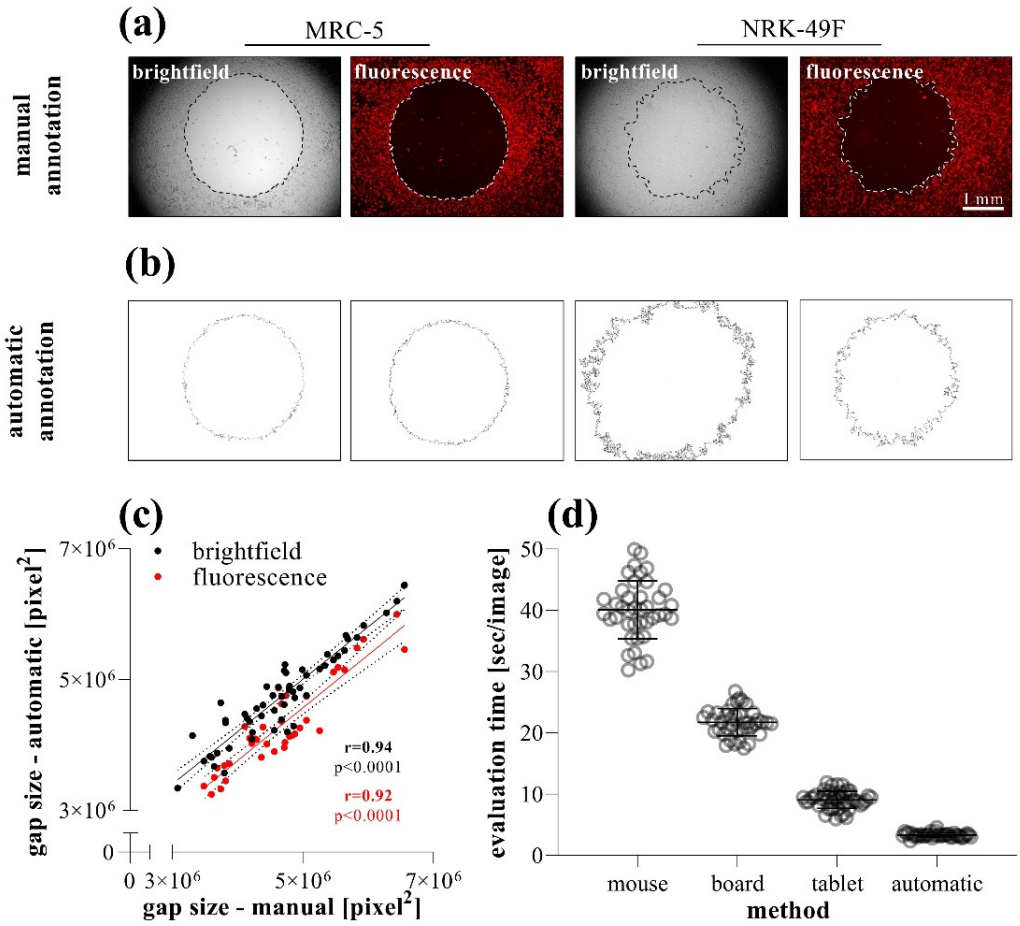

Figure 6. Comparison of data evaluation methods in TAS migration assay. (**a**) Brightfield and (**b**) fluorescence images were taken of DiI stained MRC-5 and NRK-49F cells. The same images (n = 40) of MRC-5 cells were analyzed after manual and automatic annotation, then the (**c**) resulting gap areas and the (**d**) required evaluation times were compared. Correlation was determined by Pearson's coefficients (r).

2.4. Comparison of Scratch and TAS Migration Assays

To compare their sensitivity and reproducibility, scratch and TAS migration assays were performed in parallel using MRC-5 cells.

Based on several independent experiments we found that while the confidence interval of initial gap size varied between 23 and 30% in the case of the scratch assay, it was only about 9% in the case of the TAS assay (Figure 7a). We found similar consistency while measuring directly the agarose spots without cell seeding (Figure S8). Beside the inconsistent size, the gap closure of scratched area is uneven and can only be documented by a series of images. In the case of TAS, the entire cell-free area can be investigated in one single field of view (Figure 7b).

The gap closure of MRC-5 cells showed similar kinetics comparing scratch (Figure 8a,c) and TAS (Figure 8b,d) migration assays. However, the intra-group variance determined by the coefficient of variation of group means was on average 3-fold higher in the scratch assay compared to the TAS assay, in the case of both relative (Figure 8a,b) and absolute (Figure 8c,d) gap size values.

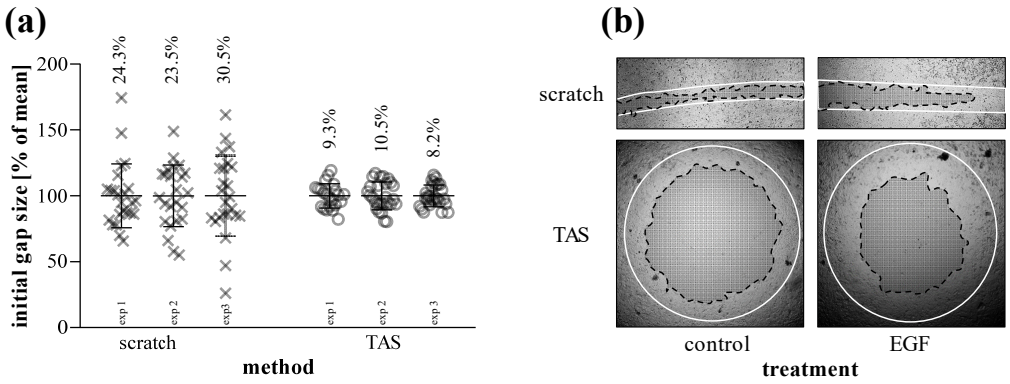

Figure 7. Reproducibility of scratch and TAS migration assays. (**a**) Consistency of initial gap sizes was determined in independent experiments performed on MRC-5 cells (n = 24–30 in each 3-3 experiments). Percentage values indicate the coefficient of variation of the concerning groups. (**b**) Evenness of gap closure was investigated on control and EGF-treated cells, as demonstrated in representative microscopic images. Lines in representative images indicate the gap edges at 0 (white) and 48 (black) hours after gel removal.

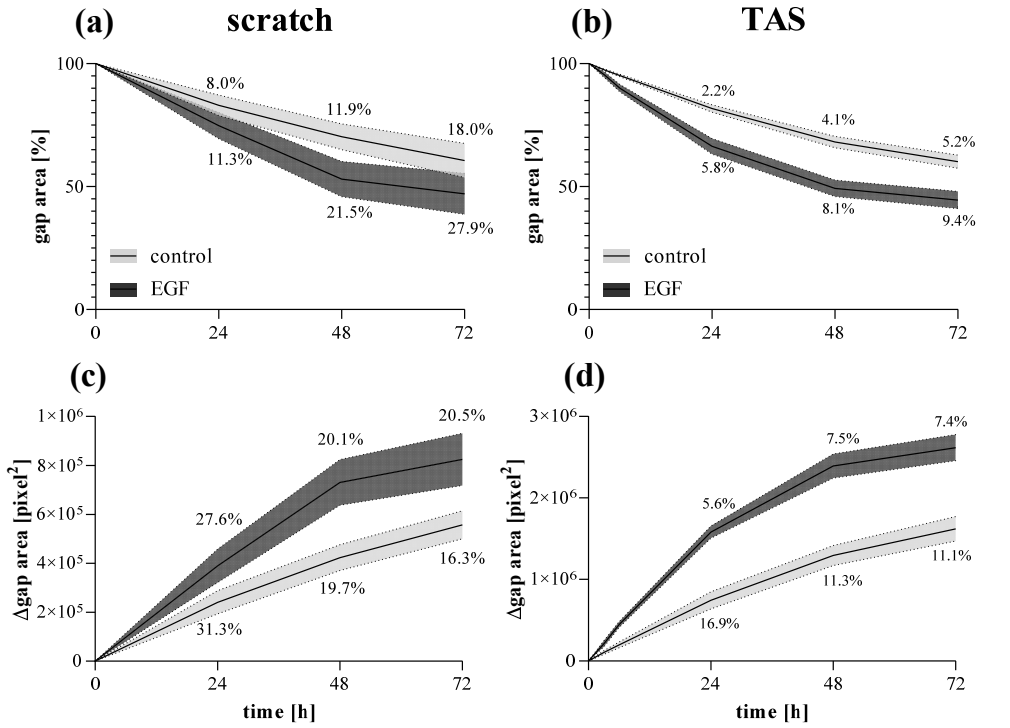

Figure 8. Fibroblast migration determined by different methods. Gap closure kinetics of control and EGF-activated MRC-5 cells were investigated by (**a**,**c**) scratch and (**b**,**d**) TAS migration assays. Alteration in gap size was determined by (**a**,**b**) relative (percentage of initial size) or (**c**,**d**) absolute (Δpixel^2) values. Results are presented as mean ± deviation, where line widths and percentage values indicate the coefficient of variation of the concerning groups (n = 6).

2.5. Antifibrotic Effect of Nintedanib

Using a complex in vitro experimental setup, we investigated the effect of nintedanib on the main properties of MRC-5 lung fibroblasts including migration, viability, proliferation, and ECM production. To describe the migration ability of MRC-5 cells, the TAS assay was performed on EGF-treated fibroblasts in the absence or presence of nintedanib. We found that nintedanib significantly decreased the gap closure kinetics of both con-

trol (Figure 9a,b) and EGF-treated (Figure 9a,c) MRC-5 cells in a dose-dependent manner (Figure 9d).

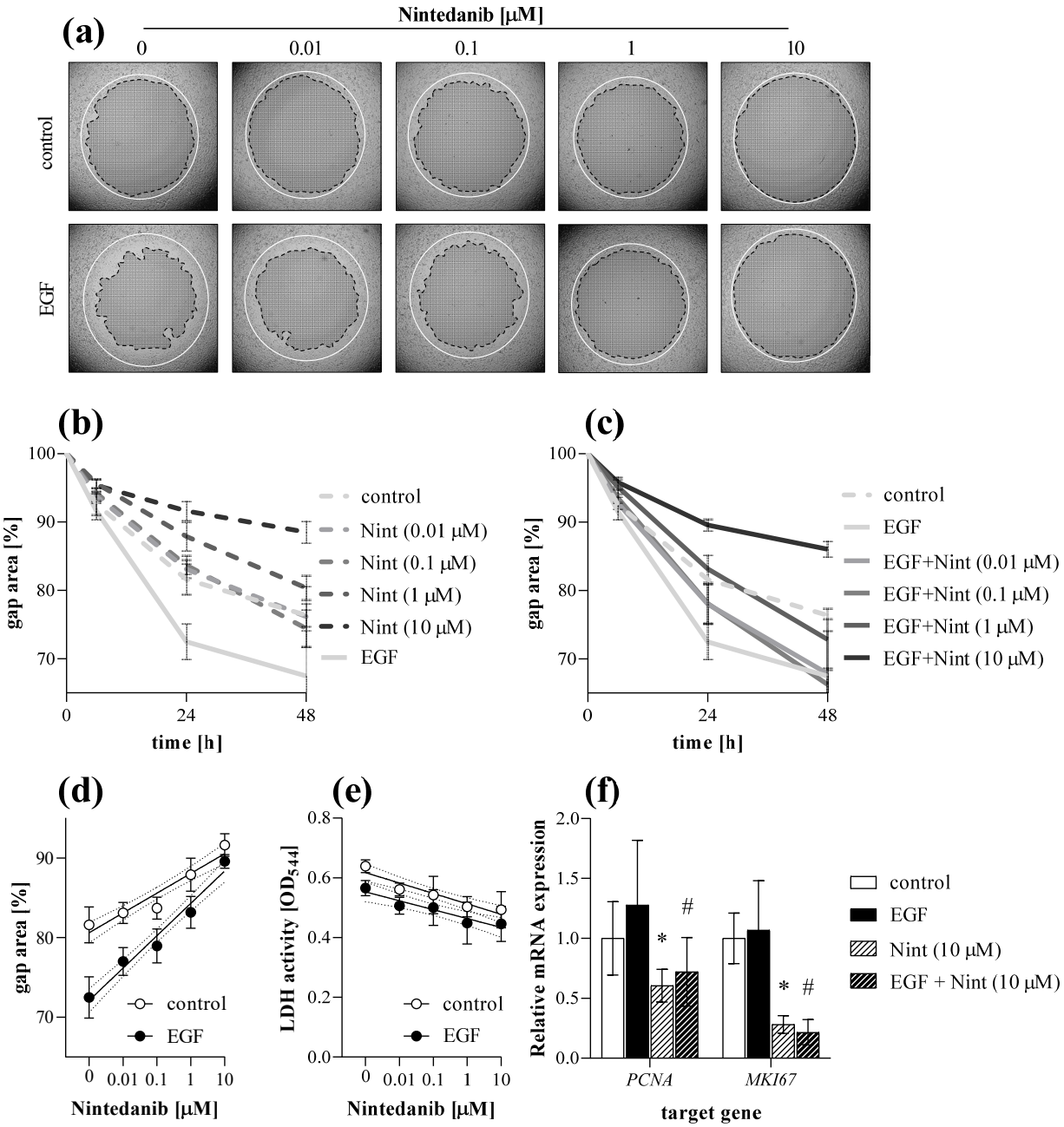

Figure 9. Effect of nintedanib on fibroblast migration. The gap closure kinetics of (**a**,**b**) control and (**a**,**c**) EGF-activated MRC-5 cells were determined by TAS assay in the absence or presence of nintedanib (Nint). Lines in section (**a**) indicate the gap edges at 0 (white) and 48 (black) hours after gel removal. (**d**) Dose-dependence was investigated on data derived from 24 h after gel removal. (**e**) To monitor cytotoxicity, LDH assay was performed on cell supernatants. (**f**) Relative mRNA expressions were determined by comparison with *RN18S* ribosomal RNA as internal control and normalized as the ratio of the control group. Results are presented as mean ± SD ($n = 6$). * $p < 0.05$ 'Nint (10 µM)' vs. 'control', # $p < 0.05$ 'EGF + Nint (10 µM)' vs. 'EGF' (two-way ANOVA).

At the end of the experiment cells were harvested and further analyzed by real-time PCR. Nintedanib decreased the mRNA expression of *PCNA* and *MKI67* in both control and EGF-treated MRC-5 cells (Figure 9f).

The proliferation of MRC-5 was investigated by MTT assay. Co-treatment with nintedanib decreased the PDGF-B-induced proliferation of fibroblasts in a dose-dependent manner (Figure 10a). Collagen deposition was determined by SiriusRed assay. Co-treatment with nintedanib decreased the TGF-ß induced collagen deposition of MRC-5 cells in a dose-dependent manner (Figure 10c).

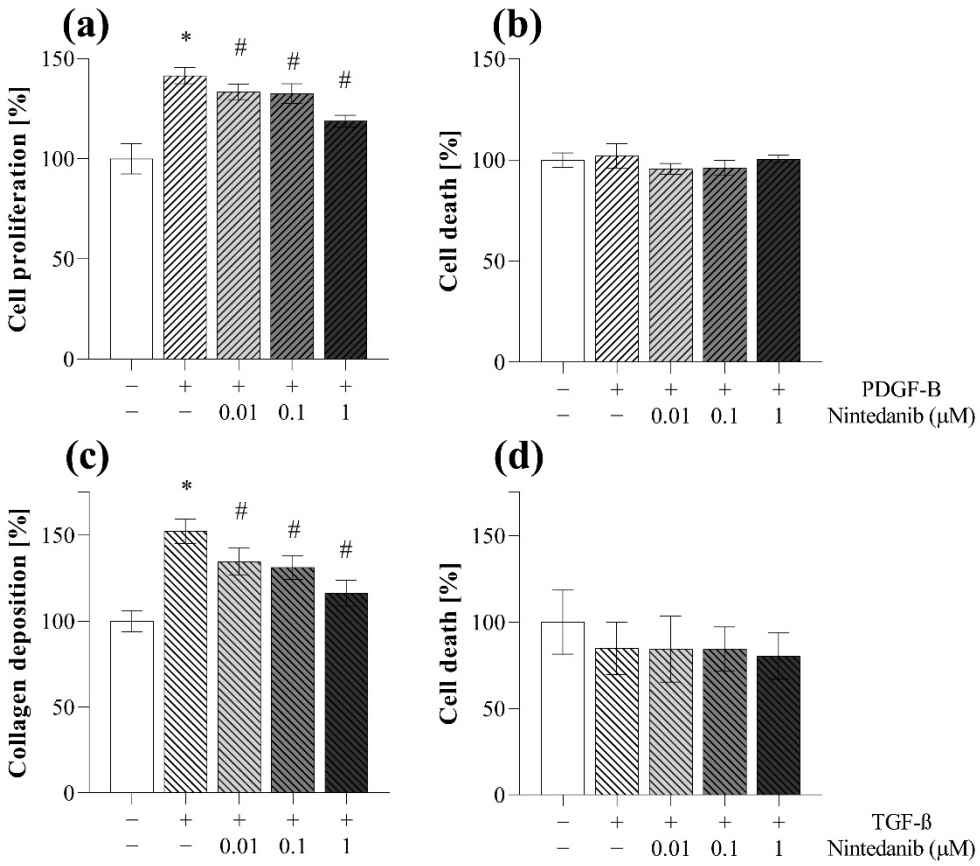

Figure 10. Effect of nintedanib on fibroblast proliferation and collagen deposition. (**a**,**b**) PDGF-B-induced cell proliferation and (**c**,**d**) TGF-ß-induced collagen deposition of MRC-5 cells in the absence or presence of nintedanib was investigated by (**a**) MTT and (**c**) SiriusRed assays. (**b**,**d**) To monitor cytotoxicity, LDH analysis was performed on cell supernatants. Results are presented as mean ± SD ($n = 6$). * $p < 0.05$ vs. control, # $p < 0.05$ vs. TGF-ß.

Viability of cells was monitored by LDH cytotoxicity assay, performed on cell supernatants derived from TAS (Figure 9e), MTT (Figure 10b), and SiriusRed (Figure 10d) assays as well. We found no sign of cell death even at the highest dose of nintedanib during the experiments.

3. Discussion

IPF is one of the most aggressive forms of interstitial lung disease associated with high mortality rate and the lack of effective therapy. Although the etiology of IPF is unknown, the molecular and cellular mechanisms leading to tissue fibrosis are relatively well described revealing the crucial role of fibroblast activation [28]. Therefore, investigating the key features of fibroblasts, including their migratory capacity [29], proliferation [30], and ECM production [31], is inevitable to identify novel therapeutic targets and develop new antifibrotic compounds.

In the investigation of cell migration on two-dimensional monolayers, the scratch assay is the most commonly used method [32]. Although this assay has many advantages, including its simplicity or affordability, it also has serious limitations, which make its use

as a high-throughput tool difficult [18]. Indeed, during the scratch assay, the cell-free gap is manually generated by scratching the surface of a confluent cell monolayer with a pipette tip on 6 or 12-well plates. Thereafter the migration of the cells and the kinetics of the gap closure is determined by graphical analysis. The main disadvantages of the scratch assay originate from the mechanical scratching itself, which causes damage of the cells, and also that of the plate surface, which has a significant impact on cell motility [33]. In addition, scratching with a pipette tip results in inconsistent initial gap sizes, which is reflected in the high intra- and inter-assay variability of the assay [32]. Therefore, alternative methods have been described to replace scratching recently. Among others, the cell-free zone can be created by heat stamp, laser, electricity, enzymatic digestion, or vacuum [20,34]. However, most of these methods have similar handicaps, including injured cells and surfaces, or resulting in gaps with irregular edges and sizes. From this point of view, a promising version could be the use of pre-installed physical barriers, where the cell-free zone is generated by plastic equipment or biocompatible gels [20–22]. Nevertheless, these commercially available kits are very expensive, and similarly to the scratch assay, work mostly with large surfaces (24 or 6-well plate) and thereby with large amounts of cells, reagents, and compounds, resulting in a low-throughput technique instead of a high-throughput one [20].

Therefore, in this study we aimed to develop a new assay eliminating the disadvantages of the above-mentioned techniques, using a simple, cost-effective, and high-throughput approach. In this method, which was termed as transient agarose spot (TAS) assay (Video S1), liquid agarose hydrogel drops were placed in the middle of the wells on a 96-well plate to exclude the fibroblasts from a consistent, circular area (Figure 2). Until the hydrogel drops were removed by pipetting, they remained stable in the middle of the wells for several days despite manipulating the cells (e.g., medium change, serum starvation, or even performing transfection). Agarose is a widely used biocompatible gel with non-toxic, non-immunogenic properties [35,36]. However, after eliminating the hydrogel drop, fibroblasts started to migrate toward the cell-free surface of the gap, as revealed by the reduction in the initial size of gap areas (Figure 2).

In the first set of experiments, we investigated the impact of the cell density on the kinetics of gap closure in TAS assay. Not surprisingly, we found that cell number significantly influences the rate of gap closure (Figure 3). Based on our experiments we suggest the use of a nearly confluent (~90%) initial cell culture in order to receive sensitive measurement, but avoid formation of overlapping cell layers, which can cause inaccuracy during the experiments. The presence of BSA in the cell culture media further accelerates the gap closure of the investigated cells (Figure 4). Moreover, fibroblast migration can also be stimulated by adding different profibrotic growth factors [37–39], as demonstrated by our experiments on EGF-treated lung fibroblasts (Figure 5). In summary, varying with the initial cell count, the amount of BSA, and other optional stimulants, our TAS assay can be easily fine-tuned to examine the effect of various factors on cell migration.

Although in this study we focused on lung fibroblasts, the TAS assay can be performed on other fibroblasts (Figures S2 and S3) or even other cell types, as well. For example, using epithelial cells (Figures S4 and S5), the mechanism of reepithelization and wound healing can be properly investigated. In the case of cancer cells (Figures S6 and S7), TAS can be interpreted as an useful assay of invasion, which is a determining process in tumor metastasis [37].

During the data evaluation of the TAS assay, the cell migration is determined after taking serial photographs of the cell-free area at certain intervals. Thereafter, the gaps can be easily assigned using graphical software (e.g., ImageJ) without any previous experience, and then the size of the gap area can be determined using a single measurement command. Nevertheless, this technique is quite time-consuming and monotonous, therefore, we investigated whether manual annotation using a standard computer mouse can be accelerated by a digitizer board (without display) or tablet (with display), or can be replaced by automatic assignment (Figure 6), using macros (described in the methods section). The automatic

annotation resulted in significantly shorter evaluation time per image (Figure 6d), however, optimal macro-options and setups should be previously adjusted in order to enable adequate recognition of gap edges. The automatic analysis proved to be well-applicable in the case of many cell types, including MRC-5 lung fibroblasts, but there are some cells, such as the more flattened NRK-49F renal fibroblasts, with their brightfield images showing lower contrast, causing difficulties in the software-driven automatic annotation of the gaps. To avoid this problem, the flattened cells can be labeled with various non-toxic stains. In our experiments, DiI membrane-dye was used to generate a stable fluorescence signal making it possible to take images with adequate contrast (Figure 6a). In this case, after a small modification in the macros, the automatic annotation became feasible with perfect correlation compared to manual ones (Figure 6b,c).

After setting up the TAS assay, we compared its laboratory use and sensitivity with that of the gold standard scratch assay on EGF-stimulated MRC-5 lung fibroblasts (Figures 7 and 8). The benefits of the 96-well plate-based TAS assay, beside the requirement of fewer raw materials, were immediately conspicuous. Indeed, in the case of TAS the whole gap area fits into a single field-of view of the microscope, which makes the easy automated documentation of the entire gap possible, reducing the need for human resources (Figure 7b). On the contrary, in the case of the scratch assay the process is more complex and the identification of the same area at the different investigated time points is a real challenge [20].

In accordance with the literature, the standard deviation of the initial gap area was about 3-fold higher in the case of the scratch compared to the TAS assay (Figure 7a) [37]. This is a serious limitation since the higher standard deviation of the initial gap area may later result in an even higher standard deviation of the remaining cell-free gap area. Indeed, in line with this consideration, we found that although the kinetics of gap closure is similar in both assays, the TAS assay seemed to have a significantly higher resolution, revealed by the 3-fold smaller deviation of the corresponding gap closure values compared to the scratch assay (Figure 8). To avoid the distortion due to the inconsistent initial gap size, which can appear in case of relative percentage values normalized to the cell-free area at 0 h (Figure 8a,b), the gap closure was also determined by absolute, pixel^2 values (Figure 8c,d). Nevertheless, we found the same difference in the intra-assay variability of the two methods in favor of the TAS assay.

The high accuracy of the TAS assay allows to detect the migration differences even in the early phase of the experiment, such as 3 h after the onset of treatments (Figure 5b). In summary, our results confirmed that the TAS assay is an improved alternative to the scratch assay, retaining its advantages and eliminating most of its limitations (Table 1). However, it should be noted that gap closure-based migration assays, including scratch or TAS assays are dedicated to investigating the collective cell migration, rather than individual single-cell motility. However, this type of cell migration is a hallmark of the tissue remodeling processes, including fibrosis, reepithelization, wound healing, and cancer invasion [40,41]. At this point it had to be noted that, despite their similar elements, the TAS assay should not be confused with the under-agarose method. In the TAS assay the agarose spot represents a mold, which excludes the cells from a certain area during their attachment to the surface of the plate. In contrast, during the under-agarose assay chemotaxis is induced by chemoattractant molecules dissolved in agarose [42–44]. Via the latter method, the individual movement of sperm cells or leukocytes can be modeled and quantified by determining the number of cells that migrated under the permanent agarose.

Finally, we demonstrated the usability of the combination of the TAS migration assay with other assays to investigate the main properties of activated fibroblasts in vitro. In these experiments, although there are commercially available kits, we used our self-optimized, 96-well plate based, cost-effective in vitro assays to determine cell migration, proliferation, and collagen deposition (for more detailed information please see the corresponding section of the methods).

Table 1. Comparison of the advantages (+) and limitations (−) of scratch and TAS migration assays.

Assay Characteristics	Scratch Assay	TAS Assay
Cost-effective	+	+
Minimal equipment	+	+
Easy to perform	+	+
Consistent gap size	−	+
Well reproducible	−	+
Easy gap relocation during repetitive imaging	−	+
Intact cells and plate surface	−	+
Small surface and volumes (96-well plate based)	−	+
Low intra- and inter-assay deviation	−	+
Automatable	−	+

First, we demonstrated that nintedanib, one of the approved drugs against lung fibrosis in IPF, decreases the migration of fibroblast in a dose-dependent manner (Figure 9a–d). As fibroblast migration can be continuously monitored during the TAS assay, even at short, hourly intervals, the experiment can be terminated at any time when significant migration is detected and both the cells, and also their supernatants, can be further analyzed. Indeed, in our present study, at the end of the TAS assay a decreasing effect of nintedanib on the expression of cell cycle regulators was demonstrated by PCR analysis (Figure 9f), revealing its effect on fibroblast proliferation and accumulation [45–47]. We confirmed the antiproliferative effect of nintedanib independently using an MTT assay on PDGF-B-stimulated cells as well (Figure 10a).

Moreover, the SiriusRed assay was also performed to determine the extent of collagen deposition of fibroblasts after their activation with TGF-ß. In this experiment we demonstrated that nintedanib decreases the ECM production of the fibroblasts (Figure 10c).

In addition to the previously described experiments, investigating the activation of fibroblasts, LDH assay was performed to gain further information. Since LDH is an intracellular enzyme, its presence in the supernatant of the cells suggests that the experimental conditions were toxic for the cells, which can significantly influence the result of the discussed assays.

Therefore, during our experiments we measured the LDH activity in the cellular supernatants derived from TAS (Figure 9e), MTT (Figure 10b) and also from SiriusRed (Figure 10d) assays. Thereby, we demonstrated that the observed inhibitory effects of nintedanib were not due to its cytotoxic effect but to its specific effects on fibroblast activation.

Taken together, these simple and cost-effective assays, including TAS, MTT, SiriusRed, and LDH are complementary and have the ability to describe the different aspects of fibroblast activation, including migration, proliferation, and ECM production of the main effector cells of fibrosis.

4. Materials and Methods

4.1. Cell Lines

MRC-5 (#CCL-171) human lung fibroblast, NRK-49F (#CRL-1570) rat kidney fibroblast, A549 (#CRM-CCL-185) human lung epithelial cell, and Caco-2 (#HTB-37) human colon carcinoma cell lines (American Type Culture Collection (ATCC), Manassas, VA, USA) were cultured in Dulbecco's Modified Eagle Medium (Thermo Fisher Scientific, Waltham, MA, USA), HT-29 (#HTB-38) human colon carcinoma cell line (ATCC) was cultured in McCoy's 5A Medium (Thermo Fisher Scientific) supplemented with 10% heat-inactivated fetal bovine serum (FBS) (Invitrogen, Waltham, MA, USA) and 1% penicillin and streptomycin (Merck, Kenilworth, NJ, USA) mixture under standard cell culture conditions (37 °C, humidified, 5% CO_2). During in vitro experiments, recombinant epidermal growth factor (EGF, 10 ng/mL, #236-EG, R&D Systems, Minneapolis, MN, USA), recombinant platelet-derived growth factor B (PDGF-B, 10 ng/mL, #520-BB, R&D Systems), recombinant transforming growth factor beta 1 (TGB-ß, 1 nM, #PHG9204, Thermo Fisher Scientific), and nintedanib (Nint,

0.01–10 μM, Vichem Chemie Research, Budapest, Hungary) were used. Control cells were treated only with the corresponding solvents (EGF, PDGF-B: phosphate buffered saline (PBS), Nint: DMSO, TGF-β: 4 mM HCl) in equal volumes.

4.2. Transient Agarose Spot (TAS) Migration Assay

To perform TAS assay, 2 μL of hot 0.1% agarose (Merck) solution (in sterile H_2O) was placed in the middle of each well of a 96-well tissue culture plate (Sarstedt, Newton, MA, USA), then gel droplets were allowed to polymerize for 15 min at room temperature. Thereafter, cells were seeded (n = 5–8 well/treatment group) at a density to reach near full confluence (2×10^4 cells/well (otherwise indicated) MRC-5, 10^4 cells/well NRK-49F, 2×10^4 cells/well A549, 6×10^4 cells/well Caco-2, 4×10^4 cells/well HT-29). After 24 h of plating, media was removed from cells and the agarose spots were gently aspirated by a 100 μL pipette from above, without touching the cell monolayer (further instruction can be found in Video S1 and in the section 'Tips and tricks'). To remove debris and unattached cells, wells were washed three times with 200 μL sterile PBS. Then, cells were treated with recombinant cytokines and/or compounds diluted in 100 μL culture medium containing 0.1% FBS, unless otherwise indicated. In certain experiments, as an additional part of TAS assay, MRC-5 cells were incubated in 0.1 mg/mL DiI solution (#D282, Thermo Fisher Scientific) for 2 h before the agarose removal and treatments. The main steps of TAS assay are illustrated in Video S1.

4.3. Scratch Assay

To perform scratch assay [18], MRC-5 cells were seeded (n = 6 well/treatment group) into 12-well tissue culture plates (Sarstedt) at a density of 4×10^5 cells/well. After 24 h of plating, media were aspired from cells and the monolayer was scratched with a single decisive movement using a 200 μL pipette tip. To remove debris and unattached cells, wells were washed three times with 2 mL sterile PBS. Then, cells were treated with recombinant EGF diluted in 1 mL culture medium containing 0.1% FBS.

4.4. Data Acquisition

Brightfield or fluorescence images of each well were taken using an Olympus IX81 microscope system (Olympus Corporation, Tokyo, Japan) at various time points after the treatments. Cell-free gap areas were annotated manually by standard computer mouse, digitizer board without display or tablet or automatically and measured using ImageJ 1.48v software (National Institutes of Health, Bethesda, Rockville, MD, USA), finally determined as a ratio (%) of initial gap area at 0 h:

$$\text{gap area } [\%] = \frac{\text{actual gap area}}{\text{initial gap area}} \times 100 \quad (1)$$

In some cases, the gap closure was described by the absolute value decrease in cell-free area:

$$\Delta\text{gap area } \left[\text{pixel}^2\right] = \text{initial gap area} - \text{actual gap area} \quad (2)$$

During automatic data analysis, the following macros were used. ***Highlighted parameters*** were set up and verified in each individual experiment.

- Brightfield images:

```
run("Find Edges");
setAutoThreshold("Default");
//run("Threshold...");
setThreshold(0, 20);
run("Analyze Particles...", "size=2,000,000-Infinity show=Outlines summarize");
close();
```

- Fluorescence images:

```
run("RGB Stack");
run("Next Slice [>]");
run("Delete Slice");
run("Next Slice [>]");
run("Delete Slice");
run("Find Edges", "slice");
setAutoThreshold("Default");
//run("Threshold...");
setThreshold(0, 20);
run("Analyze Particles...", "size=2,000,000-Infinity show=Outlines display clear
summarize slice");
close();
```

4.5. Cell Confluency

To determine the cell confluency, cells were labeled with DiI as described above in the section 'Transient agarose spot (TAS) migration assay'. Thereafter fluorescent images were taken with wide field of view and analyzed using ImageJ software. During the data acquisition, the extent of black pixels was measured using 'color threshold' and 'measure' commands, the gel spot area was determined by annotation, and the confluency was calculated based on the following equation:

$$\text{confluency } [\%] = \left(1 - \frac{\text{black pixel area} - \text{gel spot area}}{\text{total area} - \text{gel spot area}}\right) \times 100 \quad (3)$$

4.6. LDH Cytotoxicity Assay

The extent of cell death was determined by a colorimetric method, based on the lactate dehydrogenase (LDH) enzyme activity in the supernatant, released from damaged cells [48]. Equal volumes (40 µL) of aspired media were mixed in a sterile 96-well plate with LDH reagent, containing 109 mM lactate, 3.3 mM ß-nicotinamide-adenine-dinucleotide-hydrate (#N7004), 2.2 U/mL diaphorase (#D2197), 3 mM TRIS, 30 mM HEPES, 10 mM NaCl, 350 µM thiazolyl blue tetrazolium bromide (all reagents were purchased from Merck), then incubated at 37 °C for 1 h. Absorbance was recorded at 570 nm and at 690 nm as background in a SPECTROstar Nano microplate reader using SPECTROstar Nano MARS v3.32 software (BMG Labtech, Ortenberg, Germany).

4.7. MTT Cell Proliferation Assay

To perform MTT assay, MRC-5 cells were seeded (n = 6 well/treatment group) into 96-well tissue culture plates at a density of 4×10^3 cells/well. After 24 h of plating, cells were treated for 24 h with recombinant PDGF-B in the absence or presence of nintedanib diluted in culture medium containing 0.1% FBS.

The rate of cell proliferation was determined by a colorimetric method, based on the intracellular mitochondrial dehydrogenase activity of the attached cells [49]. Then, 10 µL of MTT reagent, containing 5 mg/mL thiazolyl blue tetrazolium bromide (diluted in sterile H_2O) was added into each well including cells and 100 µL of supernatant as well, then incubated at 37 °C for 4 h. Thereafter, the supernatants were removed from cells using a pipette, and the intracellular MTT crystals were dissolved by adding 100 µL 1:1 mixture of DMSO and ethanol (all reagents were purchased from Merck). Absorbance was recorded at 570 nm and at 690 nm as background in a SPECTROstar Nano microplate reader using SPECTROstar Nano MARS v3.32 software.

4.8. SiriusRed Collagen Detection Assay

To perform SiriusRed assay, MRC-5 cells were seeded (n = 6 well/treatment group) into 96-well tissue culture plates at a density of 10^4 cells/well. After 24 h of plating, cells

were treated for 48 h with recombinant TGF-ß in the absence or presence of nintedanib diluted in culture medium containing 0.1% FBS and 100 µM ascorbate (Merck).

The collagen deposition was determined based on a basic histological dye SiriusRed, incorporating into the triple helical collagen molecules [50]. After removing supernatants, cells were incubated in a fixative solution containing 26% EtOH, 3.7% formaldehyde, 2% glacial acetic acid for 15 min at room temperature. Samples were stained for 1 h at room temperature with 0.1% solution of SiriusRed (DirectRed80) dissolved in 1% acetic acid, then washed three times with 200 µL of 0.1 M HCl, and finally the bounded dye was dissolved by adding 100 µL of 0.1 M NaOH (all reagents were purchased from Merck). Absorbance was recorded at 544 nm and at 690 nm as background in a SPECTROstar Nano microplate reader using SPECTROstar Nano MARS v3.32 software.

4.9. RNA Isolation and cDNA Synthesis

Total RNA was isolated from MRC-5 cells by Geneaid Total RNA Mini Kit (Geneaid Biotech, New Taipei City, Taiwan). Equal RNA was reverse-transcribed using Maxima First Strand cDNA Synthesis Kit for RT-qPCR (Thermo Fisher Scientific) to generate first-stranded cDNA. The mRNA expressions were determined by real-time PCR using LightCycler 480 SYBR Green I Master enzyme mix on a LightCycler 96 system (Roche Diagnostics, Indianapolis, IN, USA). PCR primers (Table 2) were designed as previously described [51,52] and synthetized by Integrated DNA Technologies (IDT, Coralville, IA, USA). Results were analyzed using LightCycler 96 software v1.1.0.1320 (Roche Diagnostics). Relative mRNA expression was determined by comparison with *RN18S* as internal control using the ΔΔCt method [53]. Data were normalized and presented as the ratio of their control group values.

Table 2. Nucleotide sequences of primer pairs applied for the real-time PCR detection.

Gene	NCBI Ref. Seq.	Primer Pairs
MKI67	NM_002417.4	F: 5′-CCC CTA CGG ATT ATA CTC AAC TTA-3′ R: 5′-TGT AAT ATT GCC TCC TGC TCA T-3′
PCNA	NM_002592.2	F: 5′-GCG GTC TGA GGG CTT CGA CAC CTA-3′ R: 5′-CCG CGT TAT CTT CGG CCC TTA GTG-3′
RN18S	HQ387008.1	F: 5′-GGC GGC GAC GAC CCA TTC-3′ R: 5′-TGG ATG TGG TAG CCG TTT CTC AGG-3′

Abbreviations: ref. seq.: reference sequence; F: forward; R: reverse.

4.10. Statistical Analysis

Statistical evaluation of data was performed using GraphPad Prism 8.01 software (GraphPad Software Inc., San Diego, CA, USA) using an ordinary one-way or two-way ANOVAs with Dunnett's tests for multiple comparisons and Pearson's correlation for correlation analyses. $p \leq 0.05$ was considered as statistically significant. Unless otherwise indicated, results are illustrated as mean ± SD of the corresponding treatment groups. The applied tests, significances, and number of elements (n) are indicated in each figure legend.

5. Conclusions

In summary, in the present study we presented a new 96-well plate based TAS assay, developed to investigate fibroblast migration. We also demonstrated the combined use of a set of in vitro assays, which can be used in fibrosis-related basic research, and even in high-throughput drug screenings. These functional assays together widely describe the main properties of fibroblasts, including migration, proliferation, viability, and collagen deposition, thereby contributing to an increasingly urgent understanding of the scarring process.

6. Tips and Tricks for TAS Assay

- Working with hot fluids may cause pipetting inaccuracies → after boiling, agarose solution should be left for about 10 min to cool down.
- Electrostatic charging may cause difficulties in agarose dropping → static electricity should be eliminated by a grounded device or ionizing bar.
- Drop size can be decreased in order to achieve more spectacular relative values ←→ however, 2 µL droplets are optimal for microscopy using a 4× objective, and the smaller the volume is, the harder it is to ensure pipetting accuracy.
- The pipetting of agarose spots can be accelerated by using multichannel pipettes.
- Drying-up of agarose spots results in improper cell-free area-making → plates should be kept covered during gel polymerization phase.
- Some cell types (e.g., large, flat fibroblasts) may attach in a shorter amount of time → the cell seeding step can be shortened to 3–4 h instead of overnight.
- Some cell types (e.g., small, rounded carcinoma cells) may attach less strongly → the washing step should be gentle but thorough to eliminate floating cells, which could form colonies in the cell-free area.
- During the removal of agarose spots, the pipette tip should be carefully approached to the top of the gel. At the moment of contact, the refraction of the gel will change, and it can be sucked by a single movement.

Supplementary Materials: The following supporting information can be downloaded at: https://www.mdpi.com/article/10.3390/ijms23042119/s1.

Author Contributions: Conceptualization, A.V.-S. and Á.V.; methodology, A.V.-S.; formal analysis, C.S., E.L. and C.P.; resources, L.Ő. and A.J.S.; writing—original draft preparation, A.V.-S. and Á.V.; writing—review and editing, D.P., B.S.; funding acquisition, Á.V. and A.J.S. All authors have read and agreed to the published version of the manuscript.

Funding: This research was funded by Semmelweis University, STIA-KFI-2020 (61830-96319); National Research, Development and Innovation Office (NKFIH) 2020-4.1.1-TKP2020, TKP2020-NKA-09, TKP2020-NKA-13, TKP2021-EGA-24, 20382-3/2018 FEKUTSTRAT, K124549, K125470, FIKP (61830-69271) grants.

Institutional Review Board Statement: Not applicable.

Informed Consent Statement: Not applicable.

Data Availability Statement: Data is contained within the article or supplementary material.

Acknowledgments: We are grateful to Mária Bernáth for her excellent technical assistance.

Conflicts of Interest: The authors declare no conflict of interest.

References

1. Meltzer, E.B.; Noble, P.W. Idiopathic pulmonary fibrosis. *Orphanet J. Rare Dis.* **2008**, *3*, 8. [CrossRef]
2. Barratt, S.L.; Creamer, A.; Hayton, C.; Chaudhuri, N. Idiopathic pulmonary fibrosis (IPF): An overview. *J. Clin. Med.* **2018**, *7*, 201. [CrossRef]
3. Wynn, T.A. Common and unique mechanisms regulate fibrosis in various fibroproliferative diseases. *J. Clin. Investig.* **2007**, *117*, 524–529. [CrossRef] [PubMed]
4. Wynn, T.A. Fibrotic disease and the TH 1/TH 2 paradigm. *Nat. Rev. Immunol.* **2004**, *4*, 583–594. [CrossRef] [PubMed]
5. The Gene Ontology resource: Enriching a GOld mine. *Nucleic Acids Res.* **2021**, *49*, D325–D334. [CrossRef]
6. Ashburner, M.; Ball, C.A.; Blake, J.A.; Botstein, D.; Butler, H.; Cherry, J.M.; Davis, A.P.; Dolinski, K.; Dwight, S.S.; Eppig, J.T. Gene ontology: Tool for the unification of biology. *Nat. Genet.* **2000**, *25*, 25–29. [CrossRef] [PubMed]
7. Hinz, B.; Celetta, G.; Tomasek, J.J.; Gabbiani, G.; Chaponnier, C. Alpha-smooth muscle actin expression upregulates fibroblast contractile activity. *Mol. Biol. Cell* **2001**, *12*, 2730–2741. [CrossRef] [PubMed]
8. Hinz, B.; Dugina, V.; Ballestrem, C.; Wehrle-Haller, B.; Chaponnier, C. α-Smooth muscle actin is crucial for focal adhesion maturation in myofibroblasts. *Mol. Biol. Cell* **2003**, *14*, 2508–2519. [CrossRef] [PubMed]
9. Hinz, B. Formation and function of the myofibroblast during tissue repair. *J. Investig. Dermatol.* **2007**, *127*, 526–537. [CrossRef]
10. Rokonay, R.; Veres-Székely, A.; Szebeni, B.; Pap, D.; Lippai, R.; Béres, N.J.; Veres, G.; Szabó, A.J.; Vannay, Á. Role of IL-24 in the mucosal remodeling of children with coeliac disease. *J. Transl. Med.* **2020**, *18*, 36. [CrossRef]

11. McDougall, S.; Dallon, J.; Sherratt, J.; Maini, P. Fibroblast migration and collagen deposition during dermal wound healing: Mathematical modelling and clinical implications. *Philos. Trans. R. Soc. A Math. Phys. Eng. Sci.* **2006**, *364*, 1385–1405. [CrossRef]
12. Herrera, J.; Henke, C.A.; Bitterman, P.B. Extracellular matrix as a driver of progressive fibrosis. *J. Clin. Investig.* **2018**, *128*, 45–53. [CrossRef]
13. Jun, J.-I.; Lau, L.F. Resolution of organ fibrosis. *J. Clin. Investig.* **2018**, *128*, 97–107. [CrossRef]
14. Richeldi, L.; Collard, H.R.; Jones, M.G. Idiopathic pulmonary fibrosis. *Lancet* **2017**, *389*, 1941–1952. [CrossRef]
15. Behr, J.; Prasse, A.; Wirtz, H.; Koschel, D.; Pittrow, D.; Held, M.; Klotsche, J.; Andreas, S.; Claussen, M.; Grohé, C. Survival and course of lung function in the presence or absence of antifibrotic treatment in patients with idiopathic pulmonary fibrosis: Long-term results of the INSIGHTS-IPF registry. *Eur. Respir. J.* **2020**, *56*, 1902279. [CrossRef] [PubMed]
16. Vega-Avila, E.; Pugsley, M.K. An overview of colorimetric assay methods used to assess survival or proliferation of mammalian cells. In Proceedings of the Western Pharmacology Society, Mexico City, Mexico, 16–20 May 2011; pp. 10–14.
17. Chen, C.Z.; Raghunath, M. Focus on collagen: In vitro systems to study fibrogenesis and antifibrosis _ state of the art. *Fibrogenesis Tissue Repair* **2009**, *2*, 7. [CrossRef]
18. Grada, A.; Otero-Vinas, M.; Prieto-Castrillo, F.; Obagi, Z.; Falanga, V. Research techniques made simple: Analysis of collective cell migration using the wound healing assay. *J. Investig. Dermatol.* **2017**, *137*, e11–e16. [CrossRef]
19. Xu, J.; Wang, X.; Li, X.; Yang, G.; Luo, C. High-throughput cell migration assay under combinatorial chemical environments by a novel 24-well-plate based device. *Biomed. Microdevices* **2020**, *22*, 40. [CrossRef] [PubMed]
20. De Ieso, M.L.; Pei, J.V. An accurate and cost-effective alternative method for measuring cell migration with the circular wound closure assay. *Biosci. Rep.* **2018**, *38*, BSR20180698. [CrossRef]
21. Jonkman, J.E.; Cathcart, J.A.; Xu, F.; Bartolini, M.E.; Amon, J.E.; Stevens, K.M.; Colarusso, P. An introduction to the wound healing assay using live-cell microscopy. *Cell Adhes. Migr.* **2014**, *8*, 440–451. [CrossRef]
22. Lv, X.; Geng, Z.; Fan, Z.; Wang, S.; Pei, W.; Chen, H. A PDMS Device Coupled with Culture Dish for In Vitro Cell Migration Assay. *Appl. Biochem. Biotechnol.* **2018**, *186*, 633–643. [CrossRef]
23. Zhang, H.; Fu, W.; Xu, Z. Re-epithelialization: A key element in tracheal tissue engineering. *Regen. Med.* **2015**, *10*, 1005–1023. [CrossRef]
24. Iizuka, M.; Konno, S. Wound healing of intestinal epithelial cells. *World J. Gastroenterol.* **2011**, *17*, 2161–2171. [CrossRef] [PubMed]
25. Rousselle, P.; Braye, F.; Dayan, G. Re-epithelialization of adult skin wounds: Cellular mechanisms and therapeutic strategies. *Adv. Drug Deliv. Rev.* **2019**, *146*, 344–365. [CrossRef] [PubMed]
26. Gritsenko, P.G.; Ilina, O.; Friedl, P. Interstitial guidance of cancer invasion. *J. Pathol.* **2012**, *226*, 185–199. [CrossRef] [PubMed]
27. Krakhmal, N.V.; Zavyalova, M.; Denisov, E.; Vtorushin, S.; Perelmuter, V. Cancer invasion: Patterns and mechanisms. *Acta Nat.* **2015**, *7*, 17–28. [CrossRef]
28. Lederer, D.J.; Martinez, F.J. Idiopathic pulmonary fibrosis. *N. Engl. J. Med.* **2018**, *378*, 1811–1823. [CrossRef]
29. Suganuma, H.; Sato, A.; Tamura, R.; Chida, K. Enhanced migration of fibroblasts derived from lungs with fibrotic lesions. *Thorax* **1995**, *50*, 984–989. [CrossRef]
30. Vancheri, C. Idiopathic pulmonary fibrosis: An altered fibroblast proliferation linked to cancer biology. *Proc. Am. Thorac. Soc.* **2012**, *9*, 153–157. [CrossRef]
31. Burgess, J.K.; Mauad, T.; Tjin, G.; Karlsson, J.C.; Westergren-Thorsson, G. The extracellular matrix–the under-recognized element in lung disease? *J. Pathol* **2016**, *240*, 397–409. [CrossRef]
32. Liang, C.-C.; Park, A.Y.; Guan, J.-L. In vitro scratch assay: A convenient and inexpensive method for analysis of cell migration in vitro. *Nat. Protoc.* **2007**, *2*, 329–333. [CrossRef]
33. Kam, Y.; Guess, C.; Estrada, L.; Weidow, B.; Quaranta, V. A novel circular invasion assay mimics in vivo invasive behavior of cancer cell lines and distinguishes single-cell motility in vitro. *BMC Cancer* **2008**, *8*, 198. [CrossRef]
34. Stamm, A.; Reimers, K.; Strauß, S.; Vogt, P.; Scheper, T.; Pepelanova, I. In vitro wound healing assays–state of the art. *BioNanoMaterials* **2016**, *17*, 79–87. [CrossRef]
35. Salati, M.A.; Khazai, J.; Tahmuri, A.M.; Samadi, A.; Taghizadeh, A.; Taghizadeh, M.; Zarrintaj, P.; Ramsey, J.D.; Habibzadeh, S.; Seidi, F. Agarose-based biomaterials: Opportunities and challenges in cartilage tissue engineering. *Polymers* **2020**, *12*, 1150. [CrossRef] [PubMed]
36. Zarrintaj, P.; Manouchehri, S.; Ahmadi, Z.; Saeb, M.R.; Urbanska, A.M.; Kaplan, D.L.; Mozafari, M. Agarose-based biomaterials for tissue engineering. *Carbohydr. Polym.* **2018**, *187*, 66–84. [CrossRef]
37. Pijuan, J.; Barceló, C.; Moreno, D.F.; Maiques, O.; Sisó, P.; Marti, R.M.; Macià, A.; Panosa, A. In vitro cell migration, invasion, and adhesion assays: From cell imaging to data analysis. *Front. Cell Dev. Biol.* **2019**, *7*, 107. [CrossRef] [PubMed]
38. Ware, M.F.; Wells, A.; Lauffenburger, D.A. Epidermal growth factor alters fibroblast migration speed and directional persistence reciprocally and in a matrix-dependent manner. *J. Cell Sci.* **1998**, *111*, 2423–2432. [CrossRef]
39. Yu, J.; Moon, A.; Kim, H.-R.C. Both platelet-derived growth factor receptor (PDGFR)-α and PDGFR-β promote murine fibroblast cell migration. *Biochem. Biophys. Res. Commun.* **2001**, *282*, 697–700. [CrossRef]
40. Friedl, P.; Gilmour, D. Collective cell migration in morphogenesis, regeneration and cancer. *Nat. Rev. Mol. Cell Biol.* **2009**, *10*, 445–457. [CrossRef]
41. Haeger, A.; Wolf, K.; Zegers, M.M.; Friedl, P. Collective cell migration: Guidance principles and hierarchies. *Trends Cell Biol.* **2015**, *25*, 556–566. [CrossRef]

42. Heit, B.; Kubes, P. Measuring chemotaxis and chemokinesis: The under-agarose cell migration assay. *Sci. STKE* **2003**, *2003*, pl5. [CrossRef]
43. Brazill, D. Chemotaxis: Under Agarose Assay. In *Cytoskeleton Methods and Protocols*; Springer: Cham, Switzerland, 2016; pp. 339–346.
44. Ahmed, M.; Basheer, H.A.; Ayuso, J.M.; Ahmet, D.; Mazzini, M.; Patel, R.; Shnyder, S.D.; Vinader, V.; Afarinkia, K. Agarose spot as a comparative method for in situ analysis of simultaneous chemotactic responses to multiple chemokines. *Sci. Rep.* **2017**, *7*, 1075. [CrossRef]
45. Weng, T.; Poth, J.M.; Karmouty-Quintana, H.; Garcia-Morales, L.J.; Melicoff, E.; Luo, F.; Chen, N.-y.; Evans, C.M.; Bunge, R.R.; Bruckner, B.A. Hypoxia-induced deoxycytidine kinase contributes to epithelial proliferation in pulmonary fibrosis. *Am. J. Respir. Crit. Care Med.* **2014**, *190*, 1402–1412. [CrossRef] [PubMed]
46. Sun, X.; Kaufman, P.D. Ki-67: More than a proliferation marker. *Chromosoma* **2018**, *127*, 175–186. [CrossRef] [PubMed]
47. Maga, G.; Hubscher, U. Proliferating cell nuclear antigen (PCNA): A dancer with many partners. *J. Cell Sci.* **2003**, *116*, 3051–3060. [CrossRef] [PubMed]
48. Korzeniewski, C.; Callewaert, D.M. An enzyme-release assay for natural cytotoxicity. *J. Immunol. Methods* **1983**, *64*, 313–320. [CrossRef]
49. Mosmann, T. Rapid colorimetric assay for cellular growth and survival: Application to proliferation and cytotoxicity assays. *J. Immunol. Methods* **1983**, *65*, 55–63. [CrossRef]
50. Walsh, B.J.; Thornton, S.C.; Penny, R.; Breit, S.N. Microplate reader-based quantitation of collagens. *Anal. Biochem.* **1992**, *203*, 187–190. [CrossRef]
51. Veres-Székely, A.; Pap, D.; Szikszi, E.; Jávorszky, E.; Rokonay, R.; Lippai, R.; Tory, K.; Fekete, A.; Tulassay, T.; Szabó, A.J. Selective measurement of α smooth muscle actin: Why β-actin can not be used as a housekeeping gene when tissue fibrosis occurs. *BMC Mol. Biol.* **2017**, *18*, 12. [CrossRef]
52. Veres-Szekely, A.; Bernath, M.; Pap, D.; Rokonay, R.; Szebeni, B.; Takacs, I.M.; Lippai, R.; Cseh, A.; Szabo, A.J.; Vannay, A. PARK7 Diminishes Oxidative Stress-Induced Mucosal Damage in Celiac Disease. *Oxid Med. Cell Longev.* **2020**, *2020*, 4787202. [CrossRef]
53. Livak, K.J.; Schmittgen, T.D. Analysis of relative gene expression data using real-time quantitative PCR and the $2^{-\Delta\Delta CT}$ method. *Methods* **2001**, *25*, 402–408. [CrossRef]

International Journal of
Molecular Sciences

MDPI

Article

Improvement in Transient Agarose Spot (TAS) Cell Migration Assay: Microplate-Based Detection and Evaluation

Apor Veres-Székely [1,2,*], Csenge Szász [1], Domonkos Pap [1,2], Péter Bokrossy [1], Dorina Lenzinger [3], Tamás Visnovitz [3,4], Judith Mihály [5], Marcell Pálmai [5], Zoltán Varga [5,6], László Őrfi [7], Attila J. Szabó [1,2], Ádám Vannay [1,2] and Beáta Szebeni [1,2]

1 Pediatric Center, Semmelweis University, 1083 Budapest, Hungary
2 HUN-REN-SU Pediatrics and Nephrology Research Group, 1052 Budapest, Hungary
3 Institute of Genetics, Cell and Immunobiology, Semmelweis University, 1089 Budapest, Hungary
4 Department of Plant Physiology and Molecular Plant Biology, ELTE Eötvös Loránd University, 1117 Budapest, Hungary
5 TTK Biological Nanochemistry Research Group, Institute of Materials and Environmental Chemistry, Research Centre for Natural Sciences, 1117 Budapest, Hungary
6 Department of Physical Chemistry and Materials Science, Faculty of Chemical Technology and Biotechnology, Budapest University of Technology and Economics, 1111 Budapest, Hungary
7 Vichem Chemie Research Ltd., 1022 Budapest, Hungary
* Correspondence: veres-szekely.apor@semmelweis.hu

Abstract: Collective cell migration is crucial in various biological processes, including tumor progression and metastasis. The widely used scratch assay (wound healing assay) has limitations in throughput, reproducibility, and data analysis. To overcome these challenges, we previously developed the Transient Agarose Spot (TAS) assay, which enhanced assay precision and reproducibility. In this study, we present an improved microplate-based TAS assay. By using a microplate reader, we automated data acquisition, enabling the detection of cell migration in a 96-well plate format with greater throughput and accuracy. The new method applies Hoechst staining to label viable cells, providing a stable signal for kinetic analysis without compromising cell viability. We validated this approach with fluorophore-expressing cancer cells and demonstrated its ability to monitor dose-dependent effects of fetal bovine serum on cell migration. Additionally, we applied the microplate-based TAS assay to assess the anti-migratory effects of kinase inhibitors and mesenchymal stem cell-derived extracellular vesicles (EVs) on lung cancer cells. The assay accurately quantified migration inhibition and revealed the concentration-dependent effects of EVs, highlighting their potential as therapeutic agents. This microplate-based TAS assay provides a scalable, efficient, and cost-effective platform for high-throughput screening of cell migration and drug discovery, offering a robust alternative to traditional microscopy-based methods.

Keywords: cell migration; TAS assay; microplate reader; Hoechst

Academic Editor: Riccardo Alessandro

Received: 30 April 2025
Revised: 6 June 2025
Accepted: 9 June 2025
Published: 11 June 2025

Citation: Veres-Székely, A.; Szász, C.; Pap, D.; Bokrossy, P.; Lenzinger, D.; Visnovitz, T.; Mihály, J.; Pálmai, M.; Varga, Z.; Őrfi, L.; et al. Improvement in Transient Agarose Spot (TAS) Cell Migration Assay: Microplate-Based Detection and Evaluation. *Int. J. Mol. Sci.* **2025**, *26*, 5584. https://doi.org/10.3390/ijms26125584

1. Introduction

Collective cell migration is a fundamental biological process that plays a crucial role in various physiological and pathological conditions, including tumor progression [1]. The ability of cancer cells to migrate and invade surrounding tissues is a hallmark of malignancy and a major determinant of prognosis [2]. Understanding the mechanisms of cancer cell migration is essential for identifying therapeutic targets and developing novel treatment strategies aimed at limiting metastasis. While traditional microscopy-based methods, particularly the widely used scratch assay, have been extensively used

to study cell migration, their inherent limitations, such as low throughput and labor-intensive protocols, restrict their utility in both basic and applied cancer research [3–5]. In our previous work, we developed the Transient Agarose Spot (TAS) cell migration assay, which offered enhanced analytical precision and reproducibility compared to the gold-standard scratch assay [4]. Although most limitations of the scratch assay were eliminated, data acquisition still relied on microscopy, requiring expensive equipment systems and time-consuming manual work for high-throughput screening.

As phenotypic readouts such as cell migration offer integrative biological insight, phenotype-based cellular assays have gained prominence in early-stage drug discovery. These assays are increasingly recognized as valuable tools in preclinical drug development, particularly for their ability to capture complex biological responses beyond single-target effects. These assays support untargeted screening, enabling the discovery of novel mechanisms of action and phenotypic effects that might be overlooked by target-based approaches [6,7]. They are widely used for hit identification, triaging, and lead optimization, and their effectiveness depends on thoughtful assay design, the use of appropriate chemical libraries, and robust strategies for hit validation [8].

Here, we present an improved version of the TAS assay, transitioning from microscopy-based detection to a microplate-based system. This new approach significantly enhances the throughput and efficiency of the cell migration assay while preserving its sensitivity, reliability, and accuracy.

2. Results

2.1. Data Acquisition by Microplate Reader

To determine the area of cell-free zones, the wells of the TAS assay containing stained cells were detected using the "well scanning" mode of the microplate reader. The resulting heatmap comprised 708 scanning points, capturing a data range of absorbance or fluorescence that transitions sharply from the cell-free area to full confluency. The area of cell-free zones was determined by setting a threshold value to define the edge of the examined area and by quantifying the points below this threshold (Figure 1a). The optimal threshold was between 10 and 25% of the maximal intensity values, within which the resulting cell-free areas exhibited a perfect correlation with each other (Figure 1b).

To validate the detection method, an entire TAS assay plate containing RFP- and GFP-expressing HCT-116 cells was scanned using both a microplate reader and microscopy (Figure 1c,d). The calculated areas showed perfect correlation between the two methods. Furthermore, microplate-based detection of RFP- and GFP-expressing HCT-116 cells stimulated with a dilution series of FBS yielded linear dose–response relationships with very high correlation coefficients (Figure 1e).

Non-fluorescent cells were first scanned in their native, unstained state using a microplate reader by measuring absorbance in the UV range. However, detection was only reliable in a medium-free environment, requiring the replacement of the culture medium with PBS. To enhance visualization, various colorimetric and fluorescent staining methods were applied, all of which were detectable with a microplate reader (Figure 1f). These methods provided clear visualization, allowing the edge of the cell-free area to be precisely defined.

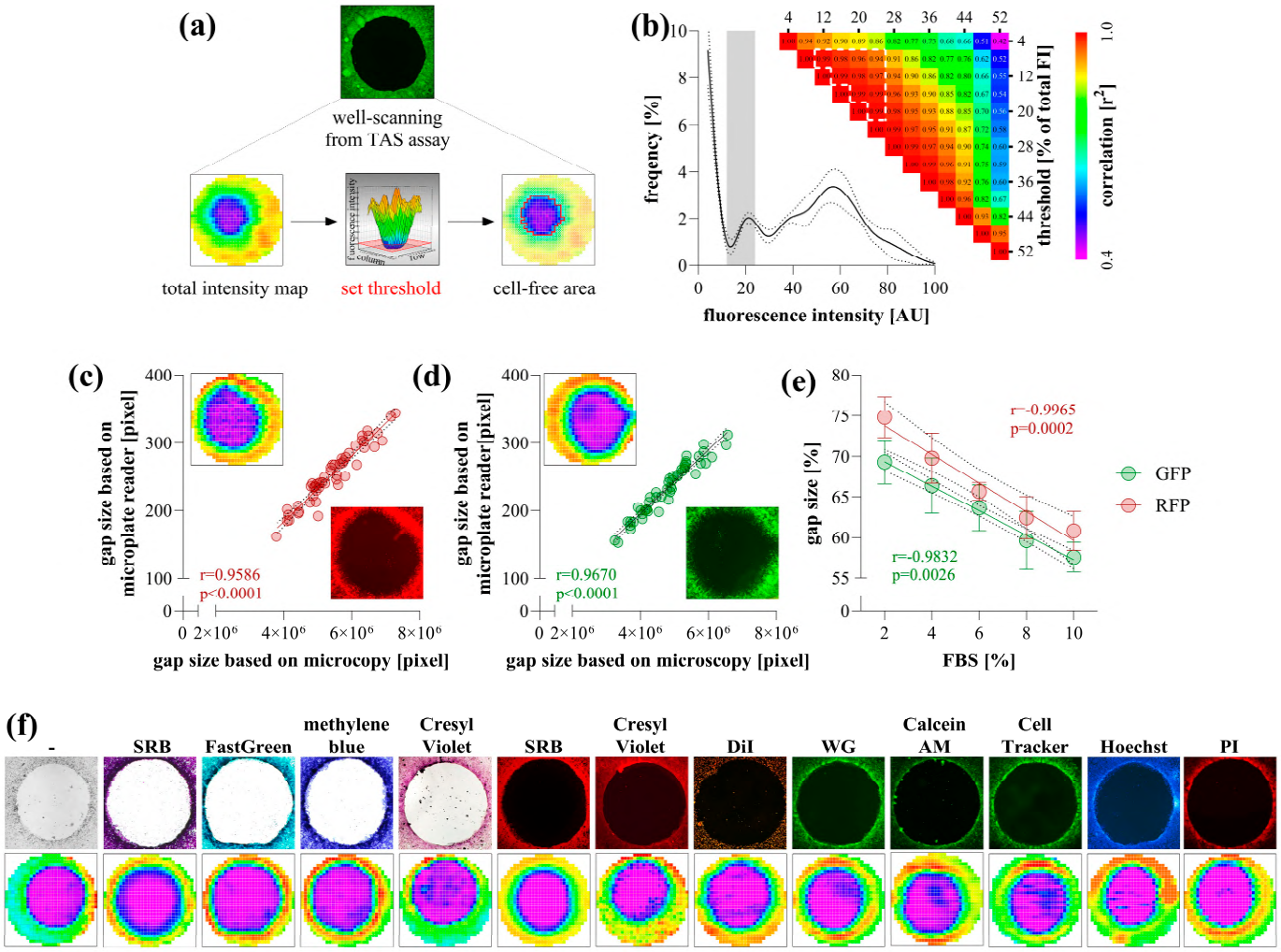

Figure 1. Data acquisition of transient agarose spot (TAS) assay using microplate reader. The well-scanning mode of the microplate reader generates an intensity heatmap of a whole well, where the cell-free area can be defined by setting a threshold value (**a**). The accuracy of threshold selection was evaluated using TAS assay wells containing GFP-expressing HCT-116 cells (n = 50) (**b**). Based on the intensity distribution of heatmap pixels, different threshold values were selected to determine cell-free areas, and a correlation matrix was generated. A nearly perfect correlation was observed for threshold values between 10 and 25% of the maximal intensity (highlighted with white outline). Validation of the microplate-based detection was carried out by correlating gap sizes with microscopy-based measurements for RFP- (**c**) and GFP-expressing (**d**) HCT-116 cells (n = 50). The applicability of microplate reader-based quantification was investigated on RFP- and GFP-expressing HCT-116 cells after their stimulation with a dilution series of fetal bovine serum (FBS) for 72 h (n = 10/group) (**e**). Various colorimetric and fluorescent stains were tested on non-fluorescent HCT-116 cells (**f**). The same wells were captured by microscopy (top, using 4× magnification) and microplate reader (bottom). Heatmaps represent well-scanning fluorescence intensity data, where color gradients correlate with signal strength across the scanned area. Significance values (*p*) and Pearson's correlation coefficients (r) are indicated.

2.2. Optimization of Hoechst Staining

The applicability of Hoechst staining for microplate-based detection was verified on RFP-, GFP-expressing, and native HCT-116 colon cancer cells. The gap areas determined based on the Hoechst fluorescence signal detected by the microplate reader showed a high correlation with RFP or GFP signals, as well as the gap size quantified by microscopy (Figure 2a).

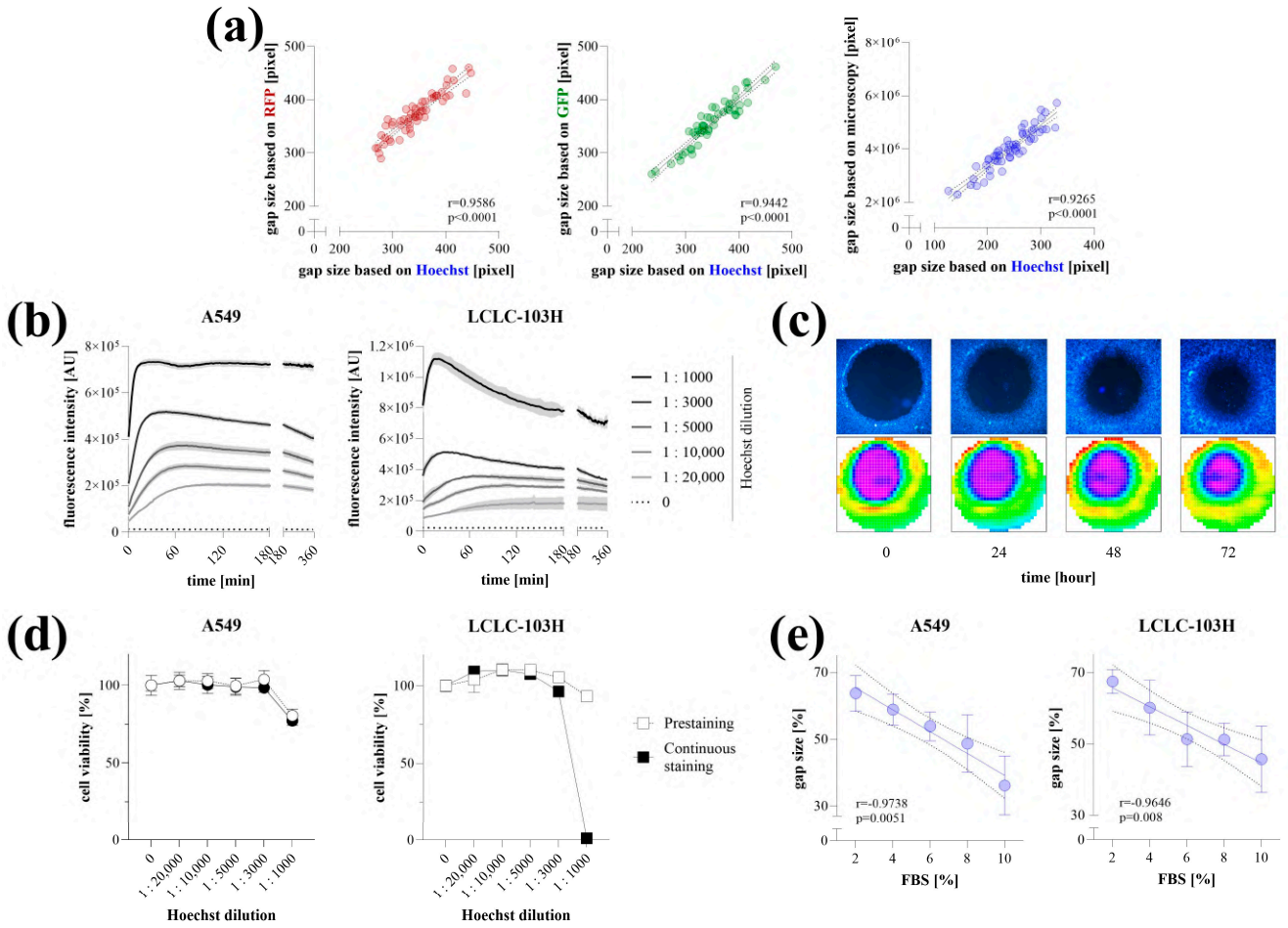

Figure 2. Optimization of Hoechst-staining. Validation of Hoechst staining for microplate-based detection was carried out in fluorescent and native HCT-116 cells (**a**). Gap areas determined by Hoechst fluorescence intensity (pre-stained cells for 4 h at 1:10,000 concentration) were correlated with RFP and GFP signals, as well as microscopy-based quantification (n = 50, using 4× magnification). Staining kinetics with various Hoechst concentrations were investigated on A549 and LCLC-103H cells (n = 5/group) with two-minute interval detection (**b**). The stability of Hoechst fluorescence signal and its detection with microscope (top) or microplate reader (bottom) was investigated for 72 h (**c**). The cytotoxicity of Hoechst staining was investigated on A549 and LCLC-103H cells using MTT cell viability assay following a 4 h prestaining or continuous staining for 72 h at 1:10,000 concentration (**d**). The applicability of microplate reader-based quantification was investigated on Hoechst-stained A549 and LCLC-103H cells after their stimulation with a dilution series of fetal bovine serum (FBS) for 72 h (n = 10/group) (**e**). Heatmaps represent well-scanning fluorescence intensity data, where color gradients correlate with signal strength across the scanned area. Results are presented as mean ± SD. Significance values (p) and Pearson's correlation coefficients (r) are indicated.

The Hoechst staining of living cells was optimized on A549 and LCLC-103H lung cancer cells. We found that even very low dye concentrations (1:20,000, 1:10,000) resulted in a stable fluorescence signal, whereas higher concentrations initially produced higher intensity, which decreased over time before finally settling at a similar value (Figure 2b). Fluorescence was detectable even 72 h after staining the cells with Hoechst at a 1:10,000 dilution for 4 h (Figure 2c). Cytotoxic effects of Hoechst staining were observed only at high concentrations, specifically when the dye-containing culture medium was not replaced after the 4 h incubation period (Figure 2d). The microplate-based detection of Hoechst-stained cells stimulated with a dilution series of FBS for 72 h yielded linear dose–response relationships with very high correlation coefficients (Figure 2e).

2.3. Representative Experiments

Representative experiments were conducted on Hoechst-stained A549 lung cancer cells stimulated with 10% FBS, with data acquisition performed using a microplate reader. Kinase inhibitors, including gefitinib, nintedanib, and sorafenib, reduced cell migration in a dose-dependent manner (Figure 3a). Similarly, EV1 and EV2 extracellular vesicles, isolated from the supernatant of MSCs, inhibited the migration of A549 cells. However, this effect was diminished at high nanoparticle concentrations (Figure 3b,c). The properties of EV1 (Figure 3d) and EV2 (Figure 3e) were characterized using various analyses. Based on NTA measurements, the average particle sizes for both samples were approximately 150 nm, with a concentration of 1–2 × 10^{10} particles/mL. After buffer subtraction, surface-enhanced IR spectra of the samples revealed characteristic absorption bands of EVs, indicating a typical protein-to-lipid ratio. TEM imaging demonstrated a typical morphology of a small EV fraction. The presence of ALIX and CD81, labeled with 5 nm and 10 nm gold particles, respectively, was detectable on the surface of the EVs.

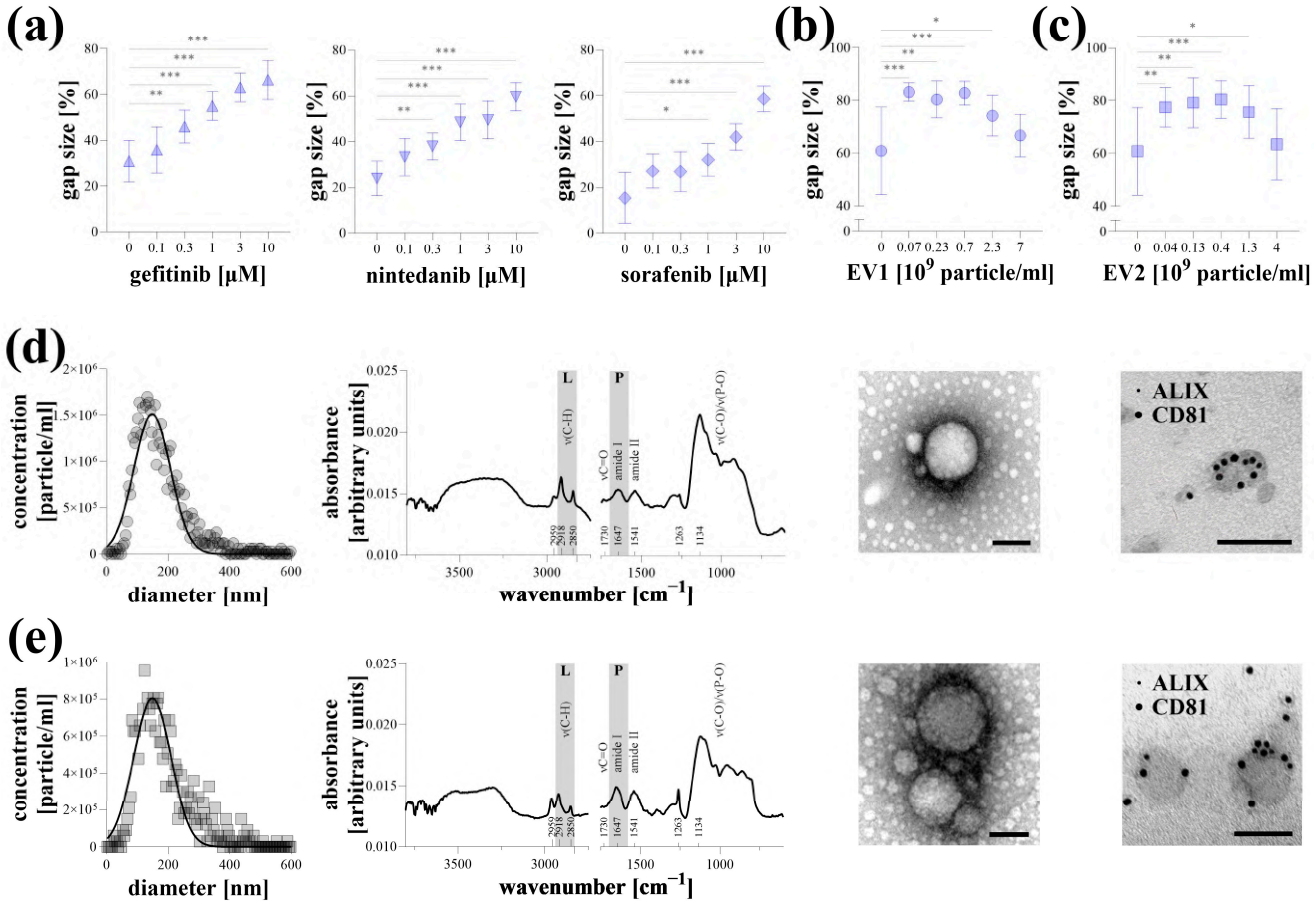

Figure 3. Representative experiments of microplate-based transient agarose spot (TAS) cell migration assay. Hoechst-stained A549 cells were stimulated with 10% FBS and the antimigratory effect of gefitinib, nintedanib, and sorafenib kinase inhibitors, (**a**) as well as EV1 (**b**) and EV2 (**c**) MSC-derived extracellular vesicles, was investigated after 72 h via microplate-based quantification (n = 10/group). Results are presented as mean ± SD. * $p < 0.05$; ** $p < 0.01$; *** $p < 0.001$; (Brown–Forsythe and Welch ANOVA with Dunnett's T3 test). Characterization of EV1 (**d**) and EV2 (**e**) samples was carried out by determining nanoparticle size distribution using nanoparticle tracking analysis, measuring protein and lipid content using surface-enhanced Fourier transform infrared spectroscopy, investigating morphology and structure using transmission electron microscopy (TEM), and demonstrating the presence of ALIX1 and CD81 markers by immuno-TEM using 5 and 10 nm gold labeled antibodies. Scale bar: 100 nm.

3. Discussion

Collective cell migration plays a crucial role in various diseases and biological processes, including embryonic development, wound healing, tumor progression, and metastasis or tissue fibrosis [9]. The scratch assay, widely considered the gold standard for studying cell migration, has several limitations, including intra- and inter-assay variability and labor-intensive data analysis [10–12]. To overcome these challenges, our research group previously developed the TAS cell migration assay, which eliminates the adverse effects of scratching the cell monolayer by using removable agarose droplets as physical barriers to create cell-free areas [4]. This innovation significantly improved assay efficiency and enabled its adaptation to a 96-well plate format, reducing material (both reagents and plastic) consumption and increasing assay accuracy and throughput. Although the TAS assay was developed on fibroblasts, its usability on cancer cells was also demonstrated. However, the detection method remained microscopy-based, which continued to face challenges due to its time and equipment requirements, thereby limiting overall efficiency [12].

In this study, we aimed to transfer data acquisition and analysis from microscopy to a microplate reader. New-generation microplate readers (e.g., devices of BMG LABTECH (Ortenberg, Germany), Tecan (Männedorf, Switzerland), and Molecular Devices (San Jose, CA, USA)) feature a well-scanning mode specifically designed to address non-homogeneous data from cell-based assays, where an uneven cell distribution across the well renders a single central measurement insufficient. This advanced scanning approach ensures more accurate and representative data acquisition by capturing multiple measurements within individual wells.

We utilized the CLARIOstar Plus microplate reader (BMG LABTECH, Ortenberg, Germany) combined with MARS software to scan a 4 mm diameter region at the center of each well in a 96-well plate. The area was scanned in a 30 × 30 matrix mode, generating absorbance or fluorescence intensity heatmaps with several hundred data points within the region of interest. The scanning points derived from TAS assay heatmaps clustered into two distinct groups: high absorbance or fluorescence values representing cell-rich regions, and near-blank values indicating cell-free zones. The border between these two groups was well-defined, enabling the establishment of a precise threshold value to demarcate and accurately measure the area of cell-free zones (Figure 1a,b). Although most limitations of the scratch assay were eliminated, data acquisition still relied on microscopy, requiring expensive equipment systems and time-consuming manual work, while the risk of bias from manual evaluation remained minimal.

The accuracy of data evaluation by the microplate reader was verified using fluorophore-expressing cancer cells (Figure 1c–e), where area quantification yielded identical gap sizes compared to the graphical analysis of the microscopic images from the same samples. The microplate reader-based evaluation has proven to be capable of tracking the dose-dependent effect of FBS on the migration of fluorescent cancer cells. FBS is an optimal inducer of cell migration due to the fact that it contains growth factors and chemoattractants [13,14]. In addition, as a general nutrient, it enhances overall metabolic activity, thereby promoting autocrine signalling, which leads to sustained receptor tyrosine kinase activation and cell proliferation, both of which are driving forces for cell migration [15,16]. However, genetically modified fluorophore-expressing cells are not always applicable. Although the UV absorbance of unlabeled cells could also be detected, this approach is impractical due to the high background signal originating from culture medium components such as phenol red, amino acids, and FBS [17]. A clear border of the cell-free area can only be detected in PBS. Therefore, various colorimetric and fluorescence staining methods were investigated to assess their suitability for microplate reader-based detection (Figure 1f).

The applied dyes, targeting intracellular proteins, cell membrane, and DNA, as well as those activated by intracellular esterase activity, yielded a satisfactory signal-to-noise ratio.

Of all the options we tested, Hoechst staining proved to be the most suitable approach for performing the TAS cell migration assay. Hoechst is a cost-effective, cell-permeable dye that allows the labeling of viable cells without fixation or permeabilization, unlike other approaches, such as colorimetric staining or using the DNA stain propidium iodide [18]. Compared to cell fixation, which converts the assay into an end-point measurement, using a non-toxic dye that labels live cells allows for multiple detections in kinetic assays. Hoechst intensity is amplified upon DNA binding; therefore, the potential leakage of free dye molecules over time does not increase the background signal, a phenomenon commonly observed in esterase-dependent approaches [19]. The use of membrane dyes can be a good alternative; however, as they are lipophilic molecules, they can be challenging to handle in water-based cellular media, and their cost is relatively higher [20]. In addition to precise area detection after Hoechst staining, a stable signal was obtained even at low concentrations, leading to high contrast at the edges of the cell-free zones for several days, while no signs of cytotoxicity were detected (Figure 2). In summary, the migration of Hoechst-stained cancer cells following FBS induction can be reliably monitored using microplate-based detection. However, it should be noted that Hoechst may interfere with drug transporters (e.g., several ATP-binding cassette (ABC) transporters, including ABCG2/BCRP, ABCB1/P-glycoprotein/MDR1, and ABCC1/MRP1), which is an important consideration when using the TAS assay for drug screening [21–23]. Since these proteins are frequently implicated in multidrug resistance, particularly in cancer cells, it is advisable to evaluate whether the compound of interest interacts with the same transport pathways as Hoechst. This can be explored using public databases such as DrugBank (for known substrates or inhibitors), via in vitro transporter-binding assays, or by comparing the compound's effective concentration in parallel experiments conducted in the absence or presence of Hoechst staining. If the tested compounds are likely to compete with Hoechst for transporter binding, using a membrane dye may be a more suitable alternative. This is supported by our previous study describing the original TAS method, where the membrane dye DiI was successfully used to label viable cells under similar experimental conditions [4]. While these offered staining procedures are generally applicable across various cell types, the intensity and kinetics of dye uptake may vary depending on the specific characteristics of each cell line. Therefore, we recommend that users perform initial optimization steps—similar to those presented here—tailored to their own experimental systems to ensure accurate and reproducible results.

Finally, in representative experiments, we demonstrated the applicability of the microplate-based TAS assay on Hoechst-stained lung cancer cells (Figure 3). Gefitinib, nintedanib, and sorafenib are kinase inhibitors widely used in the treatment of non-small-cell lung cancer [24–26]. As these drugs target receptor tyrosine kinases and other signal transduction pathways involved in cancer cell migration and proliferation, they serve as appropriate candidates for demonstration. In our experiment, these compounds exhibited a dose-dependent inhibitory effect on FBS-induced migration of A549 cancer cells (Figure 3a).

In recent years, the potential therapeutic role of MSC-derived EVs has emerged in various diseases, particularly in different cancers [27]. Although the reported data are not entirely consistent, several studies have demonstrated the anticancer effect of stem cell-derived EVs, particularly their ability to reduce the collective migration of cancer cells in vitro [28,29]. Similarly, we observed a significant anti-migratory effect of EVs isolated from the supernatant of MSCs (Figure 3b–e), which, surprisingly, was diminished at higher particle concentrations. The loss of the biological effect of EVs at elevated numbers has

also been described previously [30]. One possible explanation for this is that an increased particle concentration promotes the aggregation of extracellular vesicles [31].

In this study, we successfully developed a microplate reader-based detection method for the TAS cell migration assay, further enhancing its efficiency and applicability. Our research group previously developed the TAS assay to overcome the limitations of the widely used scratch assay, introducing advantages such as increased reproducibility, higher throughput, and reduced material consumption. By integrating microplate-based detection and Hoechst staining, we have now optimized the method for automated, high-throughput analysis, eliminating the need for a labor-intensive microscopy system. We also demonstrated its utility in assessing the effects of kinase inhibitors and MSC-derived EVs on cancer cell migration. These advancements position the TAS assay as a powerful and scalable tool for drug screening and cell migration studies, offering a robust alternative to conventional imaging techniques.

4. Materials and Methods

4.1. Cell Lines and Treatments

A549 (#CRM-CCL-185) human lung cancer cells were cultured in Dulbecco's Modified Eagle Medium (Thermo Fisher Scientific, Waltham, MA, USA), LCLC-103H (#ACC-384) human lung cancer cells, HCT-116 (#CCL-247), green fluorescent protein (GFP)-expressing HCT-116, red fluorescent protein (RFP)-expressing HCT-116 (obtained from József Tóvári, National Institute of Oncology, Budapest, Hungary), and human colon cancer cells were cultured in Roswell Park Memorial Institute (RPMI) 1640 medium (Thermo Fisher Scientific) supplemented with a 10% heat-inactivated fetal bovine serum (FBS) (Invitrogen, Waltham, MA, USA) and a 1% penicillin and streptomycin (Merck, Kenilworth, NJ, USA) mixture under standard cell culture conditions (37 °C, humidified, 5% CO_2). Mesenchymal stem cells (MSCs) were isolated from peritoneal dialysate of two individual pediatric patients treated with peritoneal dialysis at the Pediatric Center, Semmelweis University (31224-5/2017/EKU), as described previously [32,33], and cultured in Dulbecco's modified Eagle's medium/Nutrient Mixture F-12 (DMEM-F12, Thermo Fisher Scientific).

During the in vitro experiments, a dilution series (0–10 μM) of kinase inhibitors, including gefitinib, nintedanib, or sorafenib (Vichem Chemie Research Ltd., Budapest, Hungary), was used. Control cells were treated with an equivalent volume of DMSO (Merck). In addition, an alternative experimental setup involved treating the cells with extracellular vesicles (EVs; 0–7 × 10^9 particles/mL) dissolved in phosphate-buffered saline (PBS). In both experiments, the cell culture medium contained 10% FBS.

4.2. Transient Agarose Spot (TAS) Assay

TAS assay was performed according to our previously described protocol [4]. Briefly, a 0.1% agarose (Merck) solution was prepared by boiling and stirring thoroughly, then stored at 70 °C in a thermoblock until use. Subsequently, 2 μL droplets were placed in the middle of the wells of a 96-well tissue culture plate (Sarstedt, Newton, MA, USA) and left at room temperature for 15 min to polymerise. Cells were seeded (n = 6–10 well/treatment group) at a density sufficient to reach near-full confluence (1.5 × 10^4 cells/well A549, 7.5 × 10^3 cells/well LCLC-103H, 2 × 10^4 cells/well HCT-116), and incubated overnight to ensure proper attachment. Thereafter, the culture medium was removed, the agarose spots were gently aspirated from the bottom of the wells, and the cells were washed with sterile PBS. Finally, the treatment in question was applied for 72 h.

4.3. Cell Staining

Before data acquisition, various colorimetric and fluorescence-based cell staining methods were tested, with detailed staining protocols provided in Table 1. Kahle's solution was prepared using 26% ethanol, 3.7% formaldehyde, and 2% glacial acetic acid.

Table 1. Staining protocols.

	Fixation	Dye	Staining
SRB	10% TCA at 4 °C for 1 h	Sulforodamine B sodium salt (#S1402, Merck)	0.4% SRB in 1% AA for 30 min
FastGreen	Kahle's solution at RT for 15 min	FastGreen FCF (#F7252, Merck)	0.1% FastGreen in 1% AA for 5 min
methylene blue	Kahle's solution at RT for 15 min	Methylene blue solution acc. To Loeffler (#42335, Molar Chemicals, Hálasztelek, Hungary)	1% methylene blue in H_2O for 5 min
Cresyl Violet	Kahle's solution at RT for 15 min	Cresyl Fast Violet—Certistain (#K2247947, Merck)	0.14 mg/mL in 6.8 mM sodium acetate + 83 mM AA mix for 20 min
DiI	-	1,1′-Dioctadecyl-3,3,3′,3′-Tetramethylindocarbocyanine Perchlorate (#D282, Thermo Fisher Scientific)	0.1 mg/mL in cell culture medium for 24 h
WGA	-	Wheat Germ Agglutinin Alexa Fluor 488 conjugate (#W11261, Thermo Fisher Scientific)	0.01 mg/mL in cell culture medium for 4 h
Calcein AM	-	Calcein AM (#C3099, Thermo Fisher Scientific)	10 µM in cell culture medium for 1 h
Cell Tracker	-	Cell Tracker Green CMFDA (#C7025, Thermo Fisher Scientific)	5 µM in cell culture medium for 1 h
Hoechst	-	Hoechst 33,342 trihydrochloride (#B2261, Merck)	0.5 µg/mL (1:10 000) in cell culture medium for 4 h
PI	Kahle's solution at RT for 15 min	Propidium Iodide Staining Solution (#51-66211E, BD Pharmingen, San Diego, CA, USA)	0.5 µM in cell culture medium for 5 min

Abbreviations: TCA: trichloroacetic acid; AA: acetid acid; RT: room temperature.

4.4. Data Acquisition by Microscopy

Brightfield or fluorescence images of each well were captured at 0 and 72 h following the treatments using an Olympus IX81 microscope system (Olympus Corporation, Tokyo, Japan). Cell-free gap areas were manually annotated using a digitizer board and measured with ImageJ 1.48v software (National Institutes of Health, Bethesda, Rockville, MD, USA). The gap areas were finally calculated and presented as the percentage ratio (%) of the initial gap area.

4.5. Data Acquisition by Microplate Reader

Absorbance or fluorescence signal of each well was measured at 0 and 72 h, following the treatments using a CLARIOstar Plus microplate reader equipped with MARS v4.01 software (BMG Labtech, Ortenberg, Germany). During the measurements, matrix scanning mode was employed with a 30 × 30 matrix dimension focusing on a 4 mm diameter circular area in the center of each well, with a focal height set to 3.2 mm, choosing bottom

optic for fluorescence detection. The optical settings for the various staining methods are provided in Table 2. The gain parameters were manually adjusted to ensure that the resulting fluorescence data fell within the upper third of the measurement range, allowing clear distinction between cell-covered and cell-free areas. Cell-free gap areas were annotated by excluding scan points above a manually defined threshold, followed by counting the number of scan points. The gap areas were finally calculated and presented as the percentage ratio (%) of the initial gap area.

Table 2. Optical settings for data acquisition by microplate reader using various staining methods.

Staining	Measurement Method	Excitation [nm]	Emission [nm]
-	Absorbance	285	-
SRB	Absorbance	565	-
	Fluorescence	550	605
FastGreen	Absorbance	624	-
methylene blue	Absorbance	668	-
Cresyl Violet	Absorbance	590	-
	Fluorescence	583	627
DiI	Fluorescence	538	582
WGA	Fluorescence	470	515
Calcein AM	Fluorescence	490	533
Cell Tracker	Fluorescence	470	515
Hoechst	Fluorescence	355	455
PI	Fluorescence	550	605

4.6. Cell Viability Assay

Cell viability was assessed using MTT assay. At the end of the in vitro experiment, 10 µL of 5 mg/mL thiazolyl blue tetrazolium bromide (Merck), diluted in H_2O, was added to each well (containing 100 µL culture medium) and incubated at 37 °C for 4 h. Subsequently, the supernatants were aspirated from the cells, and the intracellular crystals were dissolved with 100 µL of a DMSO-ethanol (1:1) mixture. The absorbance was recorded at 570 nm, with 690 nm used as the background in a CLARIOStar Plus microplate reader using MARS v4.01 software (BMG Labtech). The results were finally normalized and presented as the percentage ratio (%) of the control group values.

4.7. Mesenchymal Stem Cell-Derived Extracellular Vesicle Isolation and Characterization

EV1 and EV2 extracellular vesicles were isolated from the medium of the two primary MSC cultures derived from different patients on peritoneal dialysis. Cells were grown in T-175 cell culture flasks (Sarstedt) until reaching full confluence. The medium was then replaced with serum-free DMEM-F12 and incubated for 24 h. Afterward, the supernatant was separated, and cells and large EVs were removed by centrifugation at 400× g for 30 min and subsequent filtration using Filtropur S syringe filter (polyethersulfone, 0.2 µm pore size, Sarstedt). EVs were then purified using tangential flow filtration (polysulfone hollow fibers, 20 nm pore size, HansaBioMed Life Sciences Ltd., Tallinn, Estonia), followed by size-exclusion chromatography (70 nm qEV columns, Izon Science, Lyon, France).

EV characterization was performed in accordance with the current guidelines from the International Society for Extracellular Vesicles (ISEV) [34]. The nanoparticle size distribution was determined by nanoparticle tracking analysis (NTA) using ZetaView PMX-120

(Particle Metrix GmbH, Meersbush, Germany) with ZetaVIEW software 8.05.12 SP2 [35]. Surface-enhanced Fourier Transform Infrared Spectroscopy (SEIRS) measurements with in-house developed gold nanoparticles were carried out to analyze the protein and lipid content, employing a Varian 2000 spectrometer (Scimitar Series, Coral Springs, FL, USA) fitted with a diamond-attenuated total reflection cell ("Golden Gate" single-reflection attenuated total reflectance (ATR) unit, Specac, Orpington, UK) [36]. The morphology and structure of nanoparticles were analyzed using transmission electron microscopy (TEM), where samples were prepared on formvar-coated copper grids, stained with uranyl acetate, and examined using a Morgagni 268D electron microscope (FEI, Eindhoven, The Netherlands) [37,38]. The presence of specific exosome markers was investigated via immune-TEM, using anti-ALIX (#SAB4200477, Merck) and anti-CD81 (#SAB3500454, Merck) primary antibodies and anti-rabbit IgG gold-conjugated secondary antibodies (5 nm gold, #G7652, and 10 nm gold, #G7277, Merck). The images were captured with a JEOL 1011 microscope (Tokyo, Japan) [39].

4.8. Statistics

Statistical evaluation of the data was performed using GraphPad Prism 9.1.2 software (GraphPad Software Inc., San Diego, CA, USA). Pearson's correlation was used for correlation analyses, and Brown–Forsythe and Welch ANOVA with Dunnett's T3 test were applied for multiple comparisons. $p \leq 0.05$ was considered statistically significant. Unless otherwise indicated, results are illustrated as mean $\pm$ SD of the corresponding groups. The applied tests, significances, and number of elements (n) are indicated in each figure legend.

Author Contributions: A.V.-S.: conceptualization, methodology, writing—original draft, investigation, visualization, project administration; C.S.: methodology, writing—original draft, investigation, visualization; D.P.: writing—review and editing, investigation; P.B.: writing—review and editing, visualization; D.L.: methodology, investigation; T.V.: methodology, investigation, resources; J.M.: methodology, investigation; M.P.: methodology, investigation; Z.V.: methodology, resources; L.Ő.: resources; A.J.S.: funding acquisition; Á.V.: writing—review and editing, supervision; B.S.: writing—review and editing, investigation. All authors have read and agreed to the published version of the manuscript.

Funding: This research was supported by the HUN-REN-SE Pediatric and Nephrology Research Group, the National Research, Development and Innovation Office (NKFIH) K-142728 (A.J.S.), TKP2021-EGA-24 (A.J.S.), TKP2021-EGA-23 (T.V.), and EKÖP-2024-53 (A.V.-S.); EKÖP-2024-160 (P.B.); EKÖP-2024-162 (C.S.); VEKOP-2.3.3-15-2017-00016 (T.V.) and RRF-2.3.121-2022-00003 (T.V.); and the Hungarian Academy of Sciences, the János Bolyai Research Scholarship (D.P., T.V., M.P.).

Institutional Review Board Statement: Not applicable.

Informed Consent Statement: Not applicable.

Data Availability Statement: Data is contained within the article.

Acknowledgments: We are grateful to Maria Bernath for her excellent technical assistance. We thank József Tóvári for kindly providing the HCT-116 cell lines.

Conflicts of Interest: Author L.Ő. was employed by the company Vichem Chemie Research Ltd. The remaining authors declare that the research was conducted in the absence of any commercial or financial relationships that could be construed as a potential conflict of interest.

Abbreviations

The following abbreviations are used in this manuscript:

EV	extracellular vesicle
FBS	fetal bovine serum

GFP	green fluorescent protein
MSC	mesenchymal stem cell
NTA	nanoparticle tracking analysis
RFP	red fluorescent protein
TAS	transient agarose spot
TEM	transmission electron microscopy

References

1. Mayor, R.; Etienne-Manneville, S. The front and rear of collective cell migration. *Nat. Rev. Mol. Cell Biol.* **2016**, *17*, 97–109. [CrossRef] [PubMed]
2. Spatarelu, C.-P.; Zhang, H.; Nguyen, D.T.; Han, X.; Liu, R.; Guo, Q.; Notbohm, J.; Fan, J.; Liu, L.; Chen, Z. Biomechanics of Collective Cell Migration in Cancer Progression: Experimental and Computational Methods. *ACS Biomater. Sci. Eng.* **2019**, *5*, 3766–3787. [CrossRef]
3. Balko, S.; Kerr, E.; Buchel, E.; Logsetty, S.; Raouf, A. A Robust and Standardized Approach to Quantify Wound Closure Using the Scratch Assay. *Methods Protoc.* **2023**, *6*, 87. [CrossRef]
4. Veres-Székely, A.; Pap, D.; Szebeni, B.; Őrfi, L.; Szász, C.; Pajtók, C.; Lévai, E.; Szabó, A.J.; Vannay, Á. Transient Agarose Spot (TAS) Assay: A New Method to Investigate Cell Migration. *Int. J. Mol. Sci.* **2022**, *23*, 2119. [CrossRef]
5. Radstake, W.E.; Gautam, K.; Van Rompay, C.; Vermeesen, R.; Tabury, K.; Verslegers, M.; Baatout, S.; Baselet, B. Comparison of in vitro scratch wound assay experimental procedures. *Biochem. Biophys. Rep.* **2023**, *33*, 101423. [CrossRef]
6. Berg, E.L. The future of phenotypic drug discovery. *Cell Chem. Biol.* **2021**, *28*, 424–430. [CrossRef] [PubMed]
7. Nyffeler, J.; Haggard, D.E.; Willis, C.; Setzer, R.W.; Judson, R.; Paul-Friedman, K.; Everett, L.J.; Harrill, J.A. Comparison of Approaches for Determining Bioactivity Hits from High-Dimensional Profiling Data. *SLAS Discov.* **2021**, *26*, 292–308. [CrossRef] [PubMed]
8. Quancard, J.; Bach, A.; Cox, B.; Craft, R.; Finsinger, D.; Guéret, S.M.; Hartung, I.V.; Laufer, S.; Messinger, J.; Sbardella, G.; et al. The European Federation for Medicinal Chemistry and Chemical Biology (EFMC) Best Practice Initiative: Phenotypic Drug Discovery. *ChemMedChem* **2021**, *16*, 1736–1739. [CrossRef]
9. Grada, A.; Otero-Vinas, M.; Prieto-Castrillo, F.; Obagi, Z.; Falanga, V. Research techniques made simple: Analysis of collective cell migration using the wound healing assay. *J. Investig. Dermatol.* **2017**, *137*, e11–e16. [CrossRef]
10. Bobadilla, A.V.P.; Arévalo, J.; Sarró, E.; Byrne, H.M.; Maini, P.K.; Carraro, T.; Balocco, S.; Meseguer, A.; Alarcón, T. In vitro cell migration quantification method for scratch assays. *J. R. Soc. Interface* **2019**, *16*, 20180709. [CrossRef]
11. Guy, J.B.; Espenel, S.; Vallard, A.; Battiston-Montagne, P.; Wozny, A.S.; Ardail, D.; Alphonse, G.; Rancoule, C.; Rodriguez-Lafrasse, C.; Magne, N. Evaluation of the Cell Invasion and Migration Process: A Comparison of the Video Microscope-based Scratch Wound Assay and the Boyden Chamber Assay. *J. Vis. Exp.* **2017**, *129*, 56337. [CrossRef]
12. Vang Mouritzen, M.; Jenssen, H. Optimized Scratch Assay for In Vitro Testing of Cell Migration with an Automated Optical Camera. *J. Vis. Exp.* **2018**, *129*, 56337. [CrossRef]
13. Omar Zaki, S.S.; Kanesan, L.; Leong, M.Y.D.; Vidyadaran, S. The influence of serum-supplemented culture media in a transwell migration assay. *Cell Biol. Int.* **2019**, *43*, 1201–1204. [CrossRef] [PubMed]
14. Lee, D.Y.; Lee, S.Y.; Yun, S.H.; Jeong, J.W.; Kim, J.H.; Kim, H.W.; Choi, J.S.; Kim, G.D.; Joo, S.T.; Choi, I.; et al. Review of the Current Research on Fetal Bovine Serum and the Development of Cultured Meat. *Food Sci. Anim. Resour.* **2022**, *42*, 775–799. [CrossRef]
15. Liu, S.; Yang, W.; Li, Y.; Sun, C. Fetal bovine serum, an important factor affecting the reproducibility of cell experiments. *Sci. Rep.* **2023**, *13*, 1942. [CrossRef] [PubMed]
16. Recho, P.; Ranft, J.; Marcq, P. One-dimensional collective migration of a proliferating cell monolayer. *Soft Matter* **2016**, *12*, 2381–2391. [CrossRef]
17. Ghasemi, M.; Turnbull, T.; Sebastian, S.; Kempson, I. The MTT Assay: Utility, Limitations, Pitfalls, and Interpretation in Bulk and Single-Cell Analysis. *Int. J. Mol. Sci.* **2021**, *22*, 12827. [CrossRef]
18. Fuchs, H.; Jahn, K.; Hu, X.; Meister, R.; Binter, M.; Framme, C. Breaking a Dogma: High-Throughput Live-Cell Imaging in Real-Time with Hoechst 33342. *Adv. Healthc. Mater.* **2023**, *12*, e2300230. [CrossRef]
19. Gillissen, M.A.; Yasuda, E.; de Jong, G.; Levie, S.E.; Go, D.; Spits, H.; van Helden, P.M.; Hazenberg, M.D. The modified FACS calcein AM retention assay: A high throughput flow cytometer based method to measure cytotoxicity. *J. Immunol. Methods* **2016**, *434*, 16–23. [CrossRef]
20. Cirulis, J.T.; Strasser, B.C.; Scott, J.A.; Ross, G.M. Optimization of staining conditions for microalgae with three lipophilic dyes to reduce precipitation and fluorescence variability. *Cytom. Part A* **2012**, *81*, 618–626. [CrossRef]
21. Swain, B.M.; Guo, D.; Singh, H.; Rawlins, P.B.; McAlister, M.; van Veen, H.W. Complexities of a protonatable substrate in measurements of Hoechst 33342 transport by multidrug transporter LmrP. *Sci. Rep.* **2020**, *10*, 20026. [CrossRef] [PubMed]

22. Kim, M.; Turnquist, H.; Jackson, J.; Sgagias, M.; Yan, Y.; Gong, M.; Dean, M.; Sharp, J.G.; Cowan, K. The multidrug resistance transporter ABCG2 (breast cancer resistance protein 1) effluxes Hoechst 33342 and is overexpressed in hematopoietic stem cells. *Clin. Cancer Res.* **2002**, *8*, 22–28. [PubMed]
23. Helms, H.C.; Hersom, M.; Kuhlmann, L.B.; Badolo, L.; Nielsen, C.U.; Brodin, B. An electrically tight in vitro blood-brain barrier model displays net brain-to-blood efflux of substrates for the ABC transporters, P-gp, Bcrp and Mrp-1. *AAPS J.* **2014**, *16*, 1046–1055. [CrossRef] [PubMed]
24. Maemondo, M.; Inoue, A.; Kobayashi, K.; Sugawara, S.; Oizumi, S.; Isobe, H.; Gemma, A.; Harada, M.; Yoshizawa, H.; Kinoshita, I.; et al. Gefitinib or chemotherapy for non-small-cell lung cancer with mutated EGFR. *N. Engl. J. Med.* **2010**, *362*, 2380–2388. [CrossRef]
25. Reck, M.; Kaiser, R.; Mellemgaard, A.; Douillard, J.-Y.; Orlov, S.; Krzakowski, M.; von Pawel, J.; Gottfried, M.; Bondarenko, I.; Liao, M.; et al. Docetaxel plus nintedanib versus docetaxel plus placebo in patients with previously treated non-small-cell lung cancer (LUME-Lung 1): A phase 3, double-blind, randomised controlled trial. *Lancet Oncol.* **2014**, *15*, 143–155. [CrossRef]
26. Scagliotti, G.; Novello, S.; Pawel, J.v.; Reck, M.; Pereira, J.R.; Thomas, M.; Miziara, J.E.A.; Balint, B.; Marinis, F.D.; Keller, A.; et al. Phase III Study of Carboplatin and Paclitaxel Alone or With Sorafenib in Advanced Non–Small-Cell Lung Cancer. *J. Clin. Oncol.* **2010**, *28*, 1835–1842. [CrossRef]
27. Weng, Z.; Zhang, B.; Wu, C.; Yu, F.; Han, B.; Li, B.; Li, L. Therapeutic roles of mesenchymal stem cell-derived extracellular vesicles in cancer. *J. Hematol. Oncol.* **2021**, *14*, 136. [CrossRef]
28. Li, T.; Zhou, X.; Wang, J.; Liu, Z.; Han, S.; Wan, L.; Sun, X.; Chen, H. Adipose-derived mesenchymal stem cells and extracellular vesicles confer antitumor activity in preclinical treatment of breast cancer. *Pharmacol. Res.* **2020**, *157*, 104843. [CrossRef]
29. Pakravan, K.; Babashah, S.; Sadeghizadeh, M.; Mowla, S.J.; Mossahebi-Mohammadi, M.; Ataei, F.; Dana, N.; Javan, M. MicroRNA-100 shuttled by mesenchymal stem cell-derived exosomes suppresses in vitro angiogenesis through modulating the mTOR/HIF-1α/VEGF signaling axis in breast cancer cells. *Cell. Oncol.* **2017**, *40*, 457–470. [CrossRef]
30. Tabak, S.; Schreiber-Avissar, S.; Beit-Yannai, E. Extracellular vesicles have variable dose-dependent effects on cultured draining cells in the eye. *J. Cell. Mol. Med.* **2018**, *22*, 1992–2000. [CrossRef]
31. Yi, J.; Kim, S.; Han, C.; Park, J. Evaluation of extracellular vesicle aggregation by single vesicle analysis. *Analyst* **2024**, *149*, 5638–5648. [CrossRef]
32. Liu, B.; Guan, Q.; Li, J.; da Roza, G.; Wang, H.; Du, C. Mesenchymal stroma cells in peritoneal dialysis effluents from patients. *Human Cell* **2017**, *30*, 51–59. [CrossRef] [PubMed]
33. Szebeni, B.; Veres-Székely, A.; Pap, D.; Bokrossy, P.; Varga, Z.; Gaál, A.; Mihály, J.; Pállinger, É.; Takács, I.M.; Pajtók, C. Extracellular Vesicles of Patients on Peritoneal Dialysis Inhibit the TGF-β-and PDGF-B-Mediated Fibrotic Processes. *Cells* **2024**, *13*, 605. [CrossRef]
34. Welsh, J.A.; Goberdhan, D.C.I.; O'Driscoll, L.; Buzas, E.I.; Blenkiron, C.; Bussolati, B.; Cai, H.; Di Vizio, D.; Driedonks, T.A.P.; Erdbrügger, U.; et al. Minimal information for studies of extracellular vesicles (MISEV2023): From basic to advanced approaches. *J. Extracell. Vesicles* **2024**, *13*, e12404. [CrossRef]
35. Kazsoki, A.; Németh, K.; Visnovitz, T.; Lenzinger, D.; Buzás, E.I.; Zelkó, R. Formulation and characterization of nanofibrous scaffolds incorporating extracellular vesicles loaded with curcumin. *Sci. Rep.* **2024**, *14*, 27574. [CrossRef] [PubMed]
36. Bebesi, T.; Pálmai, M.; Szigyártó, I.C.; Gaál, A.; Wacha, A.; Bóta, A.; Varga, Z.; Mihály, J. Surface-enhanced infrared spectroscopic study of extracellular vesicles using plasmonic gold nanoparticles. *Colloids Surf. B Biointerfaces* **2025**, *246*, 114366. [CrossRef] [PubMed]
37. Fülöp, D.; Varga, Z.; Kiss, É.; Gyulai, G. Interfacial Behavior of Biodegradable Poly(lactic-co-glycolic acid)-Pluronic F127 Nanoparticles and Its Impact on Pickering Emulsion Stability. *Langmuir* **2024**, *40*, 12353–12367. [CrossRef]
38. Théry, C.; Amigorena, S.; Raposo, G.; Clayton, A. Isolation and characterization of exosomes from cell culture supernatants and biological fluids. *Curr. Protoc. Cell Biol.* **2006**, *30*, 3–22. [CrossRef]
39. Koncz, A.; Turiák, L.; Németh, K.; Lenzinger, D.; Bárkai, T.; Lőrincz, P.; Zelenyánszki, H.; Vukman, K.V.; Buzás, E.I.; Visnovitz, T. Endoplasmin Is a Hypoxia-Inducible Endoplasmic Reticulum-Derived Cargo of Extracellular Vesicles Released by Cardiac Cell Lines. *Membranes* **2023**, *13*, 431. [CrossRef]

International Journal of
Molecular Sciences

MDPI

Article

Optimization of Sirius Red-Based Microplate Assay to Investigate Collagen Production In Vitro

Csenge Szász [1], Domonkos Pap [1,2], Beáta Szebeni [1,2], Péter Bokrossy [1], László Őrfi [3,4], Attila J. Szabó [1,2], Ádám Vannay [1,2] and Apor Veres-Székely [1,2,*]

[1] Pediatric Center, MTA Center of Excellence, Semmelweis University, 1083 Budapest, Hungary
[2] HUN-REN-SU Pediatrics and Nephrology Research Group, 1052 Budapest, Hungary
[3] Department of Pharmaceutical Chemistry, Semmelweis University, 1092 Budapest, Hungary
[4] Vichem Chemie Research Ltd., 1022 Budapest, Hungary
* Correspondence: veres-szekely.apor@med.semmelweis-univ.hu

Abstract: Tissue fibrosis is characterized by chronic fibroblast activation and consequently excessive accumulation of collagen-rich extracellular matrix. In vitro microplate-based assays are essential to investigate the underlying mechanism and the effect of antifibrotic drugs. In this study, in the absence of a gold-standard method, we optimized a simple, cost-effective, Sirius Red-based colorimetric measurement to determine the collagen production of fibroblasts grown on 96-well tissue culture plates. Based on our findings, the use of a serum-free medium is recommended to avoid aspecific signals, while ascorbate supplementation increases the collagen production of fibroblasts. The cell-associated collagens can be quantified by Sirius Red staining in acidic conditions followed by alkaline elution. Immature collagens can be precipitated from the culture medium by acidic Sirius Red solution, and after subsequent centrifugation and washing steps, their amount can be also measured. Increased attention has been paid to optimizing the assay procedure, including incubation time, temperature, and solution concentrations. The resulting assay shows high linearity and sensitivity and could serve as a useful tool in fibrosis-related basic research as well as in preclinical drug screening.

Keywords: fibroblast; collagen; extracellular matrix; Sirius Red; functional; microplate; assay

Citation: Szász, C.; Pap, D.; Szebeni, B.; Bokrossy, P.; Őrfi, L.; Szabó, A.J.; Vannay, Á.; Veres-Székely, A. Optimization of Sirius Red-Based Microplate Assay to Investigate Collagen Production In Vitro. *Int. J. Mol. Sci.* **2023**, *24*, 17435. https://doi.org/10.3390/ijms242417435

Academic Editor: Alessandro Terrinoni

Received: 4 November 2023
Revised: 4 December 2023
Accepted: 11 December 2023
Published: 13 December 2023

1. Introduction

Fibrosis is an uncontrolled, pathological process, where constant profibrotic signals promote excessive fibroblast proliferation and overproduction of extracellular matrix (ECM), mainly collagen, which displaces the functional parenchyma and eventually leads to organ dysfunction. It can affect almost every organ and plays an important role in various disorders, such as chronic autoimmune and inflammatory diseases, graft loss after transplantation, or atherosclerotic plaque formation, making fibrosis a contributor to 45% of deaths worldwide [1,2]. Currently, the only approved antifibrotic therapeutic opportunities are the multikinase inhibitors nintedanib or pirfenidone, both targeting the activation and collagen production of fibroblasts. These drugs are used to treat idiopathic pulmonary fibrosis and have been shown to reduce disease progression rate, but they cannot prevent, stop, or reverse fibrosis; moreover, they have significant, mainly gastrointestinal, side effects that lead to therapy discontinuation [3]. Although a recent study has shown that the mean survival was significantly higher among patients receiving antifibrotic treatment, it still remained for approximately 5 years [4]. This global burden makes it imperative to reveal the exact pathomechanism of fibrosis, identify potential therapeutic targets, and develop effective antifibrotic compounds.

Fibroblasts are the main executor cells in fibrotic processes. Upon activation by cytokines, chemokines, and growth factors, they migrate to the site of tissue injury, start to proliferate, and produce ECM to form the mass of scar tissue, whose primary role is to ensure tissue integrity [5]. High-throughput microplate-based in vitro systems are essential to

explore the exact pathomechanism and test the effect of antifibrotic compounds on different fibroblast functions. Cell viability or proliferation assays are used to monitor the increase in cell number through their enzyme activity, ATP production, or DNA replication [6]. Methyl thiazole tetrazolium (MTT) assay, a widely used method to investigate cell proliferation, belongs to the colorimetric assays and is based on the formation of the purple end-product formazan by mitochondrial succinate dehydrogenase enzyme in viable cells [7]. The reduction of apoptosis rate, also a sign of fibroblast activation, can be examined with the MTT dye-based lactate dehydrogenase (LDH) assay, referring to intracellular enzymes released from dead cells to the supernatant [8]. Recently, to substitute the scratch assay to evaluate the migration capacity of fibroblasts, our research group has developed a transient agarose spot (TAS) assay. This method is based on using agarose droplets as a temporary physical barrier to create a cell-free zone on the culture plate. The kinetics of gap closure and thereby the migration capacity of the examined cells can be determined by subsequent graphical analysis [9].

Although there are a variety of methods available to investigate collagen production in cell cultures, a simple, cost-effective, high-throughput assay is still lacking. Molecular biology techniques, such as immunocytochemistry, enzyme-linked immunosorbent assay, Western blot, polymerase chain reaction, or hydroxyproline assay, are expensive and often time-consuming methods that do not allow the simultaneous investigation of large numbers of samples. Of the traditional histological staining methods of collagen-rich ECM, Sirius Red has been proven to be the most specific and sensitive, compared to Masson's trichrome or Van Gieson's [10,11].

In addition to the above-mentioned difficulties in labeling and quantifying total collagen, another factor complicates the development of a biologically relevant functional cellular assay. Collagen biosynthesis is a very complex procedure, consisting of multiple intra- and extracellular steps (Figure 1). After their transcription and translation, proline and glycine-rich pre-procollagen α-chains enter the endoplasmic reticulum, where post-translation modifications, including signal peptide cleavage, prolyl, and lysyl hydroxylation and glycosylation, result in the formation of triple helix pro-collagens. These water-soluble molecules leave the intracellular space by exocytosis through the Golgi apparatus, and then the N′ and C′ terminal propeptides are enzymatically removed. This modification allows the supramolecular organization of water-insoluble tropocollagen molecules into collagen fibrils by a quarter-staggered assembly, mediated by cellular integrins and fibronectin [12–14]. Further maturation and intra- and intermolecular crosslink formation result in a network of collagen fibers that are attached to the cell surface and surrounding tissue elements to support their organization [14]. These conditions are difficult to reproduce in vitro in order to ensure the uninterrupted maturation of collagens, and it must be considered when developing an appropriate functional assay based on a two-dimensional cell culture [1,15].

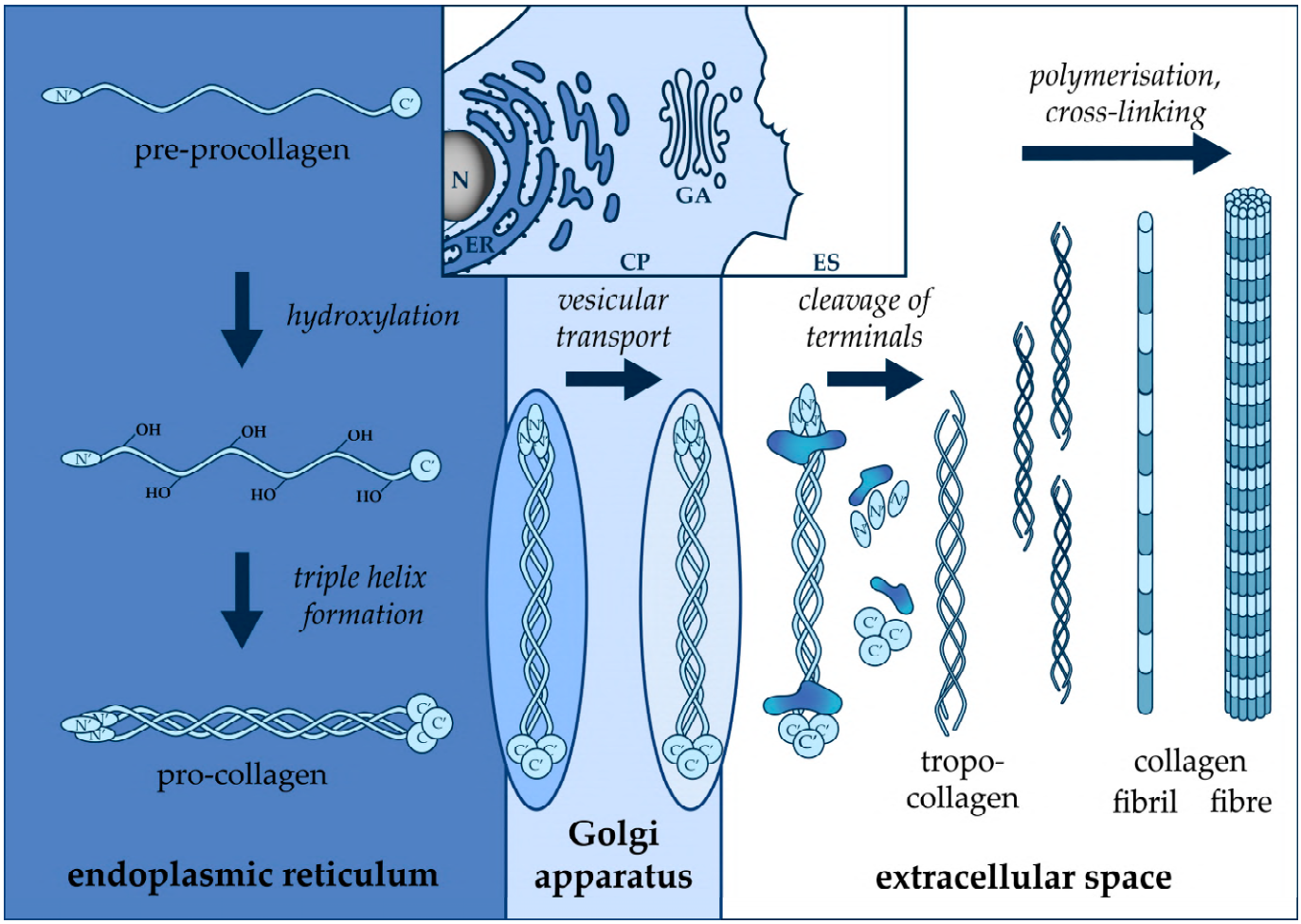

Figure 1. Collagen biosynthesis and maturation process. The **top middle** section of the figure shows the cell organelles with distinct shades of blue, involved in the post-translation modifications of collagen. Below, the schematic figure illustrates the intra- and extracellular steps of collagen fiber formation. Based on Veres-Székely et al. [16]. *N*: nucleus, *ER*: endoplasmic reticulum; *CP*: cytoplasm; *GA*: Golgi apparatus; *ES*: extracellular space.

Currently, there are two Sirius Red-based commercial kits for collagen detection. Despite their relatively high prices, Sircol Collagen Assay (Biocolor, Carrickfergus, UK) and Sirius Red Total Collagen Detection Assay Kit (Chondrex, Woodinville, WA, USA) have several limitations. The original Sircol Collagen Assay was designed for the quantification of insoluble forms of collagens after collagen extraction by acid-pepsin digestion of tissue samples. This method, including the time-consuming sample preparation, takes a whole working day, and attention is drawn to certain interfering factors, such as albumin. Indeed, several studies warn of the shortcomings of the Sircol assay, recommending additional digestion and separation steps to improve its accuracy and usability [17,18]. A new version of Sircol was released at the time of the present study, dedicated to measuring soluble collagens. Although the manufacturer promises improved specificity, no reference is yet available. However, determination of total collagen production in vitro still requires a combination of different kits and overnight sample preparation and digestion. Chondrex provides a Sirius Red Total Collagen Detection Assay Kit for detecting collagen content in tissue and cell homogenate or cell culture medium. This method is very similar to Sircol, still requiring solubilization of solid samples by acidic or enzymatic digestion and also a concentration of a high amount of culture medium (1 mL)—in which the presence of serum causes high background values.

The aim of the present study was to develop a simple, fast, cost-effective in vitro microplate-based method to quantify the amount of mature collagens attached to the cell surface and that of immature, water-soluble or floating collagens secreted by the fibroblast into the culture medium, using the collagen-specific Sirius Red dye. In addition to developing staining procedures, we also optimized the setup of experiments, including potential adjuvants during the cell treatment. The resulting method is suitable for screening the efficacy of antifibrotic drugs on the collagen production of fibroblasts.

2. Results

2.1. Detection of Cell-Associated Collagens by Sirius Red Staining

To visualize collagens in fibrotic lung tissue and cell culture, sections were stained with Sirius Red following the standard histological procedure, and then microscopic images were taken using bright-field and polarized light illumination techniques (Figure 2a). Large amounts of collagen deposition were detected in lung tissue samples, shown as red areas in bright-field images. Polarized light microscopy showed that the majority of collagens formed a complex system of fibers. In the case of adherent cell culture, the cytoplasm of fibroblasts showed Sirius Red positivity of which only a small fraction showed light scattering. Thin fibrils were mostly attached to the cell edges. Similarly, we found predominantly perinuclear and intracellular immunopositivity in fibroblasts, labeled with antibodies against pro-collagen or total collagen I (Figure 2b).

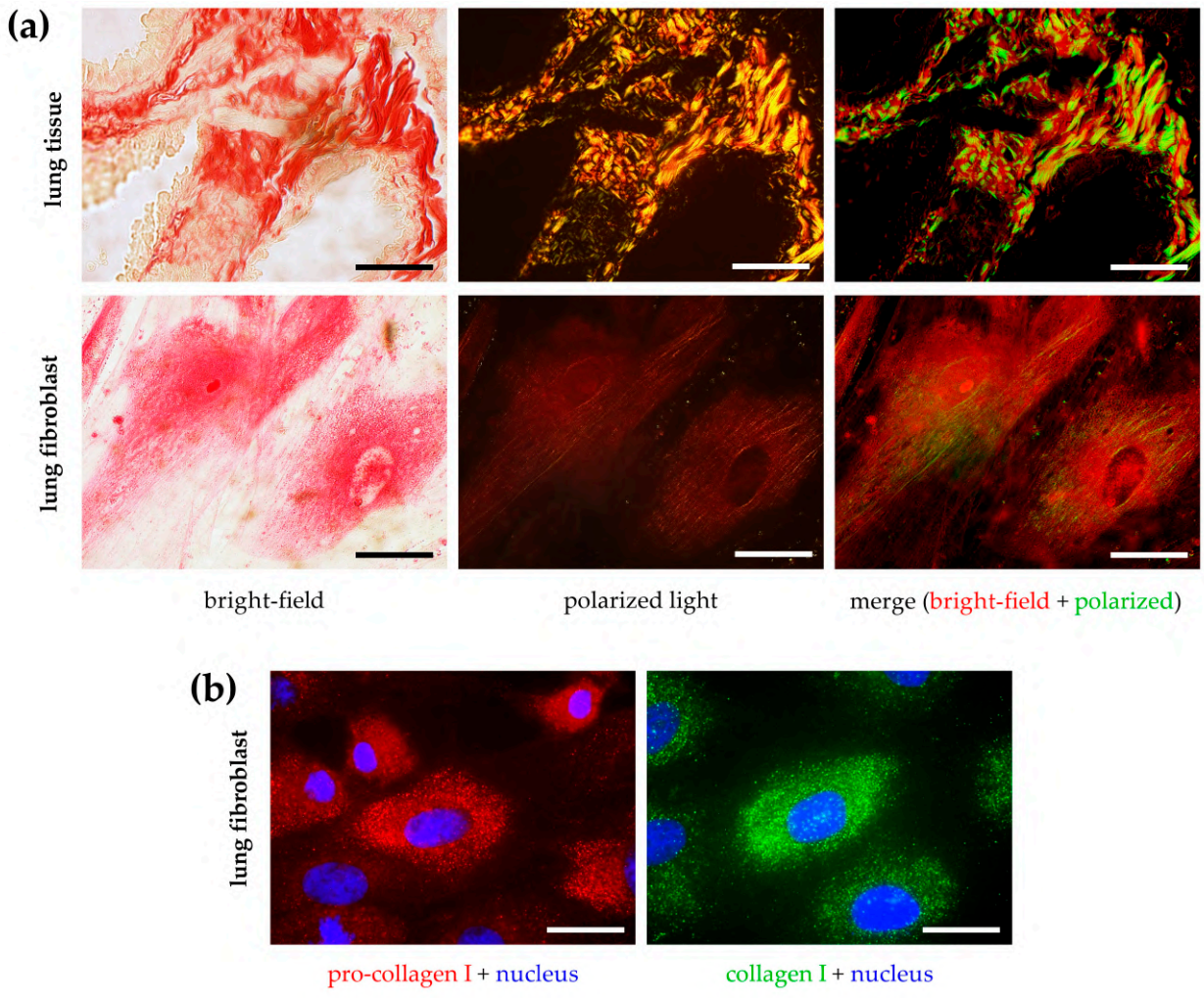

Figure 2. Detection of collagens in tissue and cell samples. (**a**) To visualize Sirius Red-stained fibrotic mouse lung tissue sections and CCD-19Lu lung fibroblasts, images were taken by bright-field and

polarized light illumination microscopy. (**b**) To visualize immunostained CCD-19Lu lung fibroblasts using antibodies raised against pro-collagen I and collagen I, images were taken by fluorescence microscopy. Scale bar: 50 µm.

To investigate collagen production of fibroblasts, unstimulated and TGF-β-treated CCD-19Lu cells, grown in 96-well plates were stained with Sirius Red (Figure 3a). The amount of dye bound to cell-associated collagens was quantified by measuring the absorbance of their eluates. Treatment with TGF-β, however, resulted in increased Sirius Red positivity of fibroblasts, and the volume exclusion effect of macromolecular crowding, investigated by the addition of various polymers (dextran, dextran sulfate sodium, polyethylene glycol, or ficoll) to the cell medium had no impact on cellular collagen deposition (Figure 3b).

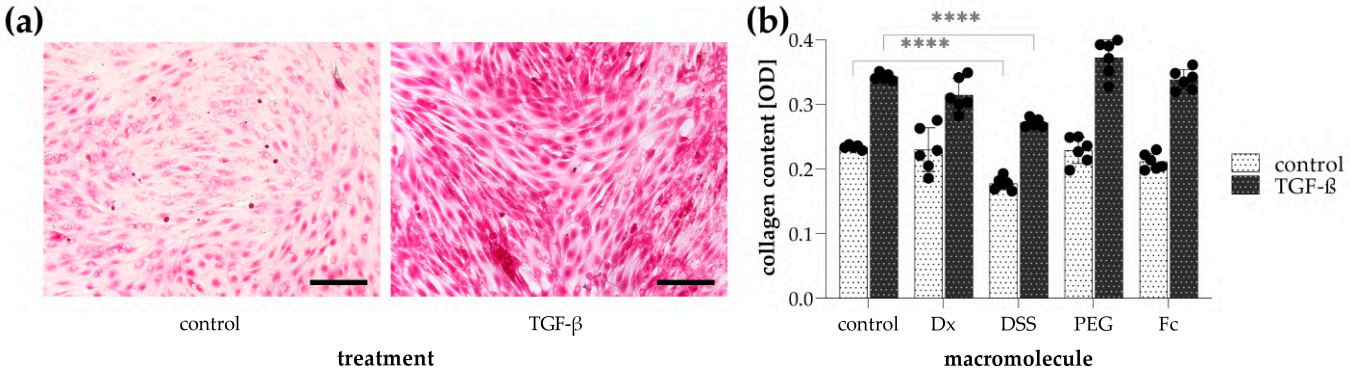

Figure 3. Detection of cell-associated collagens by Sirius Red staining on TGF-β-treated CCD-19Lu lung fibroblasts. (**a**) To visualize Sirius Red-stained cells, images were taken by bright-field microscopy. Scale bar: 200 µm. (**b**) The effect of macromolecular crowding on collagen production was investigated in the absence or presence of dextran (Dx), dextran sulfate sodium (DSS), polyethylene glycol (PEG), and ficoll (Fc). The amount of cell-associated collagens in Sirius Red-stained samples was determined by the optical density (OD) of their eluates. Results are presented as mean ± SD, dots represent individual values ($n = 6$). **** $p < 0.0001$ (two-way ANOVA with Dunnett's test).

2.2. Detection of Collagens in Cell Culture Medium by Sirius Red Staining

To establish the staining method for the determination of soluble collagen amount in the cell media, collagen solutions were incubated with Sirius Red and the collagen-dye precipitates were separated by centrifugation. Microscopic observations revealed strong and specific labeling of fibrillar collagens (Figure 4a).

An increase in Sirius Red concentration in the staining solution resulted in higher absorbance of the eluates derived from the centrifuged collagen-dye pellets, but meanwhile, the intraassay variability was also multiplied (Figure 4b). The high deviation could be the consequence of auto-precipitation and the instability of dye crystals observed in the supersaturated solution. The impact of the acetic acid concentration of Sirius Red dye solution on the labeling efficiency was investigated in collagen solutions diluted with water or cell culture medium (Figure 4c). Low acid concentration resulted in decreased binding capacity of Sirius Red, presumably due to the buffer capacity of the medium, resulting in an alkalic pH shift of the solution mix from the optimal range.

We found that performing the staining and washing procedures at room temperature resulted in reliable and accurate data; however, the sensitivity of the Sirius Red assay can be further increased by cooling the reagents, thereby increasing the read signal (Figure 4d). Stable collagen-dye formation was detected at 15 min of staining of collagen solution, which could not be further increased by the elongation of incubation time (Figure 4e). When we compared the different microplate types used in the washing process, V-bottom plates gave the best results, whereas filters or flat-bottom plates with relatively large surfaces resulted in a loss of collagen-dye precipitates (Figure 4f).

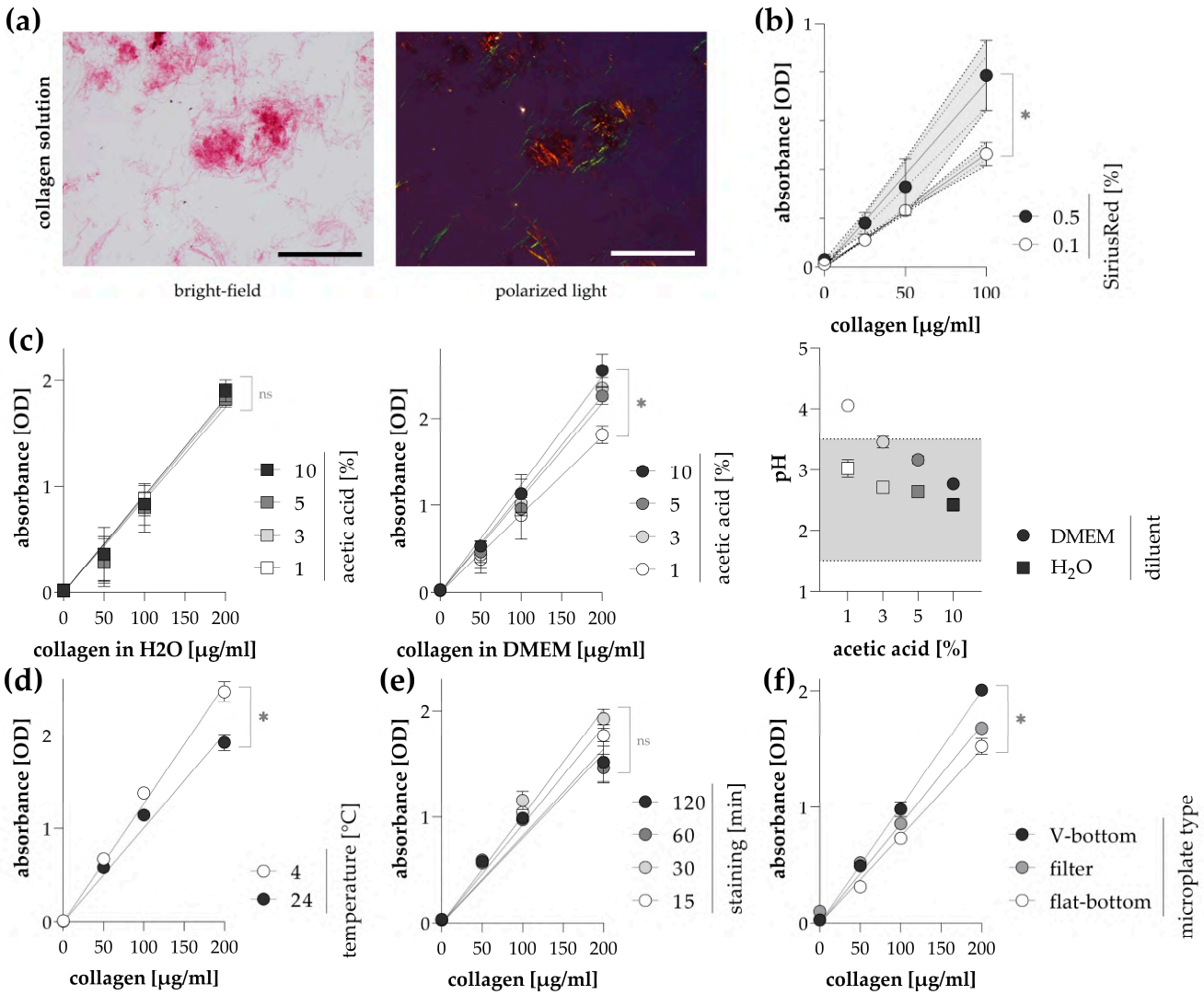

Figure 4. Detection of collagens in solution by Sirius Red staining. (**a**) To visualize Sirius Red stained collagen I solution (200 µg/mL diluted in culture medium), images were taken with a bright-field and polarized light illumination microscopy. Scale bar: 200 µm. The effect of (**b**) dye and (**c**) acetic acid concentration of the Sirius Red solution on its collagen labeling efficiency was investigated on collagen solution diluted with distilled water (H_2O) or culture medium (DMEM). The pH of the resulting mixtures was also determined. The gray bar shows the optimal binding pH range of Sirius Red on tissue sections based on literary data. The effects of (**d**) temperature and (**e**) incubation time on the labeling efficiency were investigated on collagen solution diluted in a culture medium. (**f**) Different microplate types used during the washing steps were also compared. The labeling efficiency of Sirius Red-stained samples was determined by the optical density (OD) of their eluates. Results are presented as mean ± SD ($n = 6$). ns: non-significant, * $p < 0.05$ (linear regression).

To validate the Sirius Red staining procedure of cell culture supernatants based on our results and impressions described above, a wide range of collagen dilution series were stained according to the chosen setup: 0.1% Sirius Red in 3% acetic acid, incubated at room temperature for 30 min, washed in V-bottom plate. The data obtained confirmed the good quality of our assay, characterized by a wide range of detection, high sensitivity, and very low (below 10%) intra- and inter-assay variability (Figure 5).

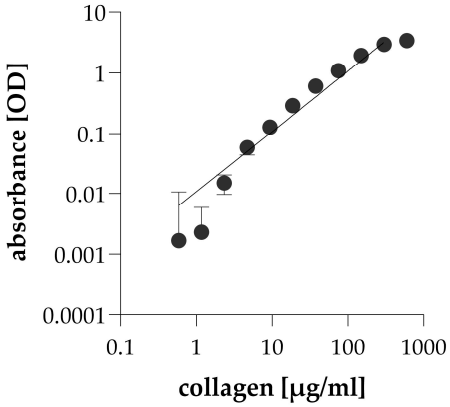

Linearity:	0–300 µg/ml
Limit of detection:	2 µg/ml
Accuracy:	±3.5 µg/ml
Intra-assay variability:	7.7 %
Inter-assay variability:	9.5 %

Figure 5. Validation of the established assay for collagen detection in solution by Sirius Red staining. To describe the efficacy of the method, collagen I solution series (0–600 ng/mL) diluted in cell culture medium (DMEM) were stained with 0.1% Sirius Red in 3% acetic acid, incubated at room temperature for 30 min, washed in V-bottom plate. The amount of collagens in Sirius Red-stained samples was determined by the optical density (OD) of their eluates. The efficiency of the method was described by determining linearity, sensitivity, and precision. Results are presented as mean ± SD (n = 6).

2.3. Optimization of In Vitro Experimental Setup to Detect Collagen Production of Fibroblasts

The effect of FBS concentration on collagen production of CCD-19Lu fibroblasts was investigated by simultaneous Sirius Red staining of the cells and their culture medium. We found that FBS itself formed flake-like precipitation with Sirius Red dye, resulting in a potential non-specific signal in cell culture medium samples (Figure 6a,b). Although the addition of FBS slightly increased the amount of cell-associated collagens, it also caused a high aspecific signal during the Sirius Red staining of cell culture medium samples (Figure 6c).

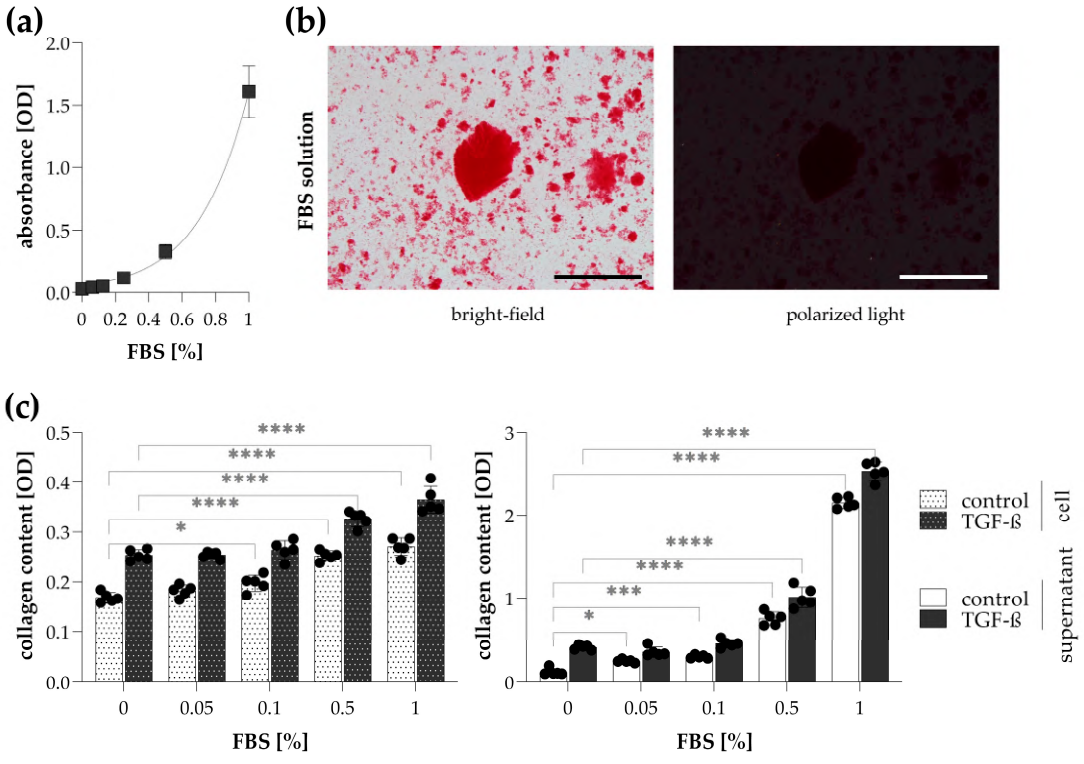

Figure 6. Effect of fetal bovine serum (FBS) on the detection of collagens in cell culture medium. (**a**) The non-specific binding of Sirius Red was investigated on FBS solution diluted in a culture

medium. (**b**) To visualize Sirius Red precipitates in 1% FBS solution, images were taken by bright-field and polarized light illumination microscopy. Scale bar: 200 µm. (**c**) To investigate the effect of FBS on the detection of collagens, TGF-β-treated CCD-19Lu lung fibroblasts, and their culture supernatant were stained with Sirius Red. The amount of collagens in Sirius Red-stained samples was determined by the optical density (OD) of their eluates. Results are presented as mean ± SD, dots represent individual values (n = 5). * $p < 0.05$; *** $p < 0.001$; **** $p < 0.0001$ (two-way ANOVA with Dunnett's test).

The impact of ascorbate on cellular collagen production was also investigated. Ascorbate solution formed no aggregates with Sirius Red dye (Figure 7a). Red precipitates separated from stained cell culture medium showed light scattering parts in polarized light (Figure 7b). The addition of ascorbate into the culture medium resulted in a dose-dependent increase in the collagen production of TGF-β-stimulated fibroblasts measured both on attached cells and in their culture medium (Figure 7c).

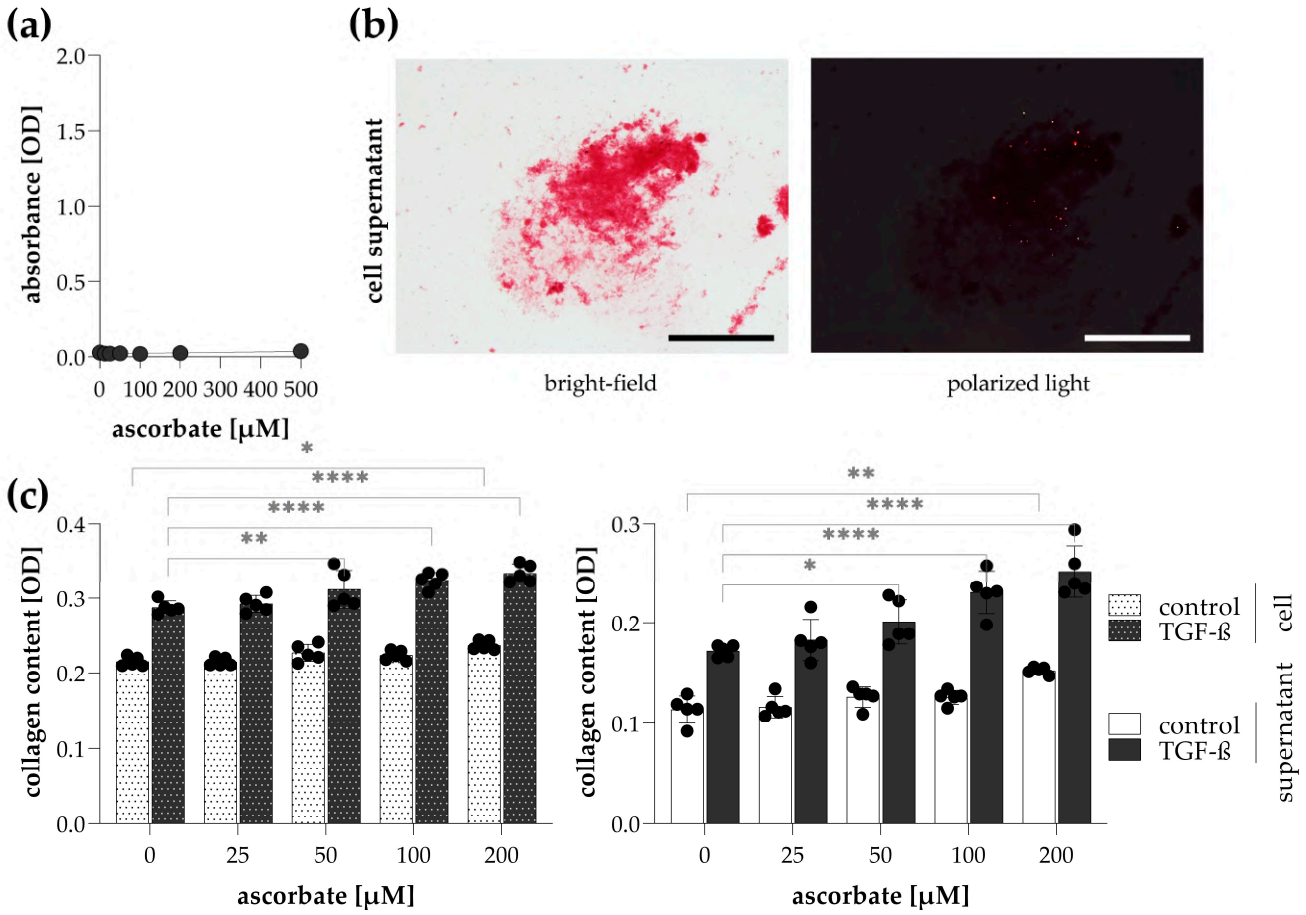

Figure 7. Effect of ascorbate on the detection of collagens in cell supernatants. (**a**) The non-specific binding of Sirius Red was investigated on an ascorbate solution diluted in a culture medium. (**b**) To visualize Sirius Red precipitates in a culture medium (200 µM ascorbate, TGF-β treatment), images were taken by bright-field and polarized light illumination microscopy. Scale bar: 200 µm. (**c**) To investigate the effect of ascorbate on the detection of collagens, TGF-β-treated CCD-19Lu lung fibroblasts and their supernatant were stained with Sirius Red. The amount of collagens in Sirius Red-stained samples was determined by the optical density (OD) of their eluates. Results are presented as mean ± SD, dots represent individual values (n = 5). * $p < 0.05$; ** $p < 0.01$; **** $p < 0.0001$ (two-way ANOVA with Dunnett's test).

2.4. In Vitro Sirius Red Assay to Investigate the Efficacy of Antifibrotic Drugs

In representative experiments, we investigated the effects of nintedanib and pirfenidone on the collagen production of TGF-β-stimulated CCD-19Lu fibroblasts by simultaneous Sirius Red staining of the cells and their culture medium. We found that, although, treatment with nintedanib also reduced the amount of cell-associated collagens in a dose-dependent manner, with the effect of collagen levels being strong in culture supernatants, where it completely neutralized the inducing effect of TGF-β (Figure 8a). This difference was even more spectacular in the case of pirfenidone, which had little effect on cell-associated collagens, but even more so on those in cell culture medium (Figure 8b).

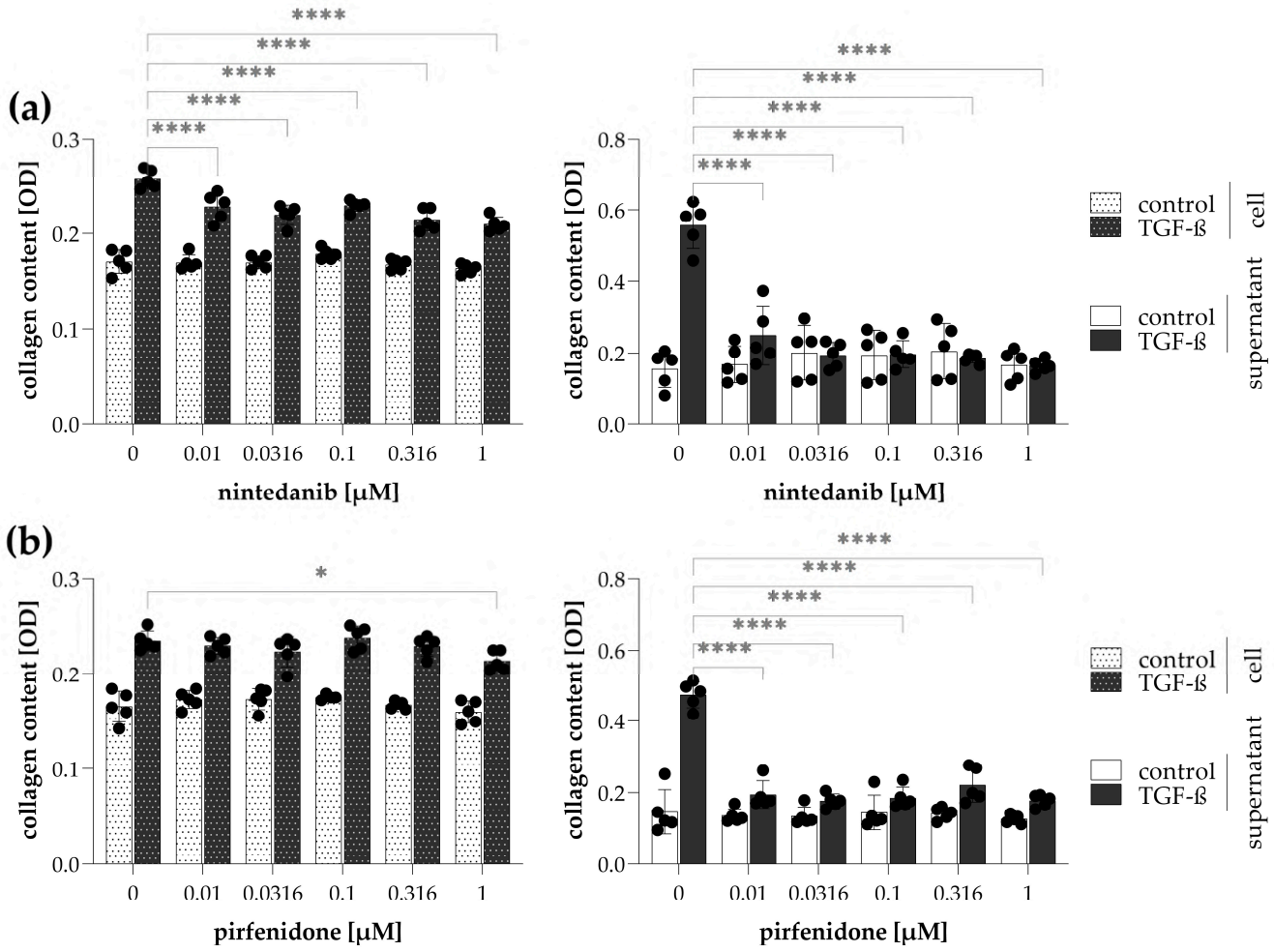

Figure 8. Sirius Red assay to screen the efficiency of antifibrotic drugs. To investigate the effect of (**a**) nintedanib or (**b**) pirfenidone, TGF-β-treated CCD-19Lu lung fibroblasts and their culture medium were stained with Sirius Red. The amount of collagens in Sirius Red-stained samples was determined by the optical density (OD) of their eluates. Results are presented as mean ± SD, dots represent individual values ($n = 5$). * $p < 0.05$; **** $p < 0.0001$ (two-way ANOVA with Dunnett's test).

3. Discussion

To complete the assay arsenal that can be effectively used in fibrosis-related research, there is a need to develop a suitable method for the measurement of collagen production in a near high-throughput manner, in addition to fibroblast proliferation and migration assays [9]. In this study, we used lung fibroblasts to optimize the in vitro experimental setup to quantify collagens while considering the related challenges described above.

The collagen-detection method of our choice was based on Sirius Red dye. This traditional histological staining method has been used since the late 1960s as a potential

substitution for Van Gieson's picrofuchsin to detect connective tissue [19]. Initially, the labeling specificity of Sirius Red was investigated on amyloid plaques, but its usability proved to be inferior to its rivals [20,21]. In contrast, when Sirius Red was used in combination with picric acid, its specific collagen-binding affinity was found to be excellent; furthermore, the labeled collagen fibers showed intensely positive birefringence under polarized light [11]. There has been a debate about whether Sirius Red is able to differentiate between collagen types based on their color changes under polarized light, but this is more likely to be due to the orientation and thickness of the labeled fibers [10,22]. Indeed, it has been shown in several studies that Sirius Red stains various types (fibrillar I, II, III, V or network forming IV) of mature and pro-collagens with similar efficiency and also their native and digested forms [23–25]. Thanks to its above-mentioned properties, Sirius Red has become one of the most widely used histological staining techniques to detect fibrotic areas on certain tissue types [22,26–29]. As shown in Figure 2, Sirius Red staining can also be used to stain cellular collagens, not only on tissue sections.

The traditional analysis of Sirius Red-stained tissue samples is based on a scoring system and is evaluated by an experienced pathologist, where digitization and subsequent graphical analysis of sections is a well-established method that provides reliable and trustworthy results [30–32]. Data acquisition approaches for Sirius Red can be further extended to include its chemical properties. The dye molecule is characterized by an elongated structure with multiple anionic azo (sulfonic acid) groups, which allow Sirius Red to bind parallelly to the collagen triple helix, which contains mostly cationic amino acid residues [11]. By the way, this orientation of Sirius Red molecules arranged by the parallelly connected tropocollagens ensures the birefringence of fibrillar collagens, including type I and III [22,33]. As acidic conditions are required for the positive charge of collagen residues, the bound dye can be eluted with an alkaline solution, allowing its quantification based on optical density [18,25]. This approach of staining the fixed cells and then releasing the dye is much simpler and faster than the commercial kits discussed in the introduction, which require overnight sample preparation and solubilization.

In this study, we propose Sirius Red staining of fibroblast to determine the amount of cell-associated collagens. As shown in Figure 3a, fibroblast activation by treatment with profibrotic growth factor resulted in more intense staining and, consequently, higher absorbance of the eluted solution. However, as mentioned in the introduction, the maturation of collagens, which results in the cell-associated fiber form, is a complex multistep process, which is challenging to model in vitro. Indeed, due to the insufficient tropocollagen conversion, fiber arrangement, and cell linkage, a significant part of the biologically relevant collagen fractions cannot be measured as the cell culture medium is usually discarded during the staining procedure [1,15]. This is well illustrated by our microscopic images, which show that even after 7 days of culture, no significant collagen fiber alignment is found (Figure 2). Previously, it has been shown that the supplementation of cell culture medium with large macromolecules accelerated the mature collagen deposition in fibroblasts, which originally required several weeks under standard experimental conditions [34–36]. This phenomenon is known as the volume exclusion effect, based on the fact that in vivo both intra- and extracellular proteins are surrounded by other macromolecules, thereby reducing the actual, available volume of the aqueous environment [34,37]. Molecular crowding mediates protein interactions, including conformational changes, enzymatic reactions, and other biological processes. In spite of all these, we found no beneficial effect on the deposition of cell-associated collagens when large polymers (e.g., dextran, polyethylene glycol, ficoll) are added to the cell culture medium (Figure 3b), most probably due to the duration of the experiment. As time saving is also an important feature of the high-throughput in vitro assays, we looked for an alternative solution instead of extending the treatment from 48 h to 1–2 weeks.

Therefore, we preferred an alternative option to detect non-cell-associated collagens. As Sirius Red dye molecules bind to the collagen triple helix via ionic interactions, soluble pro-collagen, tropocollagen, and floating mature collagen forms can also be labeled

(Figure 4a) [25]. The collagen-dye precipitates can be separated by centrifugation, and similarly to stained cells, pellets can be washed with an acid solution, thereby removing the excess dye, and then the bound dye can be eluted with an alkaline solution and its absorbance can be recorded. In the following, the optimization of collagen staining in a cell culture medium by Sirius Red will be discussed.

In the first step of our experiments, we investigated the effect of the staining environment on Sirius Red binding using a collagen solution. We found that the Sirius Red concentration we selected based on the original histological staining protocols [11] resulted in a stable, strong signal and that its enhancement was not expedient (Figure 4b). In contrast, a small modification of the acidity of the staining solution needed to be made, increasing the acetic acid concentration up to 3% (Figure 4c). This is most likely due to a pH shift of the sample-staining solution from the optimal range [11], caused by the buffer capacity of the cell culture medium. As previously discussed, an acidic environment is required for ionic interaction between Sirius Red and collagen molecules [25]. It has been previously shown that cooling staining reagents can improve the binding capacity of Sirius Red dye [38]. Similarly, we obtained higher absorbance values when collagen solutions were stained at 4 °C than at room temperature (Figure 4d). We found that providing low temperature during the implementation of the Sirius Red assay did not cause any difficulties in the treatment, and thus it was feasible to increase the sensitivity even for samples with low collagen concentration. We also examined the optimal incubation time of samples with Sirius Red solution. A stable signal was observed already at 15 min, which was not improved by longer staining (Figure 4e). On the basis of the literary data, long incubation times (usually 60 min) of fixed tissue samples are required due to the time-consuming diffusion of dye molecules into the tightly arranged collagen fibers, attached to the cells [11,24,39]. As the present assay is performed on 96-well culture plates, we compared different types of microplates to find the optimal one for multiple staining, centrifugation, and washing steps of cell culture supernatants. We found that the transparent V-bottomed plate was the most suitable for Sirius Red staining of solutions due to its small bottom surface, which results in well-formed precipitates, firmly attached to the bottom of the wells (Figure 4f). The efficacy and sensitivity of the final, optimized staining process is comparable to commercially available kits (Figure 5).

In the next step of the study, we optimized the in vitro experimental setup to investigate the collagen production of fibroblasts by Sirius Red staining on both cells and their culture medium, as described above. The majority of fibroblast-based methods to investigate collagen production is performed on prolonged or hyperconfluent cell culture, stimulated by TGF-β-treatment [35]. Therefore, in our experiments, cell seeding was followed by a proliferation phase triggered by high FBS concentration, which is one of the main components of the culture medium, containing large amounts of nutrients, ensuring cell growth [40]. However, it is known that FBS contains high amounts of albumin, a well-known carrier protein, rich in basic amino acid residues, which results in non-specific binding with various macromolecules, including Sirius Red [18,25,38]. Indeed, this was supported by our findings when staining culture media containing FBS with Sirius Red (Figure 6a,b). Meanwhile, our results showed that FBS supplementation during the fibroblast activation by TGF-β treatment had only a moderate effect on the amount of cell-associated collagens, but at the same time, it masked the specific signal detected in the culture medium (Figure 6b). Moreover, previously, it has been shown that collagen production can be increased by cultivating fibroblasts at high confluency and serum deprivation [41–43]. Therefore, we recommend the use of 0% FBS supplementation in cell treatments, in which case collagen production can be measured in a specific and sensitive manner in both cells and their medium by Sirius Red staining.

Finally, we investigated the effect of ascorbate supplementation on the collagen production of fibroblasts. Ascorbate, also known as ascorbic acid or vitamin C, is an essential cofactor of prolyl- and lysyl hydroxylase enzymes that perform the post-translational modification of collagen α chains, thereby ensuring their formation into triple helixes [44].

In addition, ascorbate has also been shown to affect collagen production and the transcriptional level by increasing the translation and the stability of collagen mRNAs [45–47]. The essential role of ascorbate on collagen biosynthesis is well illustrated by the typical symptoms of scurvy, a disease of ascorbate deficiency, affecting skin, gums, and joints among others due to collagen underproduction, leading to abnormal extracellular matrix formation in connective tissue [48,49]. We found that ascorbate increased the collagen production of fibroblasts in a dose-dependent manner, measured both on cells and in their culture medium (Figure 7). As ascorbate does not form precipitates with Sirius Red dye, we recommend 200 µM of ascorbate as a culture medium supplement during cell treatments.

As a result, we established an in vitro experimental system that allowed us to investigate the effects of various factors on collagen production. Our assay is based on a similar principle as commercially available Sirius Red-based kits; however, due to our specific recommendations for experimental setup, it finally provides more specific and sensitive results with a fraction of the cost (approx. 1/100) and time (approx. 2 h instead of a whole workday) required.

Our representative measurements on lung fibroblasts showing the antifibrotic effect of the two FDA-approved drugs nintedanib and pirfenidone demonstrate the applicability of Sirius Red assay as an in vitro screening method (Figure 8). The combination of these two staining methods together provides biologically relevant and reliable data on cellular collagen production, simultaneously determining the amount of cell-attached and soluble form of collagens (Figure 9). The simplicity and cost-effectiveness of this microplate-based method further support its applicability in fibrosis-related research both in basic science and in preclinical drug development.

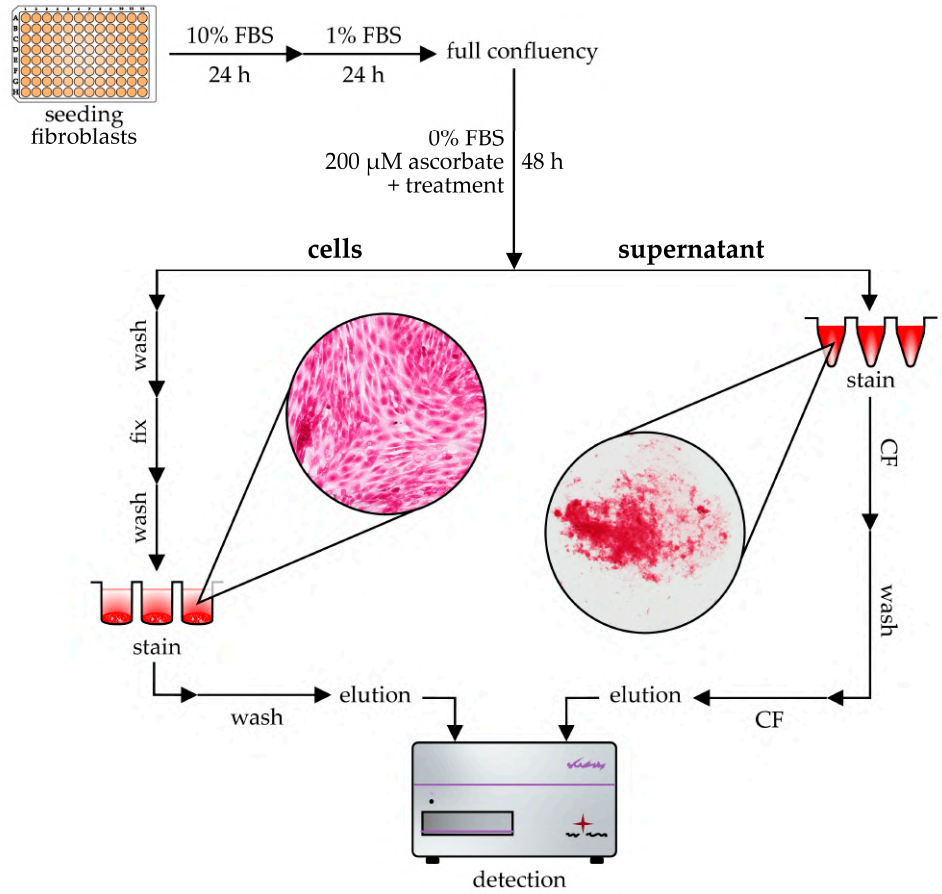

Figure 9. Schematic illustration of Sirius Red-based microplate assay to investigate collagen production in vitro. The figure shows the simultaneous staining and detection process of cell-attached and soluble collagens. *FBS*: fetal bovine serum; *h*: hours; *CF*: centrifugation.

4. Materials and Methods

4.1. Cell Lines and Treatments

CCD-19Lu (#CCL-210, American Type Culture Collection, Manassas, VA, USA) human lung fibroblast cells were cultured in Dulbecco's Modified Eagle Medium (DMEM) (Thermo Fisher Scientific, Waltham, MA, USA) supplemented with a 10% heat-inactivated fetal bovine serum (FBS) (Invitrogen, Waltham, MA, USA) and a 1% penicillin and streptomycin (Merck, Kenilworth, NJ, USA) mixture under standard cell culture conditions (37 °C, humidified, 5% CO_2).

For in vitro experiments, CCD-19Lu cells were seeded into 96-well tissue culture plates (Sarstedt, Newton, MA, USA) at a density of 10^4 cells/well (n = 5–6 wells/treatment group) and grown in DMEM with 10% FBS for 24 h, followed by 1% FBS in DMEM for an additional 24 h to achieve full confluence. Cells were then treated with 1 nM recombinant transforming growth factor beta 1 (TGF-β, #PHG9204, Thermo Fisher Scientific) diluted in FBS-free DMEM containing 200 μM ascorbate (Merck) for 48 h unless otherwise indicated.

To investigate the effect of volume exclusion, co-treatment with dextran 40 (Dx) (40 kDa, 50 mg/mL, Reanal Ltd., Budapest, Hungary), dextran sulfate sodium salt (DSS) (40 kDa, 100 μg/mL, MP Biomedicals, LLC, Irvine, CA, USA), polyethylene glycol (PEG) (20 kDa, 50 mg/mL, Merck) or ficoll 400 (Fc) (400 kDa, 50 mg/mL, Pharmacia Fine Chemicals, Uppsala, Sweden) were applied.

In representative experiments, co-treatment with 0.01–1 μM of nintedanib or pirfenidone (Vichem Chemie Research, Budapest, Hungary) was also investigated. Control cells were treated only with the respective solvents in equal volumes (TGF-β: 4 mM HCl, nintedanib, pirfenidone: DMSO).

4.2. Sirius Red Collagen Detection Assay for Cells

At the end of the in vitro experiments, after the removal of the culture medium, the cells were washed with 200 μL of phosphate-buffered saline (PBS) and fixed with 50 μL of Kahle's solution, containing 26% ethanol, 3.7% formaldehyde, and 2% glacial acetic acid, at room temperature for 15 min. After another washing step with 200 μL of PBS, cells were stained by adding 50 μL of 0.1% Sirius Red (Direct Red 80) solution dissolved in 1% acetic. The plates were incubated at room temperature for 1 h, then wells were washed with 400 μL of 0.1 M HCl. Next, 100 μL of 0.1 M NaOH solution was added to each well to eluate the bound dye from the cell-associated collagens. Microscopic images were taken from Sirius Red-stained cells right before the elution step. All reagents were purchased from Merck. The absorbance of solutions was determined as optical density (OD) on 540 nm wavelength using a CLARIOstar microplate reader with MARS Data Analysis Software v4.01 (BMG Labtech, Ortenberg, Germany).

4.3. Sirius Red Collagen Detection Assay for Cell Culture Medium

A series of dilutions of rat tail-derived collagen type I (#A10483-01; Thermo Fisher Scientific) in distilled water or DMEM was used in the optimization steps of collagen staining in the culture medium. Centrifugation and washing steps were performed and compared in various 96-well microplates, including flat-bottom (Sarstedt), V-bottom (Thermo Fisher Scientific), or 0.45 μm low-binding hydrophilic polytetrafluoroethylene (PTFE) filter plate (Merck).

At the end of the in vitro experiments, cell culture medium with a volume of 100 μL was transferred into a V-bottom 96-well microplate (Sarstedt) and was stained by adding 50 μL of 0.1% Sirius Red solution dissolved in 3% acetic acid. The samples were mixed thoroughly and incubated at room temperature for 30 min. To separate the collagen-dye precipitates, the plates were centrifuged at 3000× g for 6 min. The unbound dye solution was aspirated with a multichannel pipette; thereafter, the wells were washed with 150 μL of 0.1 M HCl solution and subsequent centrifugation. To each well, 100 μL of 0.1 M NaOH solution was added to eluate the bound dye, thereafter samples were transferred into a transparent flat-bottom 96-well plate and their absorbance was measured as previously

described. Microscopic images were taken from Sirius Red-stained collagen solutions or cell culture medium right before the elution step when collagen-dye precipitates were resuspended in an HCl solution and dripped onto a slide and covered by a glass coverslip.

4.4. Immunofluorescence Staining

CCD-19Lu cells were seeded into 4-well chambers (Sarstedt) at a density of 6×10^4 cells/well and cultured in DMEM containing 10% FBS for 7 days. Subsequently, cells were rinsed with 500 µL of PBS, fixed and permeabilized with 300 µL of BD Cytofix/Cytoperm™ (BD Biosciences, Franklin Lakes, NJ, USA) at room temperature for 15 min, then rinsed with 500 µL of BD Perm/Wash™ (BD Biosciences). Cells were incubated with primary antibodies specific for either procollagen 1α2 (sc-166572; mouse, 1:100, Santa Cruz Biotechnology, Dallas, TX, USA) or collagen type I alpha 1 (sc-293182; mouse, 1:100, Santa Cruz Biotechnology) at room temperature for 1 h, washed with 500 µL BD Perm/Wash™ for 2 min, incubated with goat anti-mouse Alexa Fluor® 568-conjugated IgG secondary antibody (A11004; 1:500, Thermo Fischer Scientific) at room temperature for 1 h and washed again with 500 µL of BD Perm/Wash™ for 2 min. Appropriate controls were performed omitting the primary antibodies to ensure their specificity and to avoid autofluorescence. Finally, slides were cover slipped using ProLong™ Gold Antifade Mountant (Thermo Fischer Scientific).

4.5. Microscopy

Microscopic images were taken with fluorescence, bright-field, or polarized light illumination techniques using the Olympus IX81 microscope system (Olympus Corporation, Tokyo, Japan) with 20× or 100× objectives.

Subsequent merging steps of corresponding image pairs were performed using ImageJ 1.48v software (National Institutes of Health, Bethesda, Rockville, MD, USA). Briefly, color images taken with bright-field and polarized light illumination from the same field of view were transformed into 8-bit format, then merged together using red (bright-field) and green (polarized) channels to visualize and compare the detected signals.

4.6. Statistical Analysis

Statistical evaluation of the data was performed using GraphPad Prism 9.1.2 software (GraphPad Software Inc., San Diego, CA, USA). Curves from the dilution series were compared by linear regression analysis. For the multiple comparisons of data from in vitro measurements, ordinary two-way ANOVA with Dunnett's tests were used. Unless otherwise indicated, results are presented as mean ± SD of the corresponding groups. The tests applied, significance (p), and number of elements (n) are indicated in each figure legend.

Descriptive statistics were performed to describe the performance of 'Sirius Red Collagen Detection Assay for Cell Culture Medium'. Linearity was determined based on the range of the collagen concentration for which a linear curve could be fitted, while regression (R^2) < 0.95 was met. The limit of detection was determined based on the minimal collagen concentration at which the absorbance was significantly different from the baseline. Accuracy was defined as the mean difference between nominal and measured collagen concentrations in the linear range. Intra-assay variability was defined based on the average coefficient of variations from the samples of linear range measured in a single experiment. Inter-assay variability was determined as the coefficient of variation derived from the mean values of samples of linear range measured in six independent experiments.

4.7. Step-by-Step Protocol of In Vitro Sirius Red Assay

4.7.1. Preparing Reagents

- Kahle's fixative solution: 26% ethanol, 3.7% formaldehyde, and 2% glacial acetic acid diluted in distilled water
- Sirius Red solution for cell staining: 0.1% Direct Red 80 dissolved in 1% acetic acid containing distilled water

- Sirius Red solution for cell medium staining: 0.1% Direct Red 80 dissolved in 3% acetic acid containing distilled water
- HCl solution: 0.1 M HCl in distilled water
- NaOH solution: 0.1 M NaOH in distilled water

4.7.2. Cell Culture and Treatment

- seed cells into 96-well plates to reach near-full confluence and culture them for 24 h in a culture medium containing 10% FBS
- change to medium containing 1% FBS for 24 h to reach full confluence
- change to medium containing 0% FBS, 200 μM ascorbate, and treat cells with the examined agents or factors for 48 h

4.7.3. Sirius Red Staining of Cells

- transfer the cell culture medium into a V-bottom 96-well microplate
- carefully wash cells with 200 μL/well PBS
- fix cells with 50 μL/well Kahle's solution at room temperature for 15 min
- wash cells with 200 μL/well PBS
- stain cells with 50 μL/well Sirius Red solution at room temperature for 1 h
- wash cells with 400 μL/well HCl solution
- elute collagen-bound dye with 100 μL/well NaOH solution

4.7.4. Sirius Red Staining of Cell Culture Medium

- add 50 μL/well Sirius Red solution to the previously transferred 100 μL/well medium, mix thoroughly, and incubate at room temperature for 30 min
- centrifuge the plates at 3000× *g* for 6 min to precipitate the collagen-dye complex from the solution
- remove the remaining fluid carefully without touching the precipitates
- add 150 μL/well HCl solution, then centrifuge the plates at 3000× *g* for 6 min
- remove the remaining fluid carefully without touching the precipitate
- elute collagen-bound dye with 100 μL/well NaOH solution
- transfer the eluted solution into transparent flat-bottom 96-well plates for detection

4.7.5. Detection

- measure the absorbance of the samples in a microplate reader at 540 nm wavelength
- either NaOH solution can be used as blank, or samples can be normalized on the background absorbance at 690 nm wavelength
- this method is applicable for the semi-quantitative comparison of collagen content between samples, but not for the exact quantification
- to quantify collagen content, collagen serial dilution in DMEM can be prepared and stained by the Cell Culture Medium protocol to create the standard curve

Author Contributions: Conceptualization, A.V.-S.; methodology, A.V.-S. and C.S.; formal analysis, C.S. and P.B.; resources, L.Ő., A.J.S. and Á.V.; writing—original draft preparation, C.S., A.V.-S. and Á.V.; writing—review and editing, D.P. and B.S.; visualization A.V.-S. and P.B.; funding acquisition, Á.V. and A.J.S. All authors have read and agreed to the published version of the manuscript.

Funding: This research was founded by the National Research, Development and Innovation Office (NKFIH), K-142728; Semmelweis University, TKP2021-EGA-24, STIA-KFI-2021; Hungarian Research Network, ELKH-POC-2022-024, the New National Excellence Program of the Ministry for Culture and Innovation from the Source of the National Research, Development and Innovation Fund, ÚNKP-23-3-I-SE-36, ÚNKP-23-3-I-SE-42, ÚNKP-23-4-II-SE-29, ÚNKP-23-5-SE-15; Hungarian Academic of Sciences, János Bolyai Research Scholarship.

Institutional Review Board Statement: Not applicable.

Informed Consent Statement: Not applicable.

Data Availability Statement: Data are contained within the article.

Acknowledgments: We are grateful to Mária Bernáth for her excellent technical assistance and to Erzsébet Kovács for providing histological sections.

Conflicts of Interest: The authors declare no conflict of interest.

References

1. Chen, C.Z.; Raghunath, M. Focus on collagen: In vitro systems to study fibrogenesis and antifibrosis state of the art. *Fibrogenesis Tissue Repair* **2009**, *2*, 7. [CrossRef]
2. Wynn, T.A. Fibrotic disease and the TH1/TH2 paradigm. *Nat. Rev. Immunol.* **2004**, *4*, 583–594. [CrossRef] [PubMed]
3. Hughes, G.; Toellner, H.; Morris, H.; Leonard, C.; Chaudhuri, N. Real world experiences: Pirfenidone and nintedanib are effective and well tolerated treatments for idiopathic pulmonary fibrosis. *J. Clin. Med.* **2016**, *5*, 78. [CrossRef] [PubMed]
4. Santos, G.; Fabiano, A.; Mota, P.C.; Rodrigues, I.; Carvalho, D.; Melo, N.; Novais-Bastos, H.; Alexandre, A.T.; Moura, C.S.; Guimarães, S.; et al. The impact of nintedanib and pirfenidone on lung function and survival in patients with idiopathic pulmonary fibrosis in real-life setting. *Pulm. Pharmacol. Ther.* **2023**, *83*, 102261. [CrossRef] [PubMed]
5. Kendall, R.T.; Feghali-Bostwick, C.A. Fibroblasts in fibrosis: Novel roles and mediators. *Front. Pharmacol.* **2014**, *5*, 123. [CrossRef] [PubMed]
6. Kamiloglu, S.; Sari, G.; Ozdal, T.; Capanoglu, E. Guidelines for cell viability assays. *Food Front.* **2020**, *1*, 332–349. [CrossRef]
7. Supino, R. MTT assays. *Methods Mol. Biol.* **1995**, *43*, 137–149. [PubMed]
8. Korzeniewski, C.; Callewaert, D.M. An enzyme-release assay for natural cytotoxicity. *J. Immunol. Methods* **1983**, *64*, 313–320. [CrossRef]
9. Veres-Székely, A.; Pap, D.; Szebeni, B.; Őrfi, L.; Szász, C.; Pajtók, C.; Lévai, E.; Szabó, A.J.; Vannay, Á.J. Transient Agarose Spot (TAS) Assay: A New Method to Investigate Cell Migration. *Int. J. Mol. Sci.* **2022**, *23*, 2119. [CrossRef]
10. Rich, L.; Whittaker, P. Collagen and picrosirius red staining: A polarized light assessment of fibrillar hue and spatial distribution. *J. Morphol. Sci.* **2017**, *22*, 97–104.
11. Junqueira, L.C.U.; Bignolas, G.; Brentani, R.R. Picrosirius staining plus polarization microscopy, a specific method for collagen detection in tissue sections. *Histochem. J.* **1979**, *11*, 447–455. [CrossRef]
12. Onursal, C.; Dick, E.; Angelidis, I.; Schiller, H.B.; Staab-Weijnitz, C.A. Collagen biosynthesis, processing, and maturation in lung ageing. *Front. Med.* **2021**, *8*, 593874. [CrossRef] [PubMed]
13. Canty, E.G.; Kadler, K.E. Procollagen trafficking, processing and fibrillogenesis. *J. Cell Sci.* **2005**, *118*, 1341–1353. [CrossRef] [PubMed]
14. Sorushanova, A.; Delgado, L.M.; Wu, Z.; Shologu, N.; Kshirsagar, A.; Raghunath, R.; Mullen, A.M.; Bayon, Y.; Pandit, A.; Raghunath, M. The collagen suprafamily: From biosynthesis to advanced biomaterial development. *Adv. Mater.* **2019**, *31*, 1801651. [CrossRef]
15. Lareu, R.R.; Arsianti, I.; Subramhanya, H.K.; Yanxian, P.; Raghunath, M. In vitro enhancement of collagen matrix formation and crosslinking for applications in tissue engineering: A preliminary study. *Tissue Eng.* **2007**, *13*, 385–391. [CrossRef] [PubMed]
16. Veres-Székely, A.; Szebeni, B.; Pap, D.; Bokrossy, P.; Lévai, E.; Szász, C.; Szabó, J.A.; Vannay, Á. A fibroblastok funkcionális vizsgálata–IV. rész: Az ECM-termelés mérése. *Gyermekgyógyászat* **2022**, *73*, 402–405.
17. Coentro, J.Q.; Capella-Monsonís, H.; Graceffa, V.; Wu, Z.; Mullen, A.M.; Raghunath, M.; Zeugolis, D.I. Collagen quantification in tissue specimens. *Fibros. Methods Protoc.* **2017**, *1627*, 341–350.
18. Lareu, R.R.; Zeugolis, D.I.; Abu-Rub, M.; Pandit, A.; Raghunath, M. Essential modification of the Sircol Collagen Assay for the accurate quantification of collagen content in complex protein solutions. *Acta Biomater.* **2010**, *6*, 3146–3151. [CrossRef]
19. Sweat, F. Sirius red F3BA as a stain for connective tissue. *Arch. Pathol.* **1964**, *78*, 69–72.
20. Cooper, J.H. An evaluation of current methods for the diagnostic histochemistry of amyloid. *J. Clin. Pathol.* **1969**, *22*, 410–413. [CrossRef]
21. Brigger, D.; Muckle, R.J. Comparison of Sirius red and Congo red as stains for amyloid in animal tissues. *J. Histochem. Cytochem.* **1975**, *23*, 84–88. [CrossRef] [PubMed]
22. Coleman, R. Picrosirius red staining revisited. *Acta Histochem.* **2011**, *3*, 231–233. [CrossRef] [PubMed]
23. Dayan, D.; Hiss, Y.; Hirshberg, A.; Bubis, J.; Wolman, M. Are the polarization colors of picrosirius red-stained collagen determined only by the diameter of the fibers? *Histochemistry* **1989**, *93*, 27–29. [CrossRef] [PubMed]
24. Walsh, B.J.; Thornton, S.C.; Penny, R.; Breit, S.N. Microplate reader-based quantitation of collagens. *Anal. Biochem.* **1992**, *203*, 187–190. [CrossRef]
25. Marotta, M.; Martino, G. Sensitive spectrophotometric method for the quantitative estimation of collagen. *Anal. Biochem.* **1985**, *150*, 86–90. [CrossRef]
26. Lattouf, R.; Younes, R.; Lutomski, D.; Naaman, N.; Godeau, G.; Senni, K.; Changotade, S.J. Picrosirius red staining: A useful tool to appraise collagen networks in normal and pathological tissues. *J. Histochem. Cytochem.* **2014**, *62*, 751–758. [CrossRef]
27. Whittaker, P.; Kloner, R.; Boughner, D.; Pickering, J. Quantitative assessment of myocardial collagen with picrosirius red staining and circularly polarized light. *Basic Res. Cardiol.* **1994**, *89*, 397–410. [CrossRef]

28. Kliment, C.R.; Englert, J.M.; Crum, L.P.; Oury, T.D. A novel method for accurate collagen and biochemical assessment of pulmonary tissue utilizing one animal. *Int. J. Clin. Exp. Pathol.* **2011**, *4*, 349.
29. Saxena, N.K.; Ikeda, K.; Rockey, D.C.; Friedman, S.L.; Anania, F.A. Leptin in hepatic fibrosis: Evidence for increased collagen production in stellate cells and lean littermates of ob/ob mice. *Hepatology* **2002**, *35*, 762–771. [CrossRef]
30. Courtoy, G.E.; Leclercq, I.; Froidure, A.; Schiano, G.; Morelle, J.; Devuyst, O.; Huaux, F.; Bouzin, C. Digital image analysis of picrosirius red staining: A robust method for multi-organ fibrosis quantification and characterization. *Biomolecules* **2020**, *10*, 1585. [CrossRef] [PubMed]
31. Huang, Y.; de Boer, W.B.; Adams, L.A.; MacQuillan, G.; Rossi, E.; Rigby, P.; Raftopoulos, S.C.; Bulsara, M.; Jeffrey, G.P. Image analysis of liver collagen using sirius red is more accurate and correlates better with serum fibrosis markers than trichrome. *Liver Int.* **2013**, *33*, 1249–1256. [CrossRef]
32. Segnani, C.; Ippolito, C.; Antonioli, L.; Pellegrini, C.; Blandizzi, C.; Dolfi, A.; Bernardini, N. Histochemical detection of collagen fibers by sirius red/fast green is more sensitive than van gieson or sirius red alone in normal and inflamed rat colon. *PLoS ONE* **2015**, *10*, e0144630. [CrossRef]
33. Liu, J.; Xu, M.Y.; Wu, J.; Zhang, H.; Yang, L.; Lun, D.X.; Hu, Y.C.; Liu, B. Picrosirius-Polarization Method for Collagen Fiber Detection in Tendons: A Mini-Review. *Orthop. Surg.* **2021**, *13*, 701–707. [CrossRef]
34. Zeiger, A.S.; Loe, F.C.; Li, R.; Raghunath, M.; Van Vliet, K.J. Macromolecular crowding directs extracellular matrix organization and mesenchymal stem cell behavior. *PLoS ONE* **2012**, *7*, e37904. [CrossRef]
35. Chen, C.; Peng, Y.; Wang, Z.; Fish, P.; Kaar, J.; Koepsel, R.; Russell, A.; Lareu, R.; Raghunath, M. The Scar-in-a-Jar: Studying potential antifibrotic compounds from the epigenetic to extracellular level in a single well. *Br. J. Pharmacol.* **2009**, *158*, 1196–1209. [CrossRef]
36. Lareu, R.R.; Subramhanya, K.H.; Peng, Y.; Benny, P.; Chen, C.; Wang, Z.; Rajagopalan, R.; Raghunath, M. Collagen matrix deposition is dramatically enhanced in vitro when crowded with charged macromolecules: The biological relevance of the excluded volume effect. *FEBS Lett.* **2007**, *581*, 2709–2714. [CrossRef] [PubMed]
37. Gnutt, D.; Ebbinghaus, S. The macromolecular crowding effect–from in vitro into the cell. *Biol. Chem.* **2016**, *397*, 37–44. [CrossRef] [PubMed]
38. Rodríguez-Rodríguez, P.; Arribas, S.M.; de Pablo, A.L.L.; González, M.C.; Abderrahim, F.; Condezo-Hoyos, L. A simple dot-blot–Sirius red-based assay for collagen quantification. *Anal. Bioanal. Chem.* **2013**, *405*, 6863–6871. [CrossRef] [PubMed]
39. Rowshani, A.T.; Scholten, E.M.; Bemelman, F.; Eikmans, M.; Idu, M.; van Groningen, M.C.; Surachno, J.S.; Mallat, M.J.; Paul, L.C.; de Fijter, J.W. No difference in degree of interstitial Sirius red–stained area in serial biopsies from area under concentration-over-time curves–guided cyclosporine versus tacrolimus-treated renal transplant recipients at one year. *J. Am. Soc. Nephrol.* **2006**, *17*, 305–312. [CrossRef] [PubMed]
40. Liu, S.; Yang, W.; Li, Y.; Sun, C. Fetal bovine serum, an important factor affecting the reproducibility of cell experiments. *Sci. Rep.* **2023**, *13*, 1942. [CrossRef] [PubMed]
41. Coller, H.A.; Sang, L.; Roberts, J.M. A new description of cellular quiescence. *PLoS Biol.* **2006**, *4*, e83. [CrossRef]
42. Coppock, D.L.; Kopman, C.; Scandalis, S.; Gilleran, S. Preferential gene expression in quiescent human lung fibroblasts. *Cell Growth Differ.* **1993**, *4*, 483–493. [PubMed]
43. Suh, E.J.; Remillard, M.Y.; Legesse-Miller, A.; Johnson, E.L.; Lemons, J.; Chapman, T.R.; Forman, J.J.; Kojima, M.; Silberman, E.S.; Coller, H.A. A microRNA network regulates proliferative timing and extracellular matrix synthesis during cellular quiescence in fibroblasts. *Genome Biol.* **2012**, *13*, R121. [CrossRef] [PubMed]
44. Szarka, A.; Lőrincz, T. The role of ascorbate in protein folding. *Protoplasma* **2014**, *251*, 489–497. [CrossRef]
45. Phillips, C.L.; Tajima, S.; Pinnell, S.R. Ascorbic acid and transforming growth factor-β1 increase collagen biosynthesis via different mechanisms: Coordinate regulation of proα1 (I) and proα1 (III) collagens. *Arch. Biochem. Biophys.* **1992**, *295*, 397–403. [CrossRef] [PubMed]
46. Murad, S.; Grove, D.; Lindberg, K.; Reynolds, G.; Sivarajah, A.; Pinnell, S. Regulation of collagen synthesis by ascorbic acid. *Proc. Natl. Acad. Sci. USA* **1981**, *78*, 2879–2882. [CrossRef]
47. Kishimoto, Y.; Saito, N.; Kurita, K.; Shimokado, K.; Maruyama, N.; Ishigami, A. Ascorbic acid enhances the expression of type 1 and type 4 collagen and SVCT2 in cultured human skin fibroblasts. *Biochem. Biophys. Res. Commun.* **2013**, *430*, 579–584. [CrossRef]
48. Bánhegyi, G.; Benedetti, A.; Margittai, É.; Marcolongo, P.; Fulceri, R.; Németh, C.E.; Szarka, A. Subcellular compartmentation of ascorbate and its variation in disease states. *Biochim. Et Biophys. Acta (BBA)-Mol. Cell Res.* **2014**, *1843*, 1909–1916. [CrossRef]
49. Pimentel, L. Scurvy: Historical review and current diagnostic approach. *Am. J. Emerg. Med.* **2003**, *21*, 328–332. [CrossRef]